A BIOMEDICAL ENGINEERING APPROACH TO INVESTIGATING FLOW AND WALL SHEAR STRESS IN CONTRACTING LYMPHATICS

A Dissertation

by

JAMES BRANDON DIXON

Submitted to the Office of Graduate Studies of
Texas A&M University
in partial fulfillment of the requirements for the degree of

DOCTOR OF PHILOSOPHY

May 2006

Major Subject: Biomedical Engineering

A BIOMEDICAL ENGINEERING APPROACH TO INVESTIGATING FLOW AND WALL SHEAR STRESS IN CONTRACTING LYMPHATICS

A Dissertation

by

JAMES BRANDON DIXON

Submitted to the Office of Graduate Studies of
Texas A&M University
in partial fulfillment of the requirements for the degree of

DOCTOR OF PHILOSOPHY

Approved by:

Chair of Committee,	Gerard Coté
Committee Members,	David Zawieja
	James Moore Jr.
	Lihong Wang
Head of Department,	Gerard Coté

May 2006

Major Subject: Biomedical Engineering

ABSTRACT

A Biomedical Engineering Approach to Investigating Flow and Wall Shear Stress in Contracting Lymphatics. (May 2006)

James Brandon Dixon, B.S., Texas A&M University

Chair of Advisory Committee: Dr. Gerard L. Coté

Collecting microlymphatics play a vital role in promoting lymph flow from the initial lymphatics in the interstitial spaces to the large transport lymph ducts. In most tissues, the primary mechanism for producing this flow is the spontaneous contractions of the lymphatic wall. Individual units, known as lymphangion, are separated by valves that help prevent backflow when the vessel contracts, thus promoting flow through the lymphatic network. Lymphatic contractile activity is inhibited by flow in isolated lymphatics, however there are virtually no *in situ* measurements of lymph flow in these vessels. Initially, a high speed imaging system was set up to image *in situ* preparations at 500 fps. These images were then manually processed to extract information regarding lymphocyte velocity (-4 to 10 mm/sec), vessel diameter (25 to 165 um), and particle location. Fluid modeling was performed to obtain reasonable estimates of wall shear stress (-8 to 17 dynes/cm^2). One of the difficulties encountered was the time consuming methods of manual particle tracking. Using previously captured images, an image correlation method was developed to automate lymphatic flow measurements and to track wall movements as the vessel contracts. Using this method the standard error of prediction for velocity measurements was 0.4 mm/sec and for diameter measurements it

was 7.0 μm. It was found that the actual physical quantity being measured through this approach is somewhere between the spatially averaged velocity and the maximum velocity of a Poiseuille flow model.

ACKNOWLEDGEMENTS

I would like to begin by thanking Dr. Cote for his council, encouragement, and mentoring throughout my time as a grad student at Texas A&M. I could not have asked for a better advisor, and I truly appreciate all that he has done for me. I would also like to thank each of my committee members for their help and expertise throughout my project: specifically, Dr. Zawieja, who really has served as a second advisor for me, for all his help and for forcing me to learn physiology, Dr. Moore for his expertise in the fluid mechanics portion of the project, and Dr. Wang for his ability to answer pretty much any random question I brought to him. I would also like to thank Dr. Gashev and Dr. Greiner for all of their help with the animal experiments. I consider myself to be quite lucky to have worked with people who are experts at what they do. I would like to thank all of the students of OBSL for making my experience in graduate school both humorous and educational. Of course, I can't forget to thank the numerous undergraduates who worked on this project, performing the tedious manual data analysis.

On a more personal note I would like to thank several people who have provided invaluable wisdom and support in various stages of my life. I would like to thank Brian Fisher for his wisdom and support as I struggled with the decision whether to go into full time ministry or pursue a career in academics. Thank you for always challenging me to grow in my walk with the Lord. I would also like to thank Jay Humphrey, for ultimately being the one who the Lord used to convince me to get my Ph.D. You have been quite a role model throughout my time at Texas A&M, all eight years to be exact.

Where would I be without my parents? Both of you have a faith that never waivers. I am certain that your undying love and prayers for your children will continue to produce young adults (5 to be exact!) who will walk with the Lord for a lifetime, something so much more valuable than careers or credentials. Thanks to Jeremy, Andrew, and Michael for the fun weekends in College Station when I could take a break from work and for Michael and Andrew convincing Meredith to marry me. I can't wait to see what the future has in store for both of you. Thank you, Kim, for being the gutsiest girl I know - if I could have even half of your persistence, who knows what I could do.

I have saved the best for last, the two loves of my life: my wife Meredith and my Savior Jesus Christ. Meredith, you have calmed me when I was frustrated, made me laugh when I was sad, and have been my strength when I was weak. Ok this is starting to sound like a Celine Dion song. Seriously though, I am so thankful that I have the rest of my life to love you. Also before I forget, thanks for proof-reading "the beast" (our affectionate term we came up with for this dissertation the week I was finishing up). Lastly, I would like to acknowledge God for the unmerited grace he has showered on me throughout my life: I can do all things through Christ who gives me strength.

TABLE OF CONTENTS

Page

ABSTRACT……... iii

ACKNOWLEDGEMENTS…… v

TABLE OF CONTENTS…… vii

LIST OF FIGURES……. ix

LIST OF TABLES…….. xiv

CHAPTER

I INTRODUCTION……..... 1

II DEVELOPMENT OF A HIGH SPEED IMAGING SYSTEM…... 9

2.1 Video Microscopy Analysis……... 9
2.2 Fluorescent Techniques…….. 11
2.3 Doppler Techniques…… 12
2.4 Laser Speckle Techniques…….. 14
2.5 Techniques in Nuclear Medicine…… 15
2.6 Materials and Methods…… 16
2.6.1 Hardware set-up and system specifications…. 17
2.6.2 Manual image analysis protocol…….. 19
2.6.3 *In vitro* calibration…… 22
2.6.4 *In situ* animal protocol……. 25
2.7 Results and Discussion…….. 28
2.7.1 *In vitro* calibration…….. 29
2.7.2 *In situ* experiments…….. 31
2.8 Concluding Remarks…….. 39

III CHARACTERIZATION OF THE ACTIVE LYMPH PUMP IN RAT MESENTERIC LYMPHATICS…… 40

3.1 Fluid Dynamics Theory…….. 40
3.2 Materials and Methods…… 45
3.2.1 Volume loading protocol…… 45

CHAPTER Page

3.3 Results and Discussion…… 46
3.3.1 Relationship between contractile sequence and fluid velocity……. 47
3.3.2 Wall shear stress and volume flow rate estimates…..... 54
3.3.3 Parameter averages in rat mesenteric lymphatics…..... 59
3.3.4 Lymphocyte flux data…….. 66
3.3.5 Volume loading experiments……... 67
3.4 Concluding Remarks……... 70

IV CORRELATION METHOD FOR PROCESSING LYMPHATIC IMAGES..... 71

4.1 Materials and Methods..... 72
4.1.1 Measuring lymph flow velocity..... 72
4.1.2 Measuring vessel diameter..... 75
4.1.3 Optimizing the image correlation algorithm.... 76
4.1.4 Increasing lymphocyte density..... 79
4.1.4 Isolated vessel protocol..... 80
4.2 Results and Discussion..... 82
4.2.1 *In situ* experiments..... 82
4.2.2 Increasing lymphocyte density through lipid absorption..... 95
4.2.3 Using the image correlation method with isolated vessels..... 97
4.3 Concluding Remarks..... 100

V CONCLUSION AND FUTURE WORK..... 101

REFERENCES..... 105

APPENDIX I..... 115

APPENDIX II..... 117

APPENDIX III..... 145

APPENDIX IV..... 161

VITA..... 181

LIST OF FIGURES

FIGURE Page

1.1 Confocal microscopy image of a portion of a mesenteric lymphatic vessel illustrating the structure of valve leaflets..... 3

1.2 Effects of imposed flow on contraction frequency and amplitude of a rat mesenteric lymphatic..... 7

2.1 Layout of the 1024 x 1024 imager and masking patterns to achieve 17 image frames at high frame rates within one large image..... 18

2.2 An image of a microlymphatic vessel with the measured wall coordinates (W_0, W_1, and W_2) and a lymphocyte at location (L(x,y)). The field of view is roughly 250 x 250 μm..... 20

2.3 Illustration of motor driven rotating disk. Different motor speeds and radial markings correspond to various linear velocities..... 23

2.4 *In vitro* flow sham used to calibrate system. The pressure could be adjusted by changing the height of the water level. The outflow resistance was set to center the velocity values in a physiologically relevant range..... 25

2.5 A loop of the small intestine pulled out to show the mesentery. Lymphatic vessels (too small to be visible in this picture) are dispersed throughout the mesentery..... 26

2.6 System set-up for the *in situ* preparation. The blue tube in figure passes APSS solution heated to 37° C..... 27

2.7 Actual vs. Measured velocities of *in vitro* calibration wheel with error bars..... 30

2.8 Actual vs. Measured volume flow rates of microspheres flowing through 140 μm glass tube..... 31

FIGURE Page

2.9 Vessel lumen diameter (mm) and lymphocyte velocity (mm/sec) for a 10 second interval from first data set..... 32

2.10 Vessel lumen diameter (mm) and lymphocyte velocity (mm/sec) for a 10 second interval from second data set..... 33

2.11 Vessel lumen diameter (mm) and lymphocyte velocity (mm/sec) for a 10 second interval from third data set..... 34

2.12 *In situ* image taken during 5.8 mm/sec fluid flow at time t = 0. The coordinates correspond to the lower lymphocyte..... 36

2.13 *In situ* image taken at time t = 2 ms after Figure 2.12. The lymphocyte has moved 12 pixels..... 36

2.14 *In situ* image taken at time t = 33 ms after Figure 2.12. Neither of the original lymphocytes is present in the image, however new ones have appeared..... 37

2.15 Estimation of volume flow rates (μl/hr) from velocity data in Figure 2.9..... 38

3.1 Typical relationship between fluid velocity (mm/sec) and wall diameter (mm) of a mesenteric lymphatic vessel for several contraction cycles..... 47

3.2 Figure showing how the parameters T_0 and T_w were calculated. The '--' represents the velocity pattern of tracked lymphocytes and the solid line represents a diameter tracing. T_0 is essentially a measure of phase difference while T_w is the period of the contraction cycle..... 48

3.3 Example of a contraction sequence that is irregular and contains periods of little to no contractile activity..... 50

3.4 The relationship between normalized vessel volume and normalized fluid velocity. Labeled points correspond to: A) Peak diastolic diameter and beginning of systolic contraction, B) Systolic diameter, C) Peak orthograde velocity, D) Peak retrograde velocity..... 53

3.5 Estimation of the volume flow rate (μl/hr) for the same data set represented in Figure 3.1..... 55

FIGURE Page

3.6 Estimation of wall shear stress (dynes/cm^2) for the same data set represented in Figure 3.1..... 56

3.7 Ratio of the wall velocity (Va) to the lymphocyte velocity (Vp) for the data represented in Figure 3.1..... 58

3.8 Relationship between radius^2 and volume flow rate. Data matched a linear fit with a correlation coefficient of 0.6102..... 61

3.9 Relationship between the radius^2 multiplied by the RMS contraction velocity and volume flow rate. Linear correlation statistic was improved to 0.7994..... 62

3.10 Wall shear stress estimates (dynes/cm^2) due to the imposed axial pressure gradients and phasic contractions calculated using current fluids model with previously reported isolated vessel experiments and plotted as a function of transaxial pressure gradient (cm H_2O)..... 65

4.1 Image of a lymphatic vessel illustrating the poor contrast at the imaging site. There are actually several, 15 to be exact, lymphocytes present in this image, although they are very difficult to distinguish from the background unless you can see them move from frame to frame..... 73

4.2 Illustration of the principle of the image correlation approach. Each image is taken at the same location separated by a small time interval. The displacement of the window corresponds to the movement of the fluid..... 75

4.3 Two reference windows are created around each of the vessel walls in the same vertical location. Their displacements are tracked to measure changes in vessel diameter..... 76

4.4 Correlation coefficient values for various window locations from Picg. Note the extent of the maximum as compared with the rest of the surface. This would be constituted as an acceptable match..... 77

4.5 Correlation coefficient values for various window locations from Picg. Note the extent of the maximum as compared with the rest of the surface. This would be constituted as a poor match..... 78

FIGURE Page

4.6 Mesenteric vessel of a rat approximately 45 minutes after being fed cream. Notice the increase in lymphocyte density compared to Figure 4.1..... 80

4.7 Comparison of spatially averaged velocity calculated from manually tracked data with that of the correlation algorithm. The standard error of prediction was 0.8479 mm/sec..... 83

4.8 Comparison of spatially averaged velocity calculated from manually tracked data with that calculated by the correlation algorithm after modifications were made to improve the algorithm. The standard error of prediction is 0.5009 mm/sec..... 84

4.9 Comparison of maximum velocity calculated from manually tracked data with that calculated by the correlation algorithm after modifications were made to improve the algorithm. The standard error of prediction is 0.4850 mm/sec..... 85

4.10 The standard error of prediction as the manually tracked velocity is varied from $\overline{V}$ to $V_{\max}$ where W on the x-axis is represented by the equation $V^* = W \times V_{\max} + (1-W)\overline{V}$ 86

4.11 Comparison of the optimized velocity ($V^* = W \times V_{\max} + (1-W)\overline{V}$) calculated from manually tracked data with that calculated by the correlation algorithm. The standard error of prediction is 0.4333 mm/sec..... 87

4.12 Another data sequence comparing the velocities calculated by the correlation algorithm with $\overline{V}$ calculated from the manually tracked data. The standard error of prediction is 0.3894 mm/sec..... 89

4.13 Another data sequence comparing the velocities calculated by the correlation algorithm with $\overline{V}$ calculated from the manually tracked data. The standard error of prediction is 0.2005 mm/sec..... 90

4.14 Diameter tracings calculated by the correlation algorithm compared with those calculated from the manually tracked data. The standard error of prediction is 6.8 um..... 93

FIGURE Page

4.15 Image correlation was used to track the wall at multiple locations and fit them together with a line. This image represents a snapshot of a movie showing the program's ability to continuously and accurately track wall movement..... 94

4.16 Diameter measurements taken at three different locations of the vessel (top, middle, and bottom). In this case the vessel narrows as you go from top to bottom, and the vessel also contracts more strongly at the bottom..... 95

4.17 A 3 second portion of a velocity fluctuation measured with the image correlation method for "lipid enhanced" rat with a large lymphocyte density..... 96

4.18 A 3 second portion of a velocity fluctuation (from Figure 2.11 at ~ t = 4 sec) measured with the image correlation method, lymphocyte density was very low..... 97

LIST OF TABLES

TABLE Page

3.1 Ranges of coefficient values that appear in the non-dimensionalized Navier-Stokes equations 3.4(a-c) along with their average values. All values were measured from the entire data set of seven rats…… 43

3.2 Average values and mean standard errors of various parameters from seven different rats……... 60

3.3 Values of lymphocyte density and lymphocyte flux for each of the seven rats represented in Table 3.2……... 66

3.4 Changes in contractile dynamics and average lymphocyte velocities for 5 different rats at 3 different time periods each: control, 5 minutes after loading began, 10 minutes after loading began, X's denote period where no measurement could be made due to rarity of lymphocytes…… 68

3.5 Data from Table 3.4 that has been normalized with the control period to remove animal to animal variability……... 69

4.1 Measurement of contraction and flow parameters as calculated by the correlation program for various pressure gradients for two different experiments…… 98

CHAPTER I

INTRODUCTION

The lymphatic system plays a crucial role in the transport of proteins and large particulate matter away from the interstitial spaces in the body, since the capillaries cannot move such particles directly by absorption. In addition to tissue homeostasis, the lymphatic system also plays important, although not completely understood, roles in lipid transport and metabolism, and immune function [1]. Nearly all body tissues have a supporting lymphatic system to serve these purposes; without such a system, our bodies would suffer serious consequences. About ten percent of the blood flow filtered out of the arterial capillaries is returned to the circulatory system after being absorbed by lymphatic capillaries and filtered through the lymphatic system. The total amount of flow through the lymph system is about two to three liters per day [1]. In mammals, the lymphatics push all of this fluid without the benefits of a central pumping organ like the heart. Historically, the lymphatic system was treated as a system of conduits which transported fluid from the interstitial spaces to the thoracic duct by means of interstitial fluid driving pressure, now referred to as the extrinsic pump. Certainly various factors influencing interstitial pressure play influential roles in the filling of lymphatics to increase flow. The factors include an increased rate of lymph formation, elevated

---

This dissertation follows the style and format of the *IEEE Transactions on Biomedical Engineering.*

capillary pressure, decreased plasma colloid osmotic pressure, increased interstitial fluid protein, and increased permeability of the capillaries.

However, several decades ago it was noticed that many lymphatics in a variety of mammals [2-5] and specifically humans [6-8] exhibit rhythmic contractions to aid in the promotion of lymph flow. Most physiology texts now teach this as the second mechanism, called the intrinsic pump, as also being responsible for driving flow; however, the various factors that control this pump and its significance in relation to the specific lymphatic functions are still poorly understood and not heavily emphasized. This discovery of lymphatic contractility is now referred to as the intrinsic lymphatic pump, as compared to the extrinsic lymphatic pump discussed earlier.

Anatomically, the vessels of the lymphatic system are divided into three categories: initial lymphatics, collecting lymphatics, and transport lymphatics. The origins of the lymphatic system, known as the initial lymphatics, are dispersed throughout the capillary network of the mesentery. The walls of the initial lymphatics are usually not contractile and are lined with endothelium but with no smooth muscle [9]. The main mechanism used to fill the initial lymphatics is the extrinsic pump, which responds to both steady-state lymph volumes and unsteady initial lymph volumes. While the surrounding skeletal muscle can contract to aid in the filling of initial lymphatics, the steady-state response is noted to act without contraction of the initial lymphatics in most tissues. It is hypothesized that this filling occurs through a combination of the active lymphatic wall pump downstream in the collecting lymphatics and favorable transient drops in fluid pressure due to contraction of surrounding skeletal

muscle and other factors from the interstitium to the lymphatic lumen [9-11].

Smooth muscle typically begins to line the lymphatics in the collecting lymphatics, where multiple initial lymphatics join together[12]. The sections of lymph vessels where smooth muscle is present, have the ability to perform spontaneous muscle contractions. It is also near these lymphatic sites that one begins to see lymphatic valves. Functional units of lymphatic vessels, known as lymphagions, are arranged in series, each separated by valves[13-15]. These valves occur every 600-1000 μm in rat mesentery lymphatics and smooth muscle is always present around such valves. The valves are highly competent and help prevent retrograde flow during relaxation of the vessel wall (Figure 1.1). This is needed to keep unwanted fluid and proteins from entering back into the interstitial spaces.

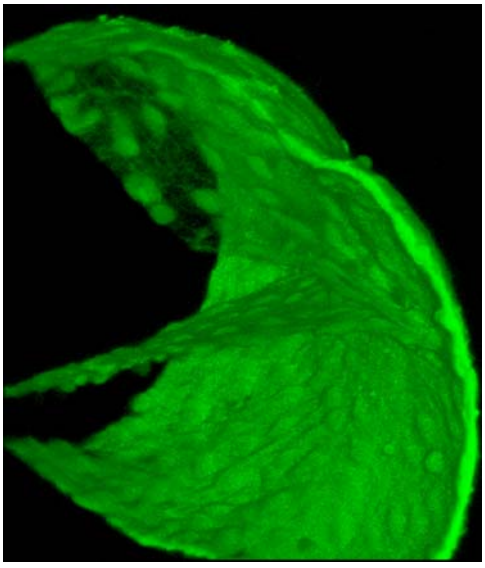

Figure 1.1: Confocal microscopy image of a portion of a mesenteric lymphatic vessel illustrating the structure of valve leaflets.

There are currently differing theories as to whether these valves play an active or a

passive role in the intrinsic pump [10, 16]. Either way, the presence of these valves, in conjunction with the active contraction cycle of individual lymphangions, makes the intrinsic pump highly effective for promoting flow.

Lymphatic muscle in rat mesenteric lymphatics has been shown to possess important differences from other smooth muscle. Lymphatic smooth muscle is composed of only SMB smooth muscle myosin heavy chain, as opposed to arterioles, which posses both SMB and SMA isoforms [12]. Contraction of this smooth muscle propagates to push lymph from one lymphagion to the next. Studies have been done on the propagation of this motion noting the phase, frequency, and amplitude of such contractions. While the majority of the propagation occurs in the downstream direction, roughly 40% of lymphatic contractions have been shown to propagate upstream [17]. It is believed that the pacemaker site for these peristaltic contractions is located at the inlet side of the valve at each lymphagion unit [18]. However, this may not be the case in all lymphatics. It is also thought that gap junctions play an important role in the coordination of contractions [19]. The conduction velocity of such contractions was found to be around 4-8 mm/sec.

Characterization of flow through the lymph system is important in order to gain a better understanding of how the system responds to the various changes in physiological parameters such as interstitial fluid pressure, fluid volume, and interstitial fluid protein concentration. There is an abundance of literature in this area of lymphatics. Studies in gross lymph flow have been an ongoing project for over the past forty years [20]. Original work did not concern itself with the mechanisms behind such flow, but rather

focused on obtaining quantitative measures of flow for the vessels of the lymphatic system in humans [9, 21-23]. The lymphatic contraction has also been investigated thoroughly and nomenclature for describing the contraction sequence has been developed [24]. However, no measurements have been reported of lymph velocities in the smaller (~ 100 μm), highly contractile lymphatic vessels. In addition to this, contraction and flow have, for the most part, been studied independently of one another. The ability to simultaneously measure both contraction and fluid velocity would be highly beneficial in understanding exactly how the intrinsic pump helps to promote lymph flow. This could also open the door for additional assessments of contraction in response to edema and various disease models. Actual velocity measurements could be compared to ejection fraction estimates used previously [25], and could be used to assess the validity of such estimates. Measurements of velocity could also be used to quantify some measure of efficiency for the valves ability to prevent backflow.

There exists an overwhelming amount of literature that shows that the mechanical environment of various tissues plays an important role in the development and function of these tissues [26-35]. Usually the forces in this environment invoke a tissue response through some biochemical regulator. With this hypothesis in mind, many investigators have studied the effects of various biochemical regulators on contraction frequency and amplitude [36-42], finding that one of the main factors shown to reduce the spontaneous transient depolarizations of the pacemaker activity in the lymph vessels is nitric oxide [25, 38, 42]. Others have shown the effects of various endothelial prostanoids on contractile activity [36, 40, 41, 43]. The main physical tissue

force whose effects on contractile function has been studied is pressure [2, 5, 24, 44]. Originally it was thought that this was the primary physical mechanism through which the lymphatic pump could be inhibited or activated. However, recently it has been shown that high flow produces an inhibition of the lymph pump when transmural pressure is kept constant [25, 45] (Figure 1.2). Presumably this occurs due to wall shear stress. This should come as no surprise because wall shear stress is one of the main mechanotransduction factors involved in vascular growth and remodeling [26-28, 30, 36]. The main question that has arisen from the flow-induced studies of isolated lymphatic pump inhibition is whether or not the imposed flows are within a reasonable physiologic range. Since the imposed flows were created by means of an axial pressure gradient, the actual velocities in these studies were not recorded, and since there is currently nothing in the literature reporting *in vivo* velocity ranges, comparisons between these isolated vessel observations and what actually might occur *in vivo* could not be made.

It was also noted in one of the above mentioned studies that this flow inhibition phenomenon was dependent upon the region from where the vessel was isolated. This dependence seems to indicate that shear stress might not only play a role in contractile function, but could also be involved in lymphatic development. This hypothesis is further supported by the observation that interstitial flow plays a vital role in lymphangiogenesis [46-48]. However, conjectures can only be taken so far without data of actual velocity measurements in shear sensitive lymphatic vessels.

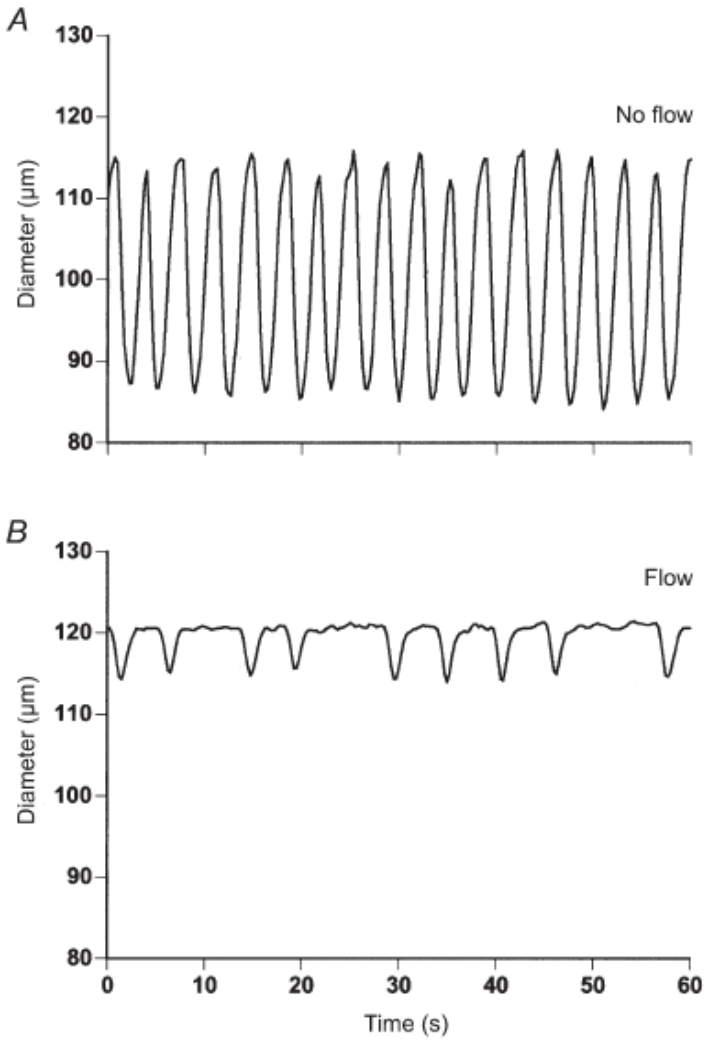

Figure 1.2: Effects of imposed flow on contraction frequency and amplitude of a rat mesenteric lymphatic[*].

These velocity measurements need to be fairly detailed so that they can be combined with some mechanical modeling to calculate an estimation of wall shear stress. To perform these calculations, we need lymph velocity measurements for the entire

[*] Reprinted with permission from "Inhibition of the active lymph pump by flow in rat mesenteric lymphatics," by Gashev et el., 2002, *Journal of Physiology*, 540, 1023-1037. Copyright 2002 by Blackwell Publishing Ltd.

contraction cycle and for the wide variety of contraction frequencies and strengths that have been observed *in vivo*. These measurements could then open the door for a wide array of isolated vessel and cell culture experiments to further characterize the biomechanical response that has been observed. They could also be used to map out the signaling pathways through which wall sheer stress regulates contraction. A comprehensive data set would also pave the way for a more detailed investigation of the fluid mechanics of lymphatic flow. Understanding the finer details of the mechanical forces involved in the regulation of the active lymphatic pump could have profound implications on our knowledge of the lymphatics' role in lipid transport and metabolism, interstitial fluid balance, and immune function. This is the first step for developing new drugs and therapies for enhancing or inhibiting lymphatic growth, and for treating various lymphatic disorders such as lymphedema and lymphoma.

CHAPTER II

DEVELOPMENT OF A HIGH SPEED IMAGING SYSTEM*

In view of our desire to measure shear stress throughout the entire contraction cycle, we needed to develop an imaging modality that would be capable of measuring both the vessel diameter and the fluid velocity simultaneously. Based on preliminary estimations the system needed to be able to measure velocities from 0.25 mm/sec to 10 mm/sec, be direction sensitive, and be able to take continuous readings for at least 30 seconds to ensure that multiple contractions cycles would be captured in a given data sequence. Due to the fluids model that was chosen, which will be discussed in further detail in the next chapter, the system also needed to be able to measure the radial profile of the velocity distribution. Since there are a wide variety of techniques that have been used in the past for velocity estimations of biological fluid flow (mostly blood flow), it is important to address the techniques and the various advantages and disadvantages of each in light of the qualifications that must be met for our specific application.

2.1 Video Microscopy Analysis

Video microscopy analysis has long been the gold standard for imaging flow through micro vessels and vessel diameter [2, 17, 20, 24, 38, 40, 49-52]. The technology itself has existed for many decades, however recent developments in computing speed

* Reprinted with permission from "Measuring microlymphatic flow using fast video microscopy" by Dixon et el., 2005. *Journal of Biomedical Optics*, 10, 064016-1 to 064016-7. Copyright 2005 by International Society for Optical Engineering.

have allowed for more exhaustive image analysis algorithms to be developed. In addition to this the development of high speed cameras have paved the way for greater temporal resolution [53, 54].

Almost all applications of such systems for lymph flow have used standard video camera capturing rates of 30 frames-per-second [17, 24, 25, 45, 55]. This has proved acceptable for measurements in contraction speed and average lymph flow, as the velocities that occur in such cases are not beyond the speed of the camera. However, we hypothesize that velocities of local flow at certain sites are much higher than those that standard video systems are capable of measuring. Our group at Texas A&M is investigating the use of a high-speed camera, with capabilities up to one million frames-per-second, to measure these higher end velocities. A similar system was used several years ago to investigate the effects of lipid absorption on lymphocyte transport [54]. However, this group did not report lymphocyte velocities but rather employed a counting technique to quantify lymphocyte flux while recording vessel diameter before and after the ingestion of olive oil. The advantage of such a technique is the ability for excellent resolution, both temporally and spatially. Temporal resolution being that which is limited by the speed of the camera and the save time of the computer, and spatial resolution being that which is limited by the magnification of the microscope and resolution of the camera. If the flow field is seeded with particles of some sort and the spatial resolution is high enough, one can get an estimation of the radial distribution of velocity across the vessel, one of the main features the velocity measurement system must have as mentioned previously. The disadvantage of this method is that real-time

velocity measurements have yet to be obtained, as all of the calculations are done with post-processing techniques that can often be time consuming and tedious. Also, the faster the frame-rate, the more data one has to analyze for a given duration of recording time. Lastly, this technique is invasive and highly sensitive to motion artifact. However, there are various *in situ* techniques that have been developed to minimize the effects of the invasive procedure on lymphatic contraction [17, 24], which will be discussed in further detail later on. Overall this technique has proved to be adequate for gaining a physiological understanding of lymphatic function, particularly lymphatic contractile activity, although it has no clinical non-invasive applications.

2.2 Fluorescent Techniques

To overcome the poor contrast that is often inherent in biological imaging, investigators have developed various fluorescent techniques to be used in combination with some form of video microscopy. Fluorescence microlymphography, a term used to describe the application of such techniques to the lymphatic vasculature, has been used to image the structure of lymphatic capillaries in various locations [23, 51, 56, 57]. Since then, many groups have quantified flow using various fluorescent techniques [21-23, 58, 59]. One fluorescent approach is to introduce into lymphatic capillaries fluorescein isothiocyanate (FITC)- labeled macromolucules such as dextran [8]. The advantage of such a technique is the accuracy of the average velocity measurements that can be achieved since the fluorescent signal detected is fairly strong. The main disadvantage of such methods is that the introduction of foreign fluorescent particles into

the system could alter the flow pattern of what normally occurs physiologically, especially since most of the techniques involve a subcutaneous injection, which creates localized edema at the site of injection. It is also difficult to measure the flow profile across the width of a vessel as current techniques concern themselves only with tracking the average speed of the fluid through the vessel and not the velocity profile.

2.3 Doppler Techniques

Doppler methods have been used with microscopy to measure flow for over thirty years [60]. Doppler-based methods for blood flow applications measure the doppler shift of a scattered source signal propagating through tissue resulting from moving blood particles within the tissue volume. This source signal can be photons [61-63], ultrasound [64], or an MR signal [65]. This method has been shown to be effective in a number of clinical scenarios where micro-vascular flow assessments are needed [66, 67] and has demonstrated some efficacy for the assessment of burn depth by measuring flow in the vascular bed at the site of the burn [68-71]. It has also been demonstrated for assessment of perfusion in skin flap procedures with limited success [72-74]. However, doppler flow through lymph vessels has proved to be more difficult as the method is dependent on the present of particles flowing through the system. In most lymphatic vessels the presence of particles, particularly white blood cells, is much scarcer than the red blood cells in the blood. In addition to this, lymph flow is much slower than that of blood as there is no “heart-like” pump driving the fluid at a constant rate through the system. The flow patterns in lymphatic capillaries are also much more

complicated due to the presence of backflow which will be discussed in further detail in the next chapter. Because of this, the measurement technique needs to be direction sensitive, which many doppler techniques are not. These complications make a doppler approach much more difficult for the lymphatic system than for blood flow measurements. However, to the knowledge of this author, one group has successfully used a doppler based approach to acquire direct measurements of lymph flow in the posterior lymph heart of toads [75]. In this specific case, many of the disadvantages discussed above do not occur here as the lymphatics system of most amphibians behaves more like the circulatory system with a pumping organ pushing flow through the vessels. No group has yet to successfully develop a doppler method to measure microlymphatic flow in mammals or humans. Traditional doppler methods are designed to give a measure of the average flow velocity through the vessel, but do not have the necessary resolution to measure the radial profile across the vessel. However, recent advances have been made to incorporate doppler imaging with optical coherence tomography (doppler OCT), to measure the radial velocity profile [67, 76-80]. As this technology advances, the speed and resolution limitations initially associated with it that would have made it difficult to apply to microlymphatics are being overcome. However, there is still a necessity for flowing scatters in your probing volume, so this technique was dismissed in our initial attempt to find the most suitable technique. We have found an interesting *in situ* method that will be presented in a few chapters that could improve this and make doppler OCT a very plausible (if not the preferable) technique for real time measurements flow patterns in contracting lymphatics. Also, since OCT is an imaging

technique, the vessel diameter associated with a particular velocity reading can be measured provided one takes enough A-scans to traverse the entire diameter.

2.4 Laser Speckle Techniques

Another optical technique that has had success in measuring fluid velocities of physiologic flow phenomenon is laser speckle [81-86]. The basic principle behind this technique is that motion in the imaging plane produces a blurring of the speckle pattern when imaging with a laser source. This speckle pattern comes from constructive and destructive interference that occurs from using a coherent light source. This blurring of the speckle pattern is proportional to the velocity and under proper calibration can be used to back out velocity measurements through evaluation of the image in the frequency domain. We chose not to pursue this technique because it was thought that the motion artifact inherent to a contracting vessel would introduce to much noise into the system to be able to separate fluid motion from the speckle statistics. In addition to this, speckle is never really a good thing in imaging but rather something one would like to avoid. If we are able to take an image of the vessel itself, it would be much better than dealing with speckle. There has been one group that has published several papers measuring lymphatic flow dynamics through a cross correlation speckle technique [87-89]. The initial paper reported the ability to measure relative changes in lymphatic flow after the administration of a lymphotropic agent [88]. The other two papers present the same 15 sec sequence of data in which the speckle technique is used to measure lymphocyte velocity and then compared with a video microscopy technique [87, 89].

However the dynamic range of the measurement is much smaller than ours as no velocities were reported over 0.5 mm/sec. Whether this limitation is due to the measurement capabilities of the physical system or to the animal preparation itself remains unclear. The authors claim that they have the capabilities to measure velocities up to 10 mm/sec, so if this assertion is true then the data represented in the paper must be from a vessel preparation with fairly weak contractions. In their most recent paper, the authors used Ringer's solution in their preparation [55], which could cause the oncotic changes in the tissue and therefore inhibit lymphatic contractility. This is very likely the reason that the authors observed that only 50% of the lymphangions had phasic contractions (see Table 1 in [55]). It has also been demonstrated [17, 24, 25, 45] that rat mesenteric lymphatics exhibit much stronger contractile and pumping characteristics *in situ* as well in isolated vessels studies. Particularly Benoit et al. [24] reported that the amplitude of contractions of rat mesenteric lymphatics *in situ* was nearly two times higher than those reported by Galanzha et al. [55]. Moreover, the low lymph velocities observed by Fedosov et al. [87-89] very well could also be a result of the limitation of the speckle technique, as very large contractions would introduce more motion artifact and a fluctuating distance between the spot size and the random phase screen from which the flow is being measured.

2.5 Techniques in Nuclear Medicine

X-ray imaging has been a diagnostic imaging tool for over a century - used to image bone structure. More recently, radioactive imaging has been used to measure

flow by injecting particles such as technetium-99m-labelled polyclonal immunoglobulin and tracing them as they flow through the vessels [90]. The return signals are generally stronger than those using fluorescence and can therefore penetrate through thicker tissue, but are more invasive than fluorescent techniques since the injected particles can potentially be more harmful. The initial cost to set such a system up is also much more expensive than both fluorescent techniques and video microscopy. As in the fluorescent technique, you run the risk of the foreign particles you are introducing into the system interfering or altering the flow patterns that occur physiologically by creating some sort of unnatural edemous situation. Other groups use various approaches (e.g. functional MRI) with contrast agents to measure lymph flow [91, 92]. These methods have shown great potential for evaluating chronic lymph disorders due to edema, but suffer speed limitations which make video microscopy techniques better for measurements of temporal shear and flow profiles.

2.6 Materials and Methods

After evaluating the above mentioned techniques available for measuring biological fluid flow, it was decided that high speed video microscopy was the technique best suited for our application because of its ability to simultaneously measure vessel diameter and particle velocity. High frame rates have enabled us to extend the detection capabilities of the velocity measurements without having to reduce magnification and compromise the spatial resolution. Since we are able to use high magnifications, we can actually measure the radial location of a moving particle and thus take this into

consideration when developing a model for estimating wall shear stress. Therefore this technique met all of the minimum criteria needed to perform our given experiments. The main drawback of this method, as we soon came to realize, was the large amount of post-processing required to extract the relevant information from the images.

2.6.1 Hardware set-up and system specifications

Initially it was uncertain as to how fast the camera (Dalstar64K1M, 1M fps 245x245, CCD camera) needed to record images since it has capabilities up to 1 million frames per second. This ultra high speed is possible by masking a 1024 x 1024 imager so that only 1 in 17 frames are exposed at a time, resulting in a 245 x 245 pixel image. The 17 frames are captured by shifting exposed pixels into the masked area. Figure 2.1 below shows the layout of the 1024 x 1024 image with each of its sub frames labeled. After capturing and saving this large image, it can later be decoded into its 17 smaller images by following the pattern shown in Figure 2.1. In order to save the images at a rate fast enough to keep pace with the camera, the images were dumped into an allocated buffer of RAM (approximately 1 GB). Once the RAM was full, the recording had to be stopped so that the images could be stored onto the hard drive. The allocation of RAM available for this allowed us to capture 6528 total images before the buffer became full. A tradeoff exists between the speed of the camera and the length of continuous imaging that can be achieved. Using prior knowledge from previous studies of lymph wall contractions done by our group [17], it was determined that the image sequences needed to be at least 15 seconds to capture several contraction cycles.

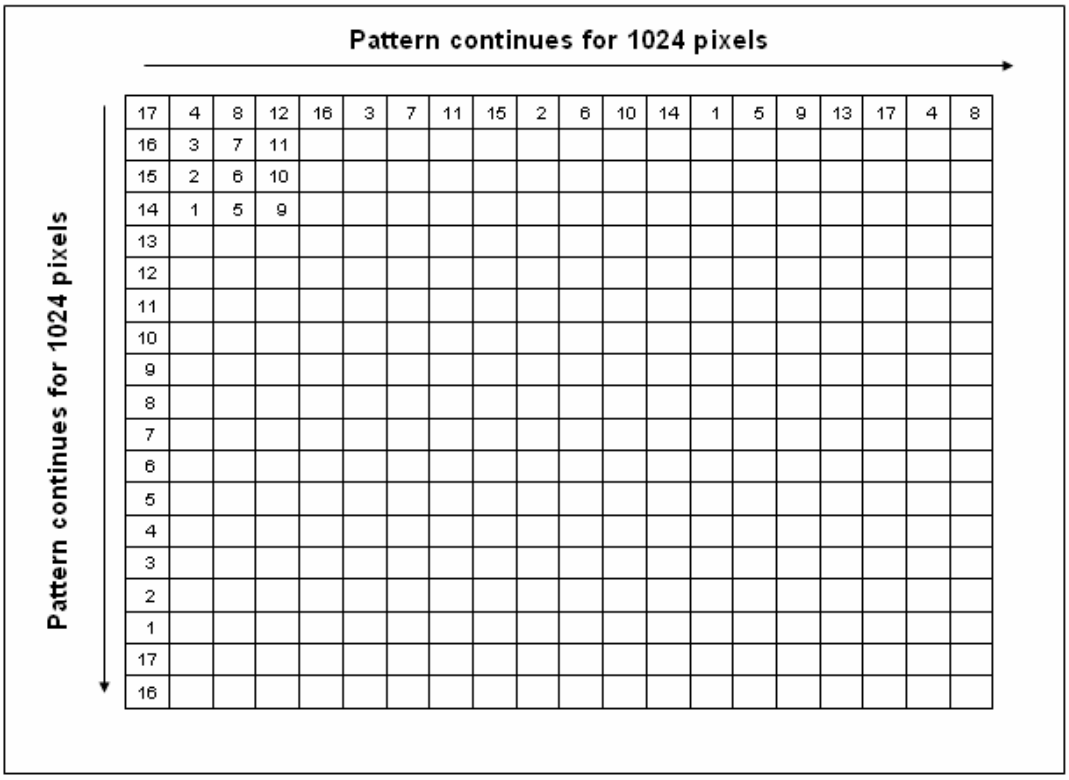

Figure 2.1: Layout of the 1024 x 1024 imager and masking patterns to achieve 17 image frames at high frame rates within one large image.

The camera speed was maximized while keeping the duration of the recording time to 30 seconds by saturating the 17th image in each image set. Within one set of 17 images, the first 16 images were captured with a 2 ms integration time per image (500 frames per second). The seventeenth image was saturated by increasing the integration time of the camera to 8 ms to extend the duration of the sequence given the limitation of RAM. This resulted in a total time of 62 ms between each set of images (16 * 2 ms + 8 ms + 22 ms memory transfer time). This allowed for the measurement of velocities, in

theory, of up to up to seventeen times faster than the capabilities of previous imaging systems used to measure lymph velocities while still maintaining the necessary dynamic range of 30 seconds to image several complete contraction cycles. These imaging parameters were set with a software interface available through Epix (XCAP-Std. V2.2, Buffalo Grove, IL). Lymphatic wall measurements were recorded at the beginning of every set of 17 images. This allowed us to measure wall contractions using a frame rate of 16 fps, a speed half of standard 30 fps cameras and sufficient to measure wall velocity throughout the phases of the contractile cycle.

2.6.2 Manual image analysis protocol

Each sequence of images had to be analyzed and processed to extract out the desired parameters: the velocity of the contractions in the lymphatic wall, the velocity of luminal lymphocytes, the diameter of the vessel, and the radial location of the lymphocytes with respect to the centerline. We used a three point method to measure the luminal diameter and provide a reference to calculate the distance of each lymphocyte from the center of the vessel (Figure 2.2). The diameter of the vessel wall (W) and distance from the centerline (D) are calculated using equations (1) and (2), given the variables as defined in Figure 2.2.

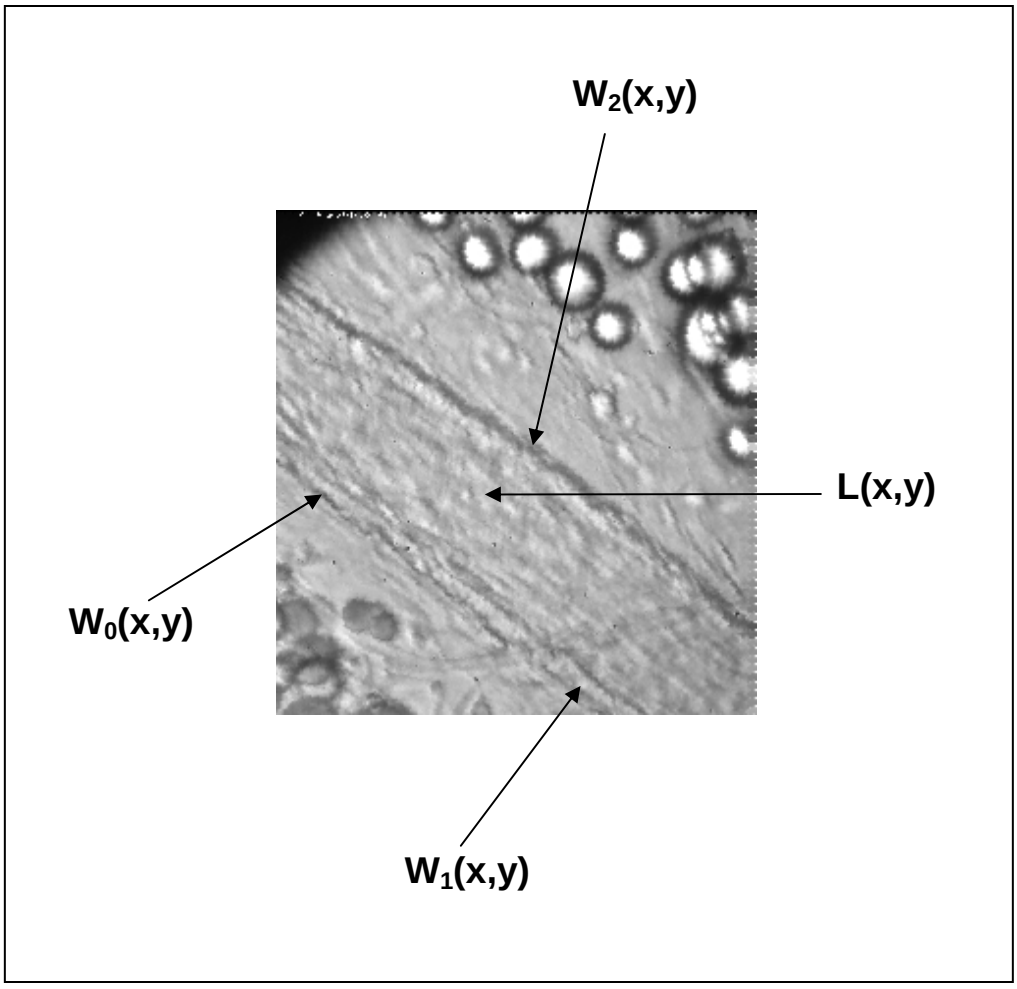

Figure 2.2: An image of a microlymphatic vessel with the measured wall coordinates (W_0, W_1, and W_2) and a lymphocyte at location (L(x,y)). The field of view is roughly 250 x 250 μm.

In the figure, W_0, W_1, W_2 are the three (x,y)-coordinates chosen along the wall of the vessel (Figure 2.2), while L is the (x,y)-coordinate of a given lymphocyte (Figure 2.2). Given this geometry, the vessel luminal diameter can be calculated as:

$$W = \sqrt{b^2 - (\frac{a^2 + b^2 - c^2}{2a})^2} \qquad (2.1)$$

in which,

$$a = \sqrt{(W_0(x) - W_1(x))^2 + (W_0(y) - W_1(y))^2}$$

$$b = \sqrt{(W_0(x) - W_2(x))^2 + (W_0(y) - W_2(y))^2}$$

$$c = \sqrt{(W_1(x) - W_2(x))^2 + (W_1(y) - W_2(y))^2}$$

Further, the distance of a given lymphocyte from the centerline can be calculated as:

$$D = \sqrt{b'^2 - (\frac{a^2 + b'^2 - c'^2}{2a})^2} - \frac{W}{2} \qquad (2.2)$$

in which,

$$b' = \sqrt{(W_0(x) - L(x))^2 + (W_0(y) - L(y))^2}$$

$$c' = \sqrt{(W_1(x) - L(x))^2 + (W_1(y) - L(y))^2} .$$

The velocities of the lymphocytes (V_L) were measured by tracking the coordinates of the lymphocyte over a sequence of images using the following equation:

$$V_L = \frac{\sqrt{(L_{t_0}(x) - L_{t_0+\Delta t}(x))^2 + (L_{t_0}(y) - L_{t_0+\Delta t}(y))^2}}{\Delta t} \qquad (2.3)$$

in which $L_{t_0}(x, y)$ is the position of some given lymphocyte at time t_0. The value, $L_{t_0+\Delta t}(x, y)$, is the position of the same lymphocyte at some time Δt past t_0, and Δt is the time interval between images.

The velocity of the wall contractions (V_W) were calculated by the following equation:

$$V_W = \frac{\sqrt{(W_{t_0} - W_{t_0+\Delta t})^2}}{\Delta t} \tag{2.4}$$

in which W_{t_0} is the diameter of the vessel at time t_0. Similarly, $W_{t_0+\Delta t}$ is the diameter of the vessel at some time Δt past t_0, and Δt is the time interval between images.

2.6.3 *In vitro* calibration

Calibration experiments were conducted in order to quantify the ability of the system to measure velocities at high frame rates using the capturing method described above. Two separate experiments were run: one to assess the sensitivity and accuracy of the velocity measurements, and another to determine the system's ability to estimate the velocity and radial position of particles moving through a tube of similar diameter to the microlymphatics. For the first set of experiments a wheel was used that rotated at various revolutions per minute and was positioned under the microscope for imaging. The wheel consisted of a motor-driven rotating disc with markings on it at a fixed radial distance as shown in Figure 2.3.

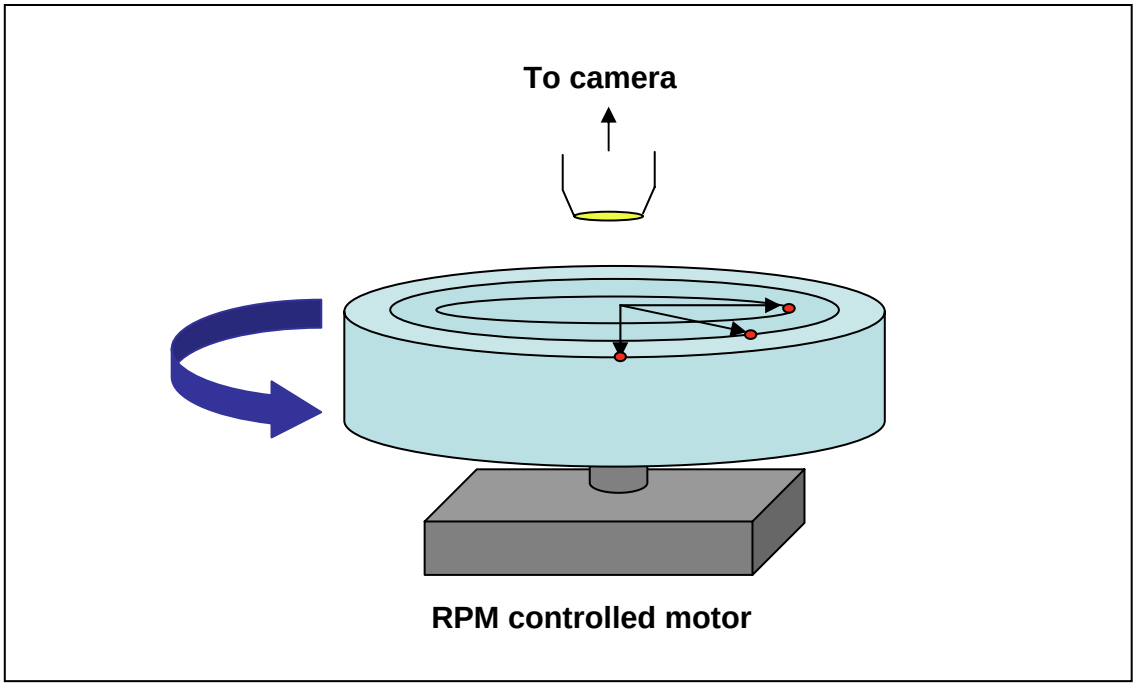

Figure 2.3: Illustration of motor driven rotating disk. Different motor speeds and radial markings correspond to various linear velocities.

Image sequences were recorded with the high-speed video camera (Dalstar64K1M, 1M fps 245x245, CCD camera) at a fixed radial distance (28.5 mm) on the wheel while varying the angular velocity so that a range of velocities could be measured that would be similar to those that were expected to occur physiologically (up to 15 mm/sec). Multiple measurements were taken while maintaining a constant speed in order to quantify the sensitivity of such measurements.

For the second set of experiments, we designed a physical model that simulated the sizes and arrangements of lymphocytes flowing through a microlymphatic using a suspension of microspheres that was passed through a glass capillary tube. A solution of sodium chloride was prepared that matched the specific gravity of the microspheres used

to simulate the white blood cells. The saline solution also served to dilute the 7.12 μm-diameter microspheres to a concentration of about $5 \cdot 10^5$ microspheres/ml approximating the size and count of lymphocytes. A glass capillary tube was heated and pulled out to a diameter of 140 μm, equivalent to the diastolic diameters of the lymphatic vessels we are studying. These values were chosen to mimic the dimensions that occur in the microlymphatics being measured in-situ as closely as possible. The fluid was passed through the tubing by applying a constant pressure with a level pressure head that could be moved up and down to control pressure. The outflow resistance was set to yield velocities that are similar to those measured *in situ* (Figure 2.4). The tubing was magnified using the same microscope optics used to record the lymphatic vessels. The images were recorded at a frame rate of 500 frames per second. Velocity measurements were made at fixed moments in time (25 ms) for a range of flow rates (15-250 μl/hr). The actual flow rate was measured by using a bubble tracking technique [93] and compared to the flow rates calculated from the images.

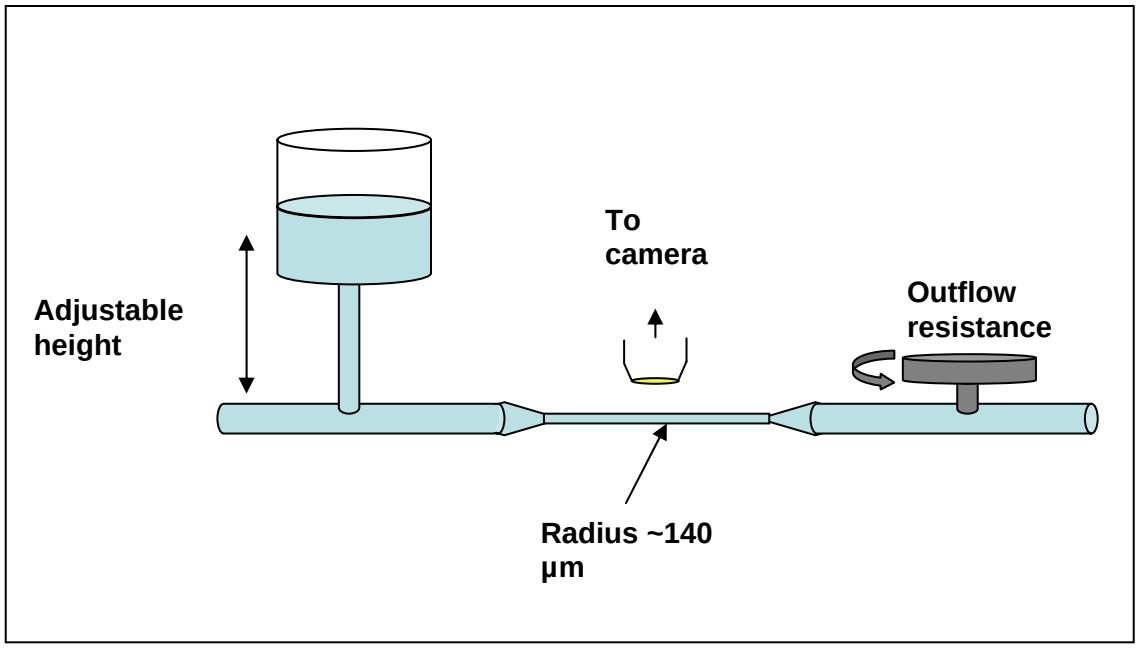

Figure 2.4: *In vitro* flow sham used to calibrate system. The pressure could be adjusted by changing the height of the water level. The outflow resistance was set to center the velocity values in a physiologically relevant range.

2.6.4 *In situ* animal protocol

Three male Sprague-Dawley rats weighing 180-220 grams were used for these initial experiments. The rats were housed in an environmentally-controlled, American Association for Accreditation of Laboratory Animal Care-approved vivarium. Each animal was fasted for 12-15 hours before the experiments, while water was available ad libitum. Each rat was anesthetized with an intramuscular injection of Fentanyl-Droperidol (0.3 ml/kg) and Diazepam (2.5 mg/kg). Supplemental doses of the anesthetic were given as needed. An abdominal incision was made to gain access to the mesenteric lymphatic vessels (Figure 2.5).

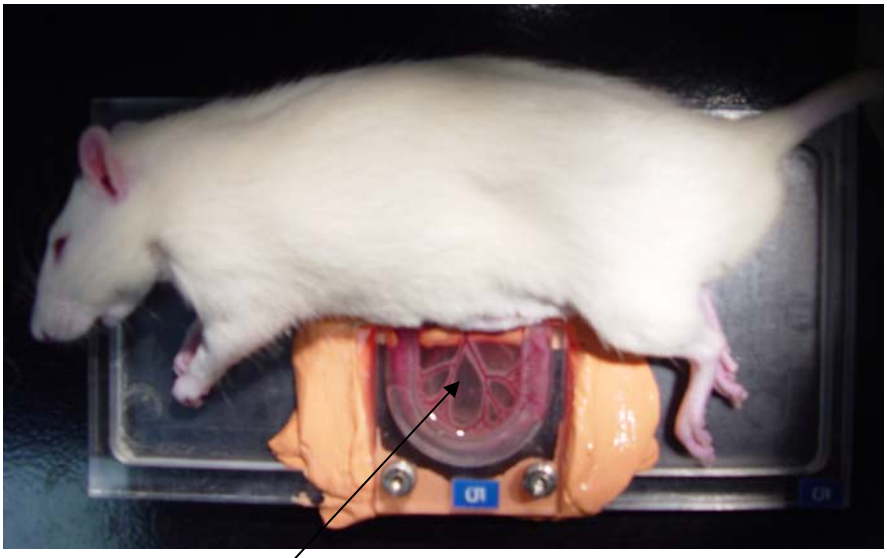

Figure 2.5: A loop of the small intestine pulled out to show the mesentery. Lymphatic vessels (too small to be visible in this picture) are dispersed throughout the mesentery.

A loop of the small intestine was exteriorized through the incision and gently positioned over a semicircular viewing pedestal on a Plexiglas preparation board capable of maintaining temperature and perfusing the vessel with a heated buffered solution (Figure 2.5). A lymphatic vessel was centered over an optical window in the preparation board. The exteriorized tissue was perfused with a phosphate buffered solution supplemented with HEPES (10mM) and 1% bovine serum albumin (Appendix II). The solution was pre-warmed to 38°C, and the pH adjusted to 7.4. The temperature of the exteriorized tissue and the animal's core were maintained at 36-38°C. The preparation board was placed on the stage of an intravital microscope (Zeiss), and the lymphatic

vessel was observed at a magnification of 100X-200X using an 80 mm projective lens, a 10X water immersion objective, and a variable magnification intermediate lens (Figure 2.6). The depth of field for this optic setup was approximately 14 μm. All the experiments were digitized with the high-speed video camera (Dalstar64K1M, 1M fps 245x245, CCD camera) using the capturing technique described previously.

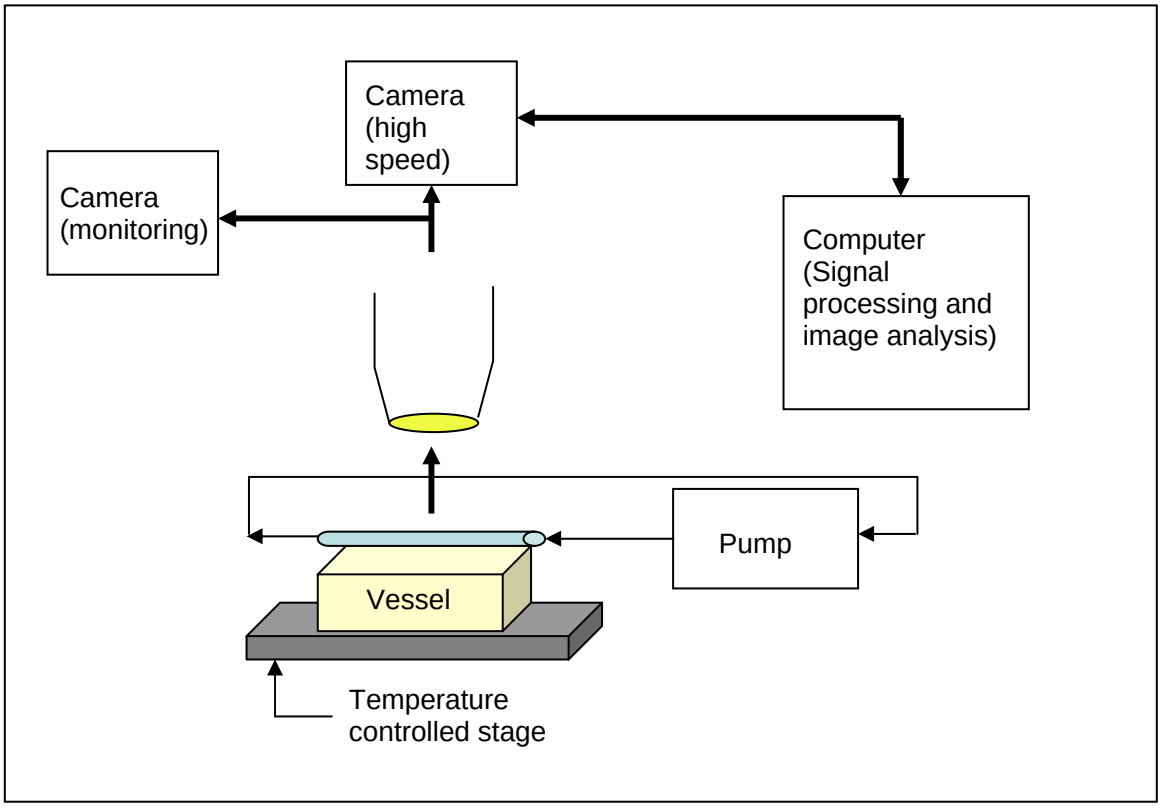

Figure 2.6: System set-up for the *in situ* preparation. The blue tube in figure passes APSS solution heated to 37° C.

After imaging and recording the specimen, the image sequences were loaded for

analysis in Epix, an image analysis software package, using the three point measuring method described in the Theory section. To record the wall measurements, a sequence of images were loaded through a program written in Matlab and three coordinates were selected with a cursor along the wall, as shown in Figure 2.2. This was done on sets of 51 images for the entire sequence of 6258 images. This ensured that the luminal diameter was being measure at the same location for the entire recording sequence. These coordinates were then imported into a program to make all of the necessary calculations. Lymphocytes were tracked manually by recording the location of the coordinates of the lymphocyte. An arbitrary lymphocyte within the field of view and depth of focus was chosen and that particle was tracked for 24 ms. Software was developed to import these coordinates and calculate the lymphocyte velocity, the distance of the particle from the centerline, and the volume flow rate (Appendix III).

2.7 Results and Discussion

Since there are currently no other developed methodologies for measuring flow in contracting mesenteric lymphatics, we had to verify that our system was working on known values of velocity. For the initial set of experiments we used a calibration wheel that was designed for calibrating a laser doppler system. This proved to work quite well however we wanted to test the frame rates and magnifications we intended to use so we needed to replicate the physical parameters we would encounter *in situ* as closely as we could *in vitro*. This led to the second set of calibration experiments. Once the system was verified to be working correctly and the correct imaging speeds were chosen, we

conducted our *in situ* experiments.

2.7.1 *In vitro* calibration

Calibration experiments were conducted to ensure the accuracy of the camera timing and our velocity estimation procedure. The calibration wheel was imaged at ten different velocities three times each and the velocities were calculated from the images and compared with the actual velocity of the wheel to test for system accuracy and sensitivity. Figure 2.7 shows the actual versus measured velocities for all measurements ($R^2 = 0.999$). The system showed accuracy, with less than 2% error when compared to actual velocities, and a sensitivity that yielded an average standard deviation of ~0.17 mm/sec for multiple measurements at a given velocity.

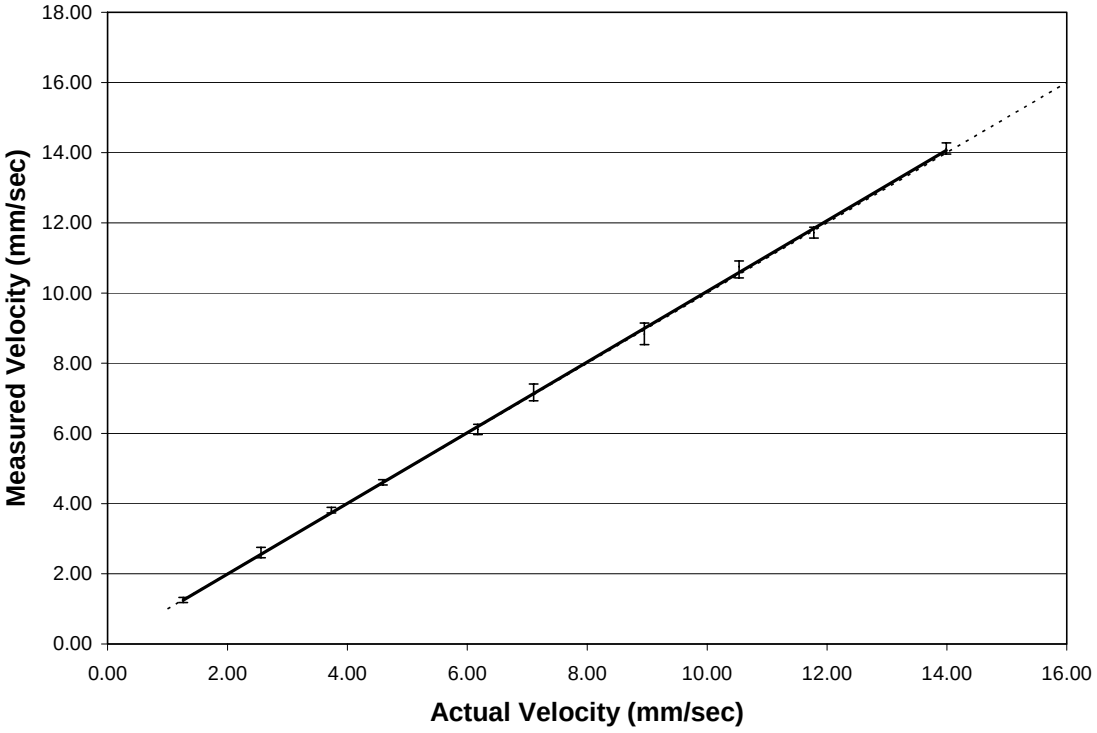

Figure 2.7: Actual vs. Measured velocities of *in vitro* calibration wheel with error bars.

For the second set of calibration experiments, images were recorded while flowing fluid and microspheres through a synthetic vessel. Velocities and the distance of the particles from the centerline were measured five different times throughout the sequence of flow for eight different flow rates. Figure 2.8 shows the actual vs. average predicted flow rates for each of the eight measurements along with error bars (R^2=0.999). Since the Reynolds number is very small (< 5), the volume flow rate could be calculated from the particle's velocity and position given by Equation 2.5, which is a derived from Navier-Stokes for laminar flow through a tube (Q = volume flow rate, $V_{\bar{r}}$ = velocity of particle measured at some distance $\bar{r}$ from the center, r = vessel radius).

$$Q = \frac{\pi V_{\bar{r}} r^4}{2(r^2 - \bar{r}^2)} \tag{2.5}$$

This approximation resulted in an average error of 5.7% with a maximum error of 10.6%. This is more than likely due to the depth of field covering more than just the center of the vessel, resulting in error in the distance from the centerline measurements. However, it was within acceptable limits to make reasonable estimations of in-situ flow rates.

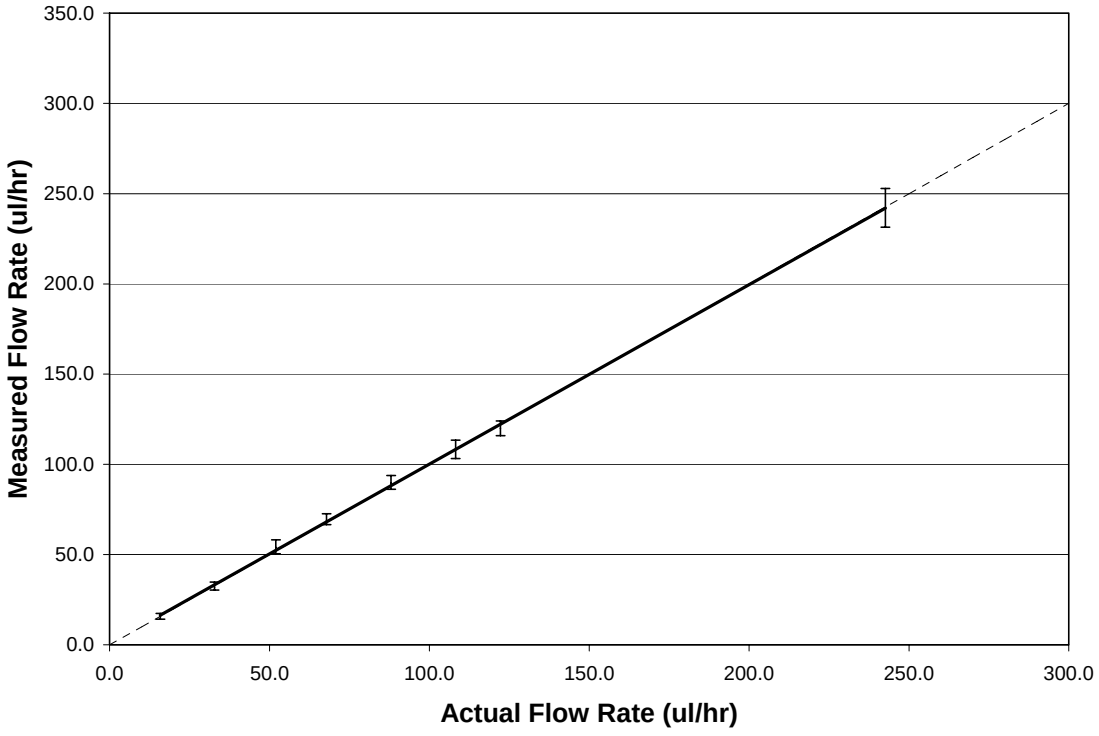

Figure 2.8: Actual vs. Measured volume flow rates of microspheres flowing through 140 μm glass tube.

2.7.2 In-situ experiments

Preliminary results for several contractions for three different rats have shown

the viability of this system to measure the velocity in the microlymphatic vessel of the rat while simultaneously recording the diameter of the vessel (Figures 2.9, 2.10, 2.11).

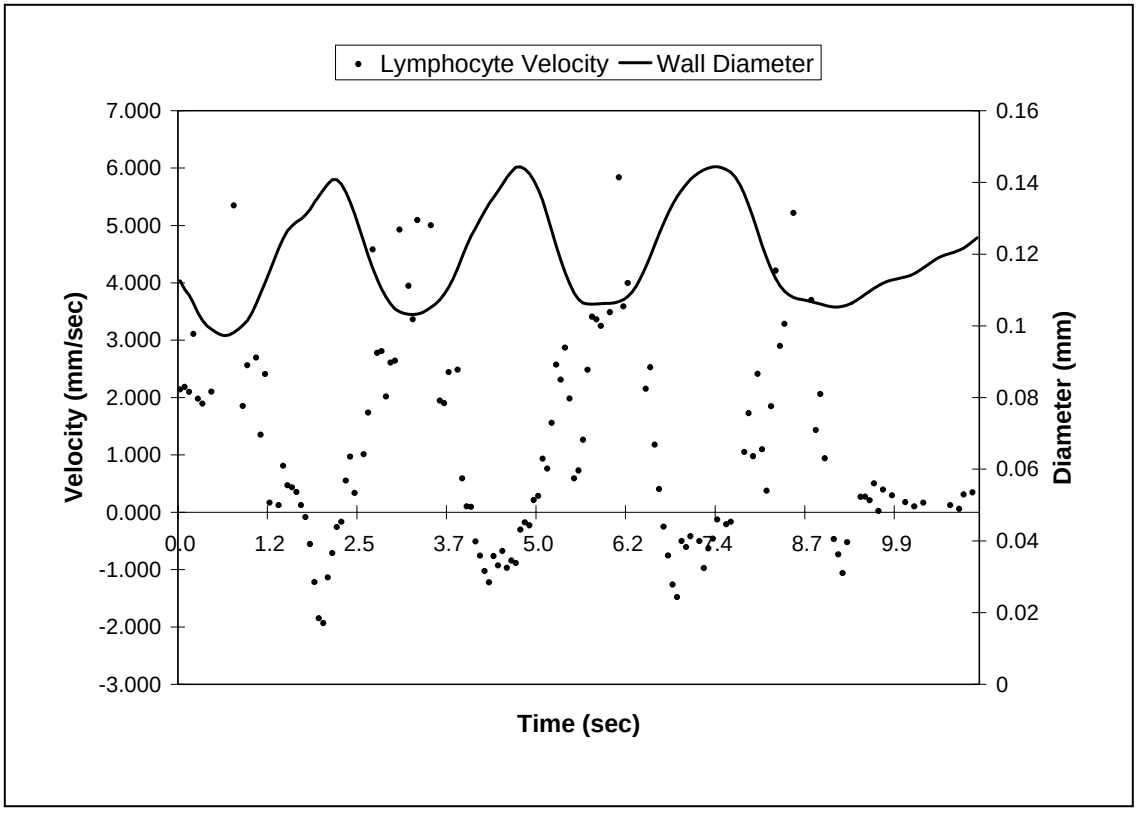

Figure 2.9: Vessel lumen diameter (mm) and lymphocyte velocity (mm/sec) for a 10 second interval from first data set.

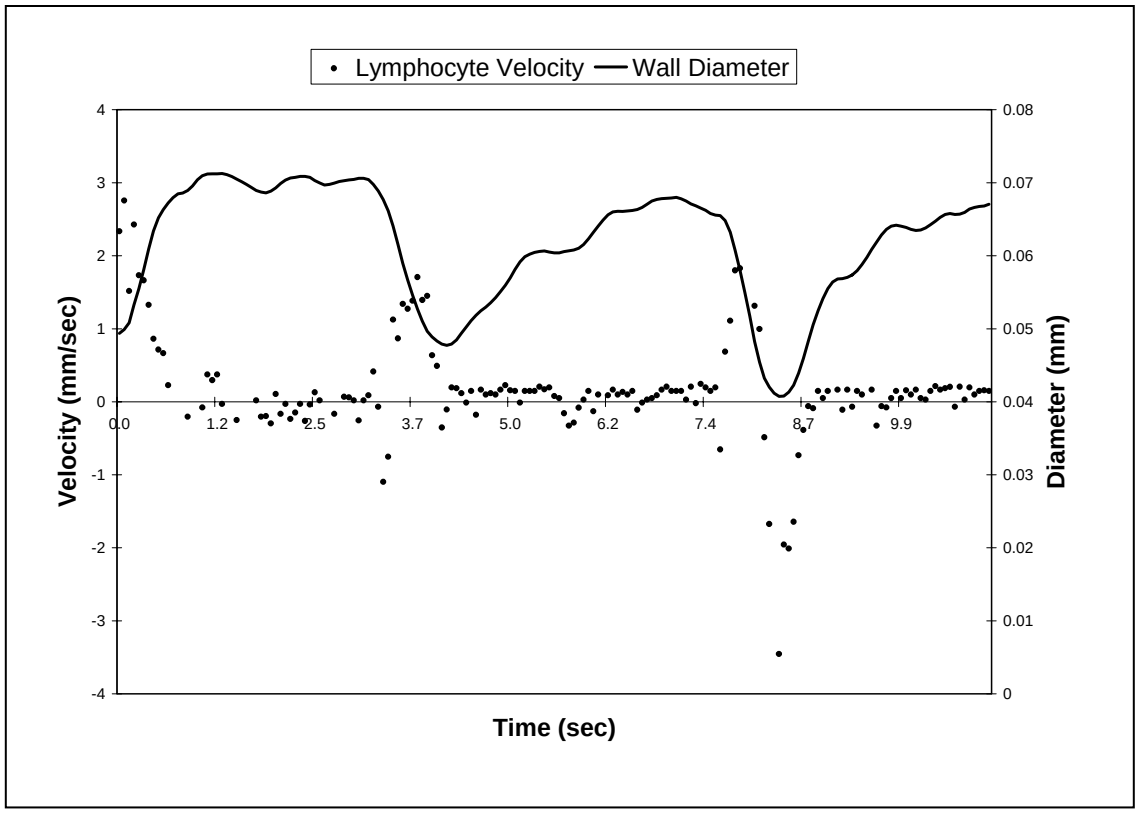

Figure 2.10: Vessel lumen diameter (mm) and lymphocyte velocity (mm/sec) for a 10 second interval from second data set.

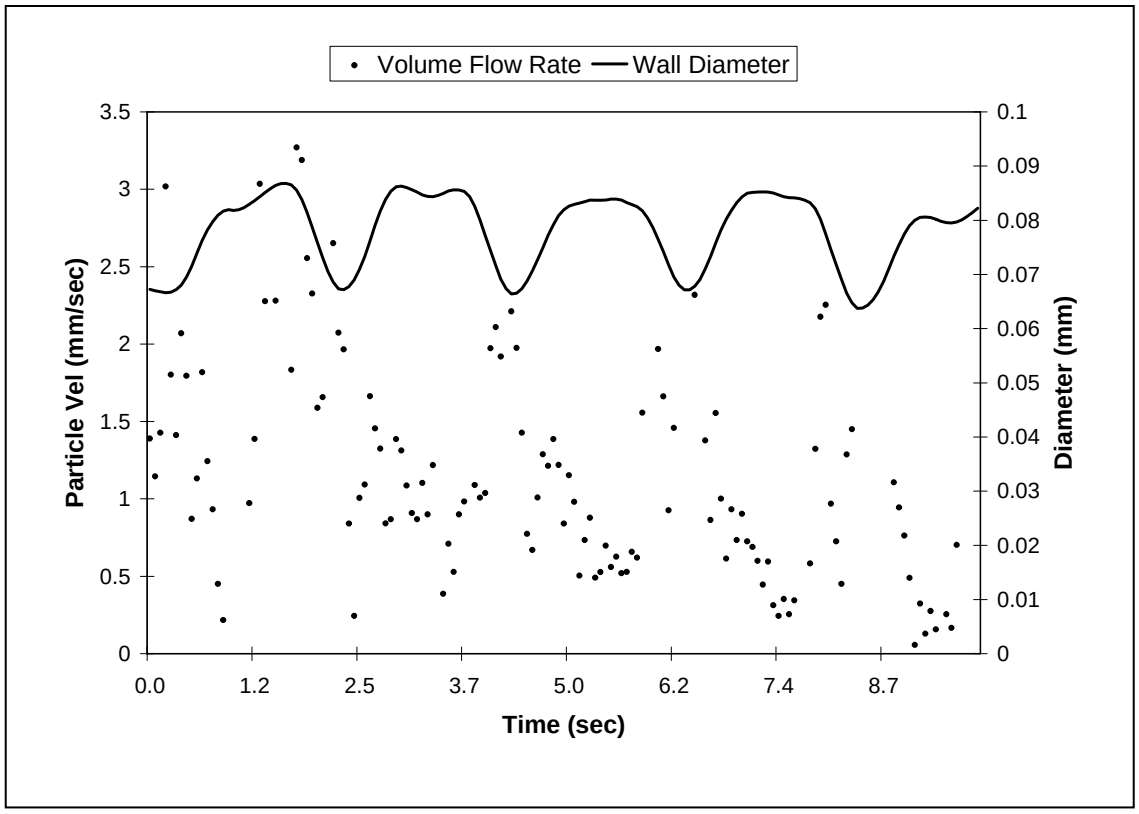

Figure 2.11: Vessel lumen diameter (mm) and lymphocyte velocity (mm/sec) for a 10 second interval from third data set.

Lymphocytes velocities ranged from -1 mm/sec to 7 mm/sec. As can be seen by the three figures, the pattern and dynamic range of the diameters and the contraction frequencies varied from rat to rat. Quantitative measurements of fluid velocities in the microlymphatics were recorded through the entire contraction cycle and fast video microscopy was used to measure velocities greater than 1 mm/sec for the first time. As expected the velocity of the lymph fluid fluctuates in a cyclical pattern at the same frequency as the wall contractions with about a 90 degree phase difference. The range of values measured for the lymphocyte velocities is much larger than previous systems

were capable of measuring using standard video microscopy. For example, the typical field of view when applying the necessary magnification to these vessels is 250 x 250 μm. In order to track a particle one must measure that particle's location at two different times. This means that the particle can travel no further than 125 μm to ensure that the particle is captured twice before it leaves the field of view. Therefore the maximum velocity a 30 frame per second camera could theoretically measure is 3.75 mm/sec (Velocity = distance/time = 125 μm/.033 s). This is under an ideal scenario in which one could resolve the 125 μm "streak" that would occur as a result of the moving particle when imaging at 30 fps (assuming that you are not electronically shuttering). This is illustrated by the images shown in Figures 2.12, 2.13, and 2.14. These images were taken during the peak velocity measurement at time t=6.08 sec from Figure 2.9, which is during a peak velocity measurement of 5.8 mm/sec (larger than the 3.75 mm/sec limit). As seen by comparing Figures 2.12 and 2.13, which occur 2 ms apart, both particles appear in the field of view. However, in Figure 2.14, taken 33 ms after Figure 2.12, neither lymphocyte is in the field of view. It should be noted that each image has been subtracted from the image immediately following it in order to remove the background and enhance objects in motion. Coordinates of the lymphocyte are also shown to illustrate the displacement of the lymphocyte from Figure 2.12 to Figure 2.13. In conclusion, a conventional 30 fps imaging system is too slow given the velocities that we have measured *in situ*.

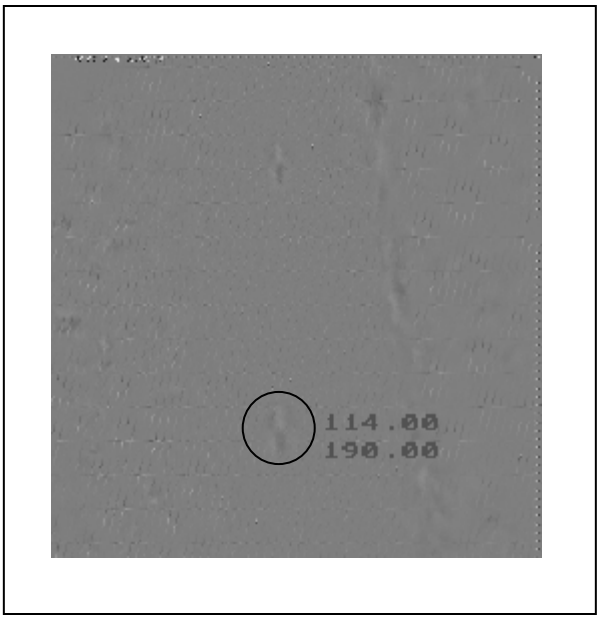

Figure 2.12: *In situ* image taken during 5.8 mm/sec fluid flow at time t = 0. The coordinates correspond to the lower lymphocyte.

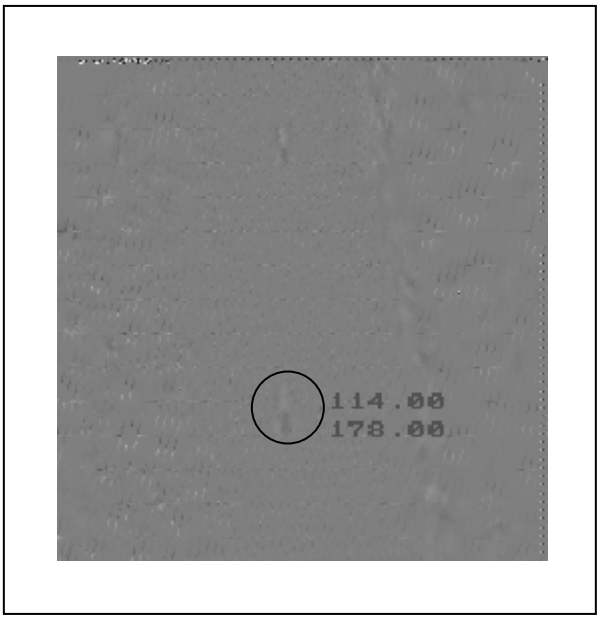

Figure 2.13: *In situ* image taken at time t = 2 ms after Figure 2.12. The lymphocyte has moved 12 pixels.

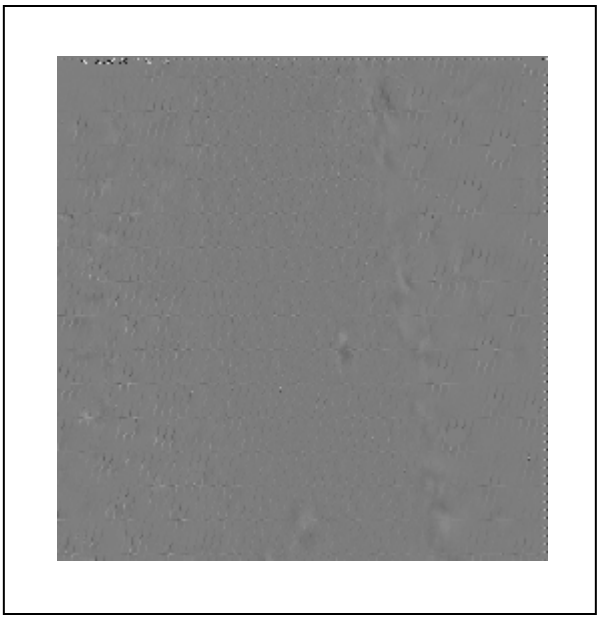

Figure 2.14: *In situ* image taken at time t = 33 ms after Figure 2.12. Neither of the original lymphocytes is present in the image, however new ones have appeared.

The maximum contractions observed in the microlymphatics of rats can be 60% of the vessel diameter, with average contractions being approximately 40-50% of the vessel diameter [17]. In this particular set of rats the contractions were about 40% of the maximum diameter. This would lead one to believe that in vessels with even larger contractions, the maximum velocities observed would be even greater than the 7 mm/sec observed in this case, further emphasizing the need for a fast imaging system. Figure 2.15, shows the estimated volume flow rate from the data sets shown in Figure 2.9. Similar plots can be generated from our measurements shown in Figures 2.10 and 2.11.

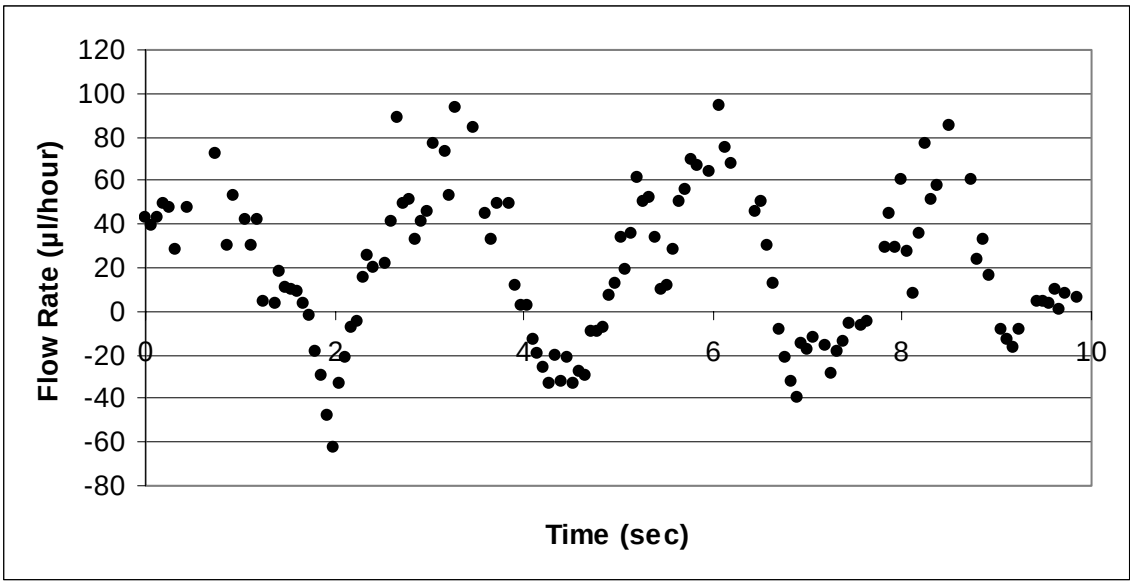

Figure 2.15: Estimation of volume flow rates (µl/hr) from velocity data in Figure 2.9.

Almost all applications of video microscopy systems for lymph flow have been captured with a standard video camera at a rate of 30 frames-per-second. This has proved acceptable for measurements in contraction speed and average lymph flow, as the velocities that occur in such cases are not beyond the speed of the camera (less than 1 mm/sec for microlymphatic flow given a magnification of around 100-200X). However, our group observed in initial experiments highly blurred particles during contractions that indicated that velocities of local flow during the phasic contractions are much higher than those that current video systems are capable of measuring. For example, a particle moving at 7 mm/sec, if imaged with a conventional video microscopy system, would in theory be a blurred streak of about 250 µm in length. The problem is that the contrast between white blood cells and the lymph media is so poor given the complex *in situ*

image that the length of this streak cannot be measured, or even seen is some cases, and the velocity cannot be deduced. Therefore, we pursued the use of a high-speed camera, using capture rates of up to five hundred frames-per-second, to measure these higher end velocities.

2.8 Concluding Remarks

There are currently a wide variety of imaging methods available for measuring lymph flow, each with their own advantages and disadvantages. With the recent developments in camera speed and the constant improvements in computer performance, some of the limitations that existed in the past for lymphatic imaging were shown to be removed in this set of data. The *in situ* data presented here corresponds to three segments of 10 seconds of continuous contractions in three different rats in order to show the feasibility of the system to accurately measure the higher end velocities that occur as well as to provide some verifiable data that such velocities exist. Through the unique image acquisition process presented in this chapter, adequate data was collected for the first time to measure fluid velocity throughout the entire contraction cycle while maximizing the hardware resources currently available for acquisition. Initial studies have shown velocities up to 7 mm/sec, which appear to occur immediately following the onset of vessel contraction. The post processing methods developed have been sufficient to measure the velocity, diameter, and distance of the lymphocyte from the centerline.

CHAPTER III

CHARACTERIZATION OF THE ACTIVE LYMPH PUMP IN RAT MESENTERIC LYMPHATICS

After developing a system, which was verified to have the necessary dynamic range and accuracy to measure lymphocyte velocities throughout the entire contraction sequence, we then sought to repeat the experiment on numerous animals to get a better representation of the ranges of values that might occur in mesenteric lymphatics under normal conditions. Subsequently, we sought to characterize flow and contraction response to edemous conditions.

3.1 Fluid Dynamics Theory

In order to estimate wall shear stress, a model was developed which would accurately reflect the fluid dynamics we were observing *in situ* and give us reasonable estimates of wall shear stress. To do this we started with Navier-Stokes equations for flow through a cylindrical tube:

$$\frac{1}{r}\frac{\delta}{\delta r}(rV_r) + \frac{\delta V_z}{\delta z} = 0 \tag{3.1a}$$

$$\rho\left(\frac{\delta V_r}{\delta t} + V_r\frac{\delta V_r}{\delta r} + V_z\frac{\delta V_r}{\delta z}\right) = \mu\left[\frac{\delta}{\delta r}\left(\frac{1}{r}\frac{\delta}{\delta r}(rV_r)\right) + \frac{\delta^2 V_r}{\delta z^2}\right] - \frac{\delta p}{\delta r} \tag{3.1b}$$

$$\rho\left(\frac{\delta V_z}{\delta t} + V_r\frac{\delta V_z}{\delta r} + V_z\frac{\delta V_z}{\delta z}\right) = \mu\left[\frac{1}{r}\frac{\delta}{\delta r}\left(r\frac{\delta V_z}{\delta r}\right) + \frac{\delta^2 V_z}{\delta z^2}\right] - \frac{\delta p}{\delta z} \tag{3.1c}$$

In choosing these equations as a starting point, we are already making some assumptions to simplify the problem. Namely, we are assuming axisymmetric flow of a Newtonian fluid through a cylindrical tube. This is reasonable since most lymphagion have a cylindrical geometry and the contraction of an individual lymphangion is not really peristaltic, but rather the entire segment contracts at roughly the same time [17]. This set of equations is still fairly difficult to solve. To reduce this system down, we started by introducing some terms that would allow us to non-dimensionalize this system and eliminate negligible terms:

$$V_a = \frac{1}{L}\int_0^L \max\left|\frac{\delta a(z,t)}{\delta t}\right| dz : \qquad \text{maximum wall velocity} \tag{3.2}$$

$$a_m = \frac{1}{LT_2}\int_0^{T_2}\int_0^L a(z,t)\,dz\,dt : \ \text{mean radius} \tag{3.3}$$

$V_p =$ average velocity that would result from steady $\frac{\delta p}{\delta z}$ at a_m

$L =$ distance between lymph valves

$$r^* = r/a_m \qquad z^* = z/L \qquad t^* = \omega_2 t \qquad V_r^* = V_r/V_a \qquad V_z^* = V_z/V_p \qquad p^* = p/P_m$$

Each of these terms is a parameter that we can actually measure from our imaging system and get a range of values that occur physiologically. After making these substitutions into the Navier-Stokes equations, we reduced the equations and dropped the star notation for convenience, yielding:

$$\frac{1}{r}\frac{\delta}{\delta r}(rV_r) + \frac{a_m}{L}\frac{V_p}{V_a}\frac{\delta V_z}{\delta z} = 0 \tag{3.4a}$$

$$\begin{aligned}&(\frac{\omega_2 a_m}{V_a}\frac{\delta V_r}{\delta t} + V_r\frac{\delta V_r}{\delta r} + \frac{V_p}{V_a}\frac{a_m}{L}V_z\frac{\delta V_r}{\delta z}) = \\ &\frac{\mu}{\rho V_a a_m}[\frac{\delta}{\delta r}(\frac{1}{r}\frac{\delta}{\delta r}(rV_r)) + \frac{{a_m}^2}{L^2}\frac{\delta^2 V_r}{\delta z^2}] - \frac{P_m}{\rho {V_a}^2}\frac{\delta p}{\delta r}\end{aligned} \tag{3.4b}$$

$$\begin{aligned}&(\frac{\omega_2 a_m}{V_p}\frac{\delta V_z}{\delta t} + \frac{V_a}{V_p}V_r\frac{\delta V_z}{\delta r} + \frac{a_m}{L}V_z\frac{\delta V_z}{\delta z}) = \\ &\frac{\mu}{\rho V_p a_m}[\frac{1}{r}\frac{\delta}{\delta r}(r\frac{\delta V_z}{\delta r}) + \frac{{a_m}^2}{L^2}\frac{\delta^2 V_z}{\delta z^2}] - \frac{a_m}{L}\frac{P_m}{\rho {V_p}^2}\frac{\delta p}{\delta z}\end{aligned} \tag{3.4c}$$

From these equations it can be seen that essentially we have a term similar to the Reynolds number ($\frac{\mu}{\rho V_p a_m}$) and a Strouhal number ($\frac{\omega_2 a_m}{V_p}$) which commonly occur in problems in fluid dynamics. We measured each of these parameters with our imaging system and can report the reasonable ranges of each that occur *in vivo* (Table 3.1).

We know that $\frac{{a_m}^2}{L^2} << 1$ and $\frac{a_m}{L} << 1$ since the distance between valves is much larger than the vessel radius, so we have

$$\frac{1}{r}\frac{\delta}{\delta r}(rV_r) + \frac{a_m}{L}\frac{V_p}{V_a}\frac{\delta V_z}{\delta z} = 0 \tag{3.5a}$$

$$\left(\frac{\omega_2 a_m}{V_a}\frac{\delta V_r}{\delta t} + V_r\frac{\delta V_r}{\delta r} + \frac{V_p}{V_a}\frac{a_m}{L}V_z\frac{\delta V_r}{\delta z}\right) = \frac{\mu}{\rho V_a a_m}\left[\frac{\delta}{\delta r}\left(\frac{1}{r}\frac{\delta}{\delta r}(rV_r)\right)\right] - \frac{P_m}{\rho {V_a}^2}\frac{\delta p}{\delta r} \tag{3.5b}$$

$$\left(\frac{\omega_2 a_m}{V_p}\frac{\delta V_z}{\delta t} + \frac{V_a}{V_p}V_r\frac{\delta V_z}{\delta r}\right) = \frac{\mu}{\rho V_p a_m}\left[\frac{1}{r}\frac{\delta}{\delta r}\left(r\frac{\delta V_z}{\delta r}\right)\right] - \frac{a_m}{L}\frac{P_m}{\rho {V_p}^2}\frac{\delta p}{\delta z} \tag{3.5c}$$

Table 3.1: Ranges of coefficient values that appear in the non-dimensionalized Navier-Stokes equations 3.4(a-c) along with their average values. All values were measured from the entire data set of seven rats.

$0.035 < \frac{a_m}{L} < 0.1$	Average = 0.047
$0 < \frac{V_a}{V_p} < \infty$	Average = 0.033
$0.014 < \frac{\omega_2 a_m}{V_a} < \infty$	Average = 0.37
$0.00035 < \frac{\omega_2 a_m}{V_p} < \infty$	Average = 0.012
$75 < \frac{\mu}{\rho V_a a_m} < \infty$	Average = 1050
$2.08 < \frac{\mu}{\rho V_p a_m} < \infty$	Average = 40

In Eq (3.5b), if we compare the terms $\frac{\mu}{\rho V_a a_m}$, $\frac{V_p}{V_a}\frac{a_m}{L}$, and $\frac{\omega_2 a_m}{V_a}$, the Reynolds term is almost always going to be much larger than the other two terms, so the Reynolds term

will dominate. In Eq (3.5c), if we compare the terms $\frac{\mu}{\rho V_p a_m}$, $\frac{V_a}{V_p}$, and $\frac{\omega_2 a_m}{V_p}$, the Reynolds term is almost always going to be much larger than the other two, so the Reynolds term will again dominate. This leaves us with:

$$\frac{1}{r}\frac{\delta}{\delta r}(rV_r) + \frac{a_m}{L}\frac{V_p}{V_a}\frac{\delta V_z}{\delta z} = 0 \tag{3.6a}$$

$$V_r \frac{\delta V_r}{\delta r} = \frac{\mu}{\rho V_a a_m}[\frac{\delta}{\delta r}(\frac{1}{r}\frac{\delta}{\delta r}(rV_r))] - \frac{P_m}{\rho {V_a}^2}\frac{\delta p}{\delta r} \tag{3.6b}$$

$$0 = \frac{\mu}{\rho V_p a_m}[\frac{1}{r}\frac{\delta}{\delta r}(r\frac{\delta V_z}{\delta r})] - \frac{a_m}{L}\frac{P_m}{\rho {V_p}^2}\frac{\delta p}{\delta z} \tag{3.6c}$$

The final assumption that can be made is that for most of the contraction cycle the velocity of fluid is much greater than the velocity of the vessel wall. This allows us to ignore the terms with $\frac{V_a}{V_p}$, thus removing equations 3.6a and 3.6b from the system and leaving us with Eq. 3.6c from which, though integration and application of the no slip boundary condition, we derive Poiseuille flow:

$$v(r') = \frac{-1}{4\rho\nu}\frac{dp}{dz}(r^2 - r'^2) \tag{3.7}$$

This simplification allows us to estimate wall shear stress from the parameters measured through our video microscopy system described in the methods section as the following:

$$\tau = \frac{4\rho\nu\bar{V}}{r} \tag{3.8}$$

where,

τ = wall shear stress

ρ = fluid density

ν = kinematic viscosity

$\overline{V}$ = spatially averaged velocity

r = radius of the wall

3.2 Materials and Methods

We used the same *in-situ* preparation described previously in Section 2.6.4. This procedure was conducted on a total of 10 animals. For each animal we recorded 6 sequences of lymphatic contractile activity for 30 seconds. Images were recorded using the high speed camera with the same hardware configuration and manual image analysis methods as described in Section 2.6.1 and Section 2.6.2 respectively. Since it is necessary to have lymphocytes present in the vessel being imaged, some animal experiments did not prove to be useful for our analysis due to the rarity of lymphocytes that occurred. Our final data set, which we used to characterize the flow response to lymphatic contraction, consisted of seven different rats.

3.2.1 Volume loading protocol

We adapted a technique previously described by Benoit [24] to increase lymph flow. The same anesthesia protocol described earlier was used to prepare the animal for surgery. A tracheotomy was performed to facilitate respiration and the right femoral artery was cannulated for monitoring arterial pressure. Experiments were terminated if the mean arterial pressure fell below 85 mmHg. The right femoral vein was also

cannulated for intravenous fluid administration. The same procedure for exposing the mesenteric lymphatics as described in Section 2.6.4 was used. Lymph formation was increased by infusing saline at a rate of 0.2 ml/min/(100 g body wt), a value of plasma dilution that has been used by other investigators to increase lymph flow [94]. One minute sequences of images were taken for three different time periods using a high speed camera: a control before saline infusion, 5 minutes after infusion, and 10 minutes after infusion. The integration time of the camera was set to 5 ms for the first 16 frames and 40 ms for the 17^{th} frame. This allowed us to extend the continuous recording time to 1 minute. Lymphatic contractility was measured using the correlation algorithm described in detail in Section 4.1.2. Lymph velocity was tracked using the manual analysis method described in Section 2.6.2.

3.3 Results and Discussion

In order to assess the effects of lymphatic contraction on lymph flow and velocity, we measured the wall contractions while simultaneously recording the fluid velocity for several contraction cycles. The data was taken from 7 different rats, 15 different vessels, and corresponds to over 125 systolic contractions occurring collectively over a period of approximately 16 minutes. The mean diameter of the lymphatics measured in this study was 91 ± 9.0 μm. The average lymph flow measured in these vessels was 13.95 ± 5.27 μl/hr with a mean velocity of 0.87 ± 0.18 mm/s. This resulted in an average wall shear stress of 0.64 ± 0.14 dynes/cm^2, where 1 Pascal = 10 dynes/cm^2.

3.3.1 Relationship between contractile sequence and fluid velocity

The pattern of lymphatic diameter and lymph flow was somewhat variable, presumably depending on the characteristics of the lymphatic contraction pattern (i.e. the direction of contraction propagation, the local versus distant contraction strength, the presence of multiple nearby pacemakers, etc.) A typical relationship between vessel contraction and the velocity pattern of the fluid in the vessel is shown in Figure 3.1. While the frequency, magnitude, and periodicity of the contraction cycle varies in the vessels, the relationship between the lymph velocity and vessel contraction remains similar.

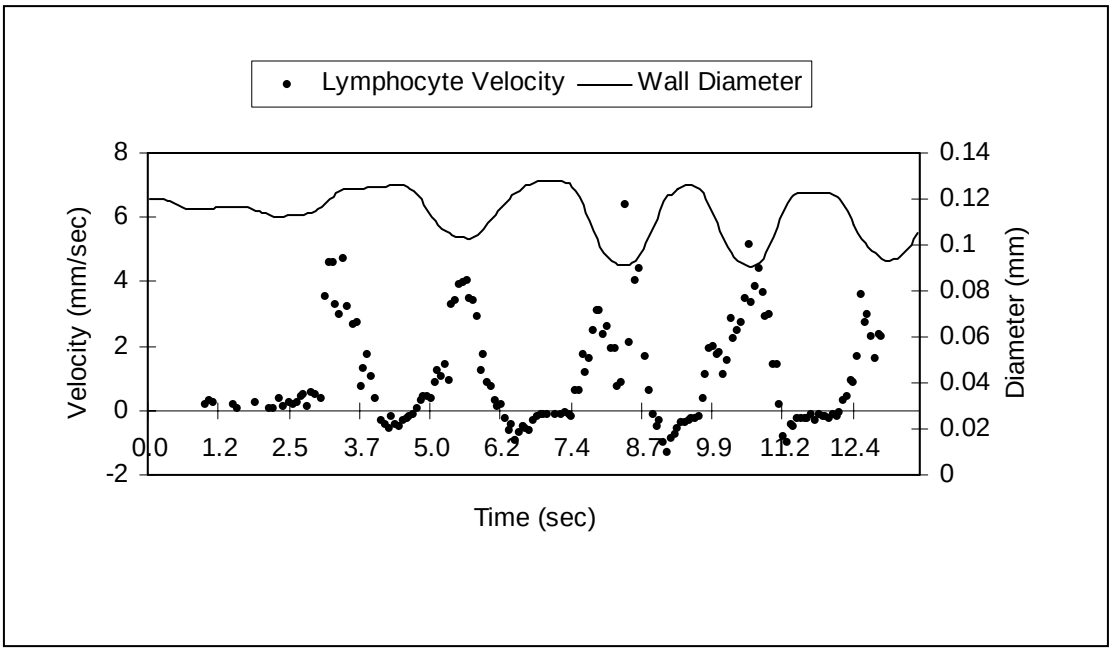

Figure 3.1: Typical relationship between fluid velocity (mm/sec) and wall diameter (mm) of a mesenteric lymphatic vessel for several contraction cycles.

The maximum orthograde lymph velocity typically occurs near or during the systolic peak of the contraction cycle while the maximum retrograde velocity occurs during the diastolic phase. In order to obtain a more thorough analysis of this relationship, we calculated the time interval between the orthograde velocity peaks and the systolic diameter peaks (minimum) shown as T_0 in Figure 3.2.

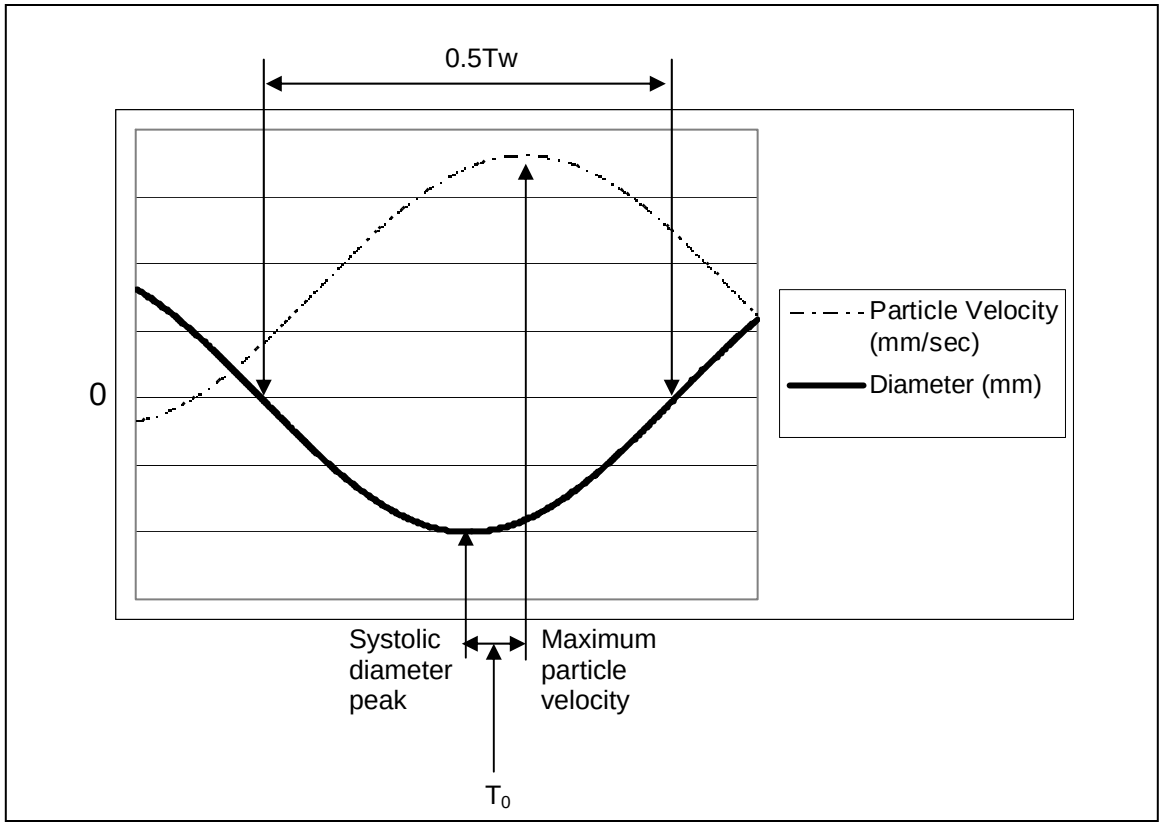

Figure 3.2: Figure showing how the parameters T_0 and T_w were calculated. The '---' represents the velocity pattern of tracked lymphocytes and the solid line represents a diameter tracing. T_0 is essentially a measure of phase difference while T_w is the period of the contraction cycle.

We then normalized this to the period of the contraction cycle (the distance between systolic peaks, T_w. The sign convention we used was negative T_0 when the orthograde velocity peak occurred before the systolic diameter peak and positive when it occured after. We performed the same comparison with the maximum retrograde velocity peaks and the diastolic diameter peaks. The maximum orthograde velocity peaks occurred $0.082T_w \pm 0.029T_w$ after the systolic diameter minimum. The maximum retrograde velocity peaks occurred $-0.115T_w \pm 0.023T_w$ before the diastolic diameter maximum. From this analysis we can see that there is a slight phase delay in the response of the fluid flow to the contraction cycle. Often the contractions are not quite as periodic as those shown in Figure 3.1. When this occurs the correlation between the fluctuations in fluid velocity and the local contraction are not as well defined (Figure 3.3).

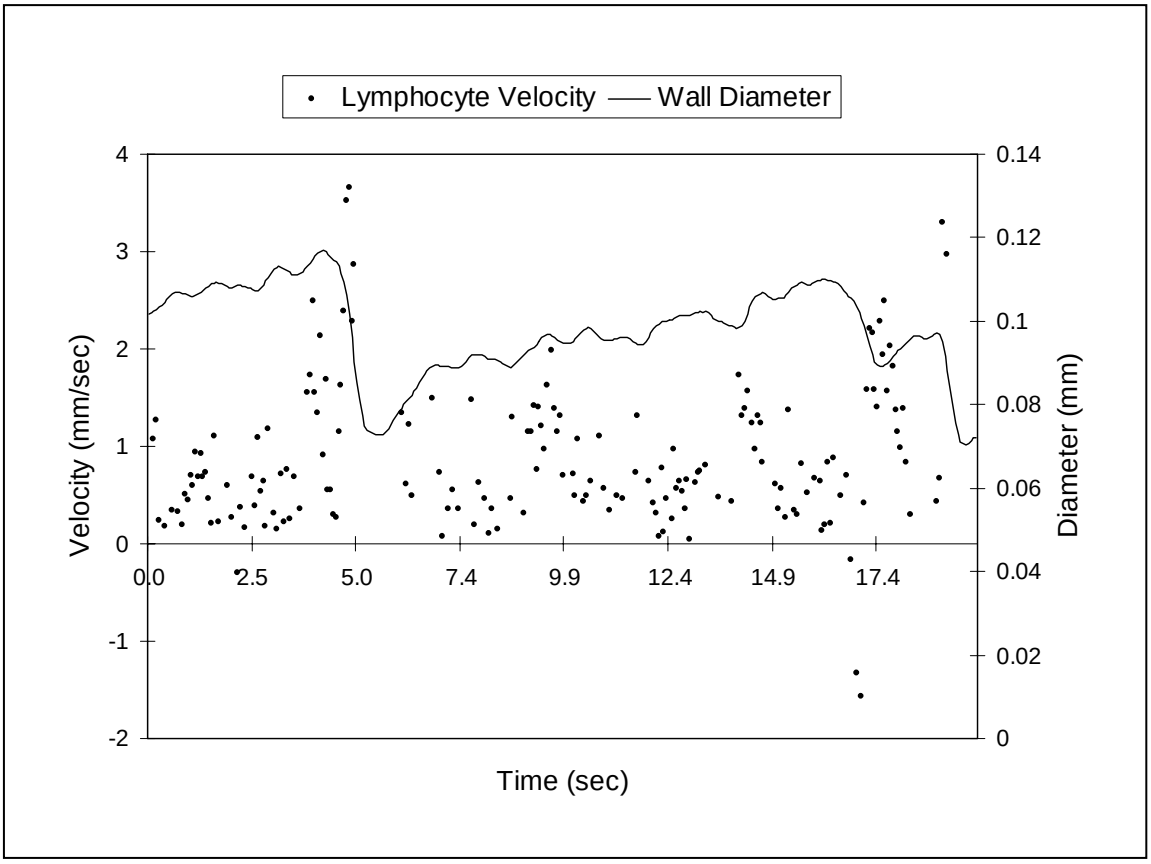

Figure 3.3: Example of a contraction sequence that is irregular and contains periods of little to no contractile activity.

Common patterns were seen throughout the sample set when comparing fluid velocity with vessel contraction. While the frequency and amplitude of contractions in mesenteric lymphatics is quite variable, the relationship between contraction and fluid velocity remains fairly consistent. This can be seen through a comparison of Figure 3.1 to Figure 3.3. The vessel in Figure 3.1 has a consistent cyclical pattern of contraction with a frequency of 0.4 cycles/sec, while the vessel in Figure 3.3 has a more complicated diameter behavior, with contractions of different strengths occurring over a 20 second interval. However, it should be noted that whenever a strong contraction at the site of

observation occurs in Figure 3.3 (t = 4 sec, 17 sec, and 19 sec), that a definite peak in velocity occurs as well. During the interval when there are no strong contractions (between t = 7 sec and 16 sec) one can still see fluctuations in the fluid velocity. These fluctuations are most likely due to the contractive or compressive effects of adjacent lymphangions (both upstream and downstream of the imaging site).

In general, a reversal of flow occurs during a brief portion of diastole (Figure 3.1). Presumably this flow reversal corresponds to the valve closure up-stream. As fluid flows in the reverse direction it pushes the valves shut, thus limiting the amount of fluid that flows back into the previous lymphangion and promoting a net effect of forward flow. The velocity of this reversal usually peaks out at approximately -1 mm/sec, although there were one or two vessels that had peak retrograde velocities as high as -3 mm/sec.

To characterize the relationship between volume and velocity we normalized several contractions from different rats and plotted volume versus velocity over one contraction (Figure 3.4). Point A corresponds to the maximum vessel diameter. Borrowing the terminology first used in describing cardiac function, this point corresponds to the very end of diastole and the beginning of systole. If this trace is followed up to point B, it can be seen that as the vessel volume decreases, the fluid velocity increases. Point B is the minimum vessel diameter or the systolic peak. The rapid increase in velocity before and after point B might be due to the expansion of a downstream lymphangion, since these contractions have been previously shown to propagate [17]. However, we cannot be certain of this since we did not have a large

enough field of view to monitor adjacent lymphangion in these studies. The point of maximum velocity, point C, occurs after the systolic peak at a slightly larger vessel volume. This agrees with the slight phase delay we reported above and is visible in Figure 3.1 as well. The velocity begins to decrease as the vessel expands until it reaches its minimum at point D. The velocity here is actually in the reverse direction, which we have termed the maximum retrograde velocity. The most interesting portion of this figure is the interval from point D back to point A. The velocity of the fluid actually increases back to zero as the vessel continues to expand. This provides additional support to the theory that the reverse velocity helps to close the valves and prevent any further back flow into the downstream lymphangion. At point A, the diastolic expansion ends and the cycle starts all over again.

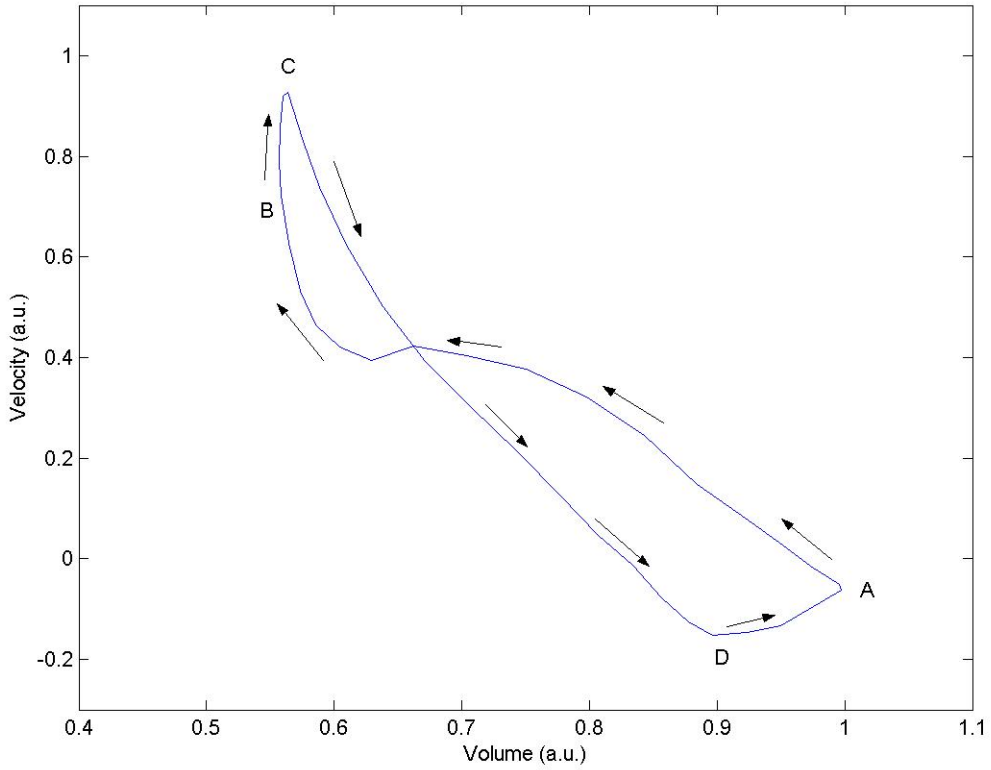

Figure 3.4: The relationship between normalized vessel volume and normalized fluid velocity. Labeled points correspond to: A) Peak diastolic diameter and beginning of systolic contraction, B) Systolic diameter, C) Peak orthograde velocity, D) Peak retrograde velocity.

It should be acknowledged that this figure was created from averaging four different contraction sequences. The selection of data was limited to segments where the contraction frequency was fairly constant. All units have been normalized due to the variations in size and average velocity from rat to rat.

3.3.2 Wall shear stress and volume flow rate estimates

Within our data set for a given moment in time, we measured the velocity of an arbitrary lymphocyte in the vessel, the distance of that cell from the vessel's centerline, and the vessel diameter. Using these parameters and our model of Pouiselle flow, we estimated the volume flow rate and wall shear stress throughout every contraction cycle. The calculations for the sequence represented in Figure 3.1 are shown in Figures 3.5 and Figure 3.6. The volume flow rate and wall shear stress plots look very similar to the velocity tracings due to the fact that all three terms are directly proportional to one another. For this particular contraction cycle, one can see that the volume flow rate reaches a value around 220 μl/hr during the peak of systole and averages 20 μl/hr. The peak wall shear stress approaches 9 dynes/cm^2, while the average wall shear stress is 0.82 dynes/cm^2

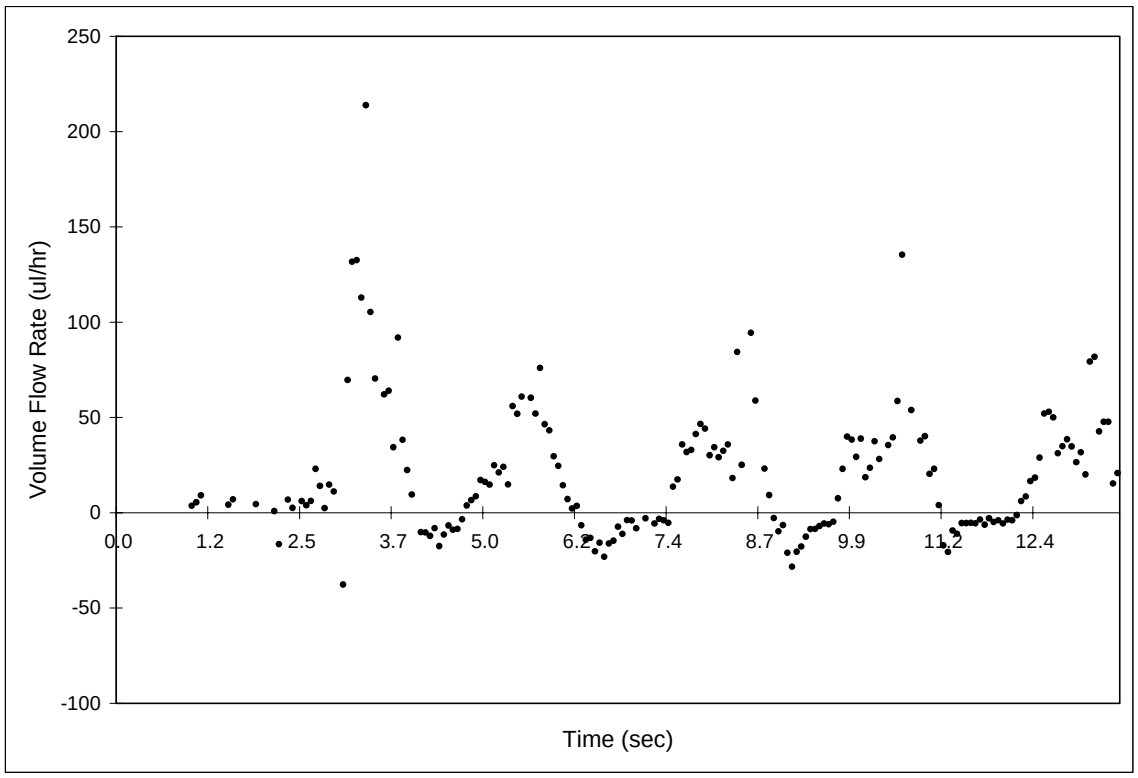

Figure 3.5: Estimation of the volume flow rate (µl/hr) for the same data set represented in Figure 3.1.

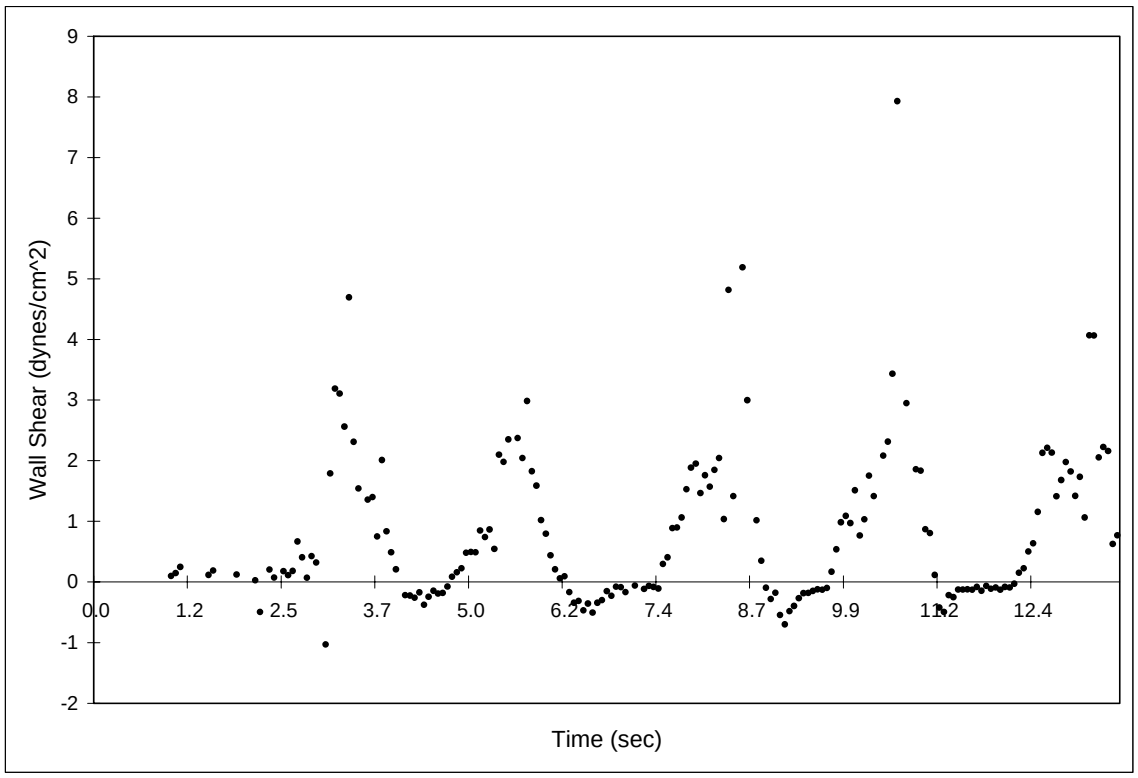

Figure 3.6: Estimation of wall shear stress (dynes/cm^2) for the same data set represented in Figure 3.1.

We also calculated volume flow rates under the assumption that no retrograde flow occurs, only taking into account the displacement of fluid due to volume changes in the vessel. To calculate this parameter we integrated the volume changes in the vessel during systole and assumed no fluid was pulled back into the vessel during diastole. We refer to this parameter as the ejection flow rate. For the data set referenced above the ejection flow rate was 34 μl/hr. From the lymphocyte velocities, we calculated the percentage of flow that was in the forward direction (% orthograde) compared to the backwards direction (% retrograde) by integrating the velocity fluctuations. For the data sequence in Figure 3.1, the percentages were 92% and 8% respectively.

It is known that in addition to pressure, lymph flow, by means of wall shear stress, plays an important role in the coordination of wall contractions and lymph propagation. This theory is supported by the study of the inhibition of the lymph pump due to flow under constant transmural pressure which was described earlier [25]. An important question that has arisen from this work is whether or not the velocities experimentally induced in the isolated vessels are physiologically relevant. If one were able to report these velocities, and more importantly approximate the shear stresses that occur *in vivo*, it would not only validate these conclusions, but it would also open the door for future work in flow-induced endothelial release of vasoactive substrates in lymphatic vessels, which could potentially play an important role in both the regulation and the development of the microlymphatic network.

Our justification of Poiseuille flow through careful analysis of the Navier-Stokes equations proved to be quite useful, since the system we developed had the capability to measure all of the necessary parameters needed in the model (namely vessel diameter, lymphocyte velocity, and lymphocyte position from the vessel centerline). However, we first needed to verify that such a model was a reasonable approximation for flow in contracting microlymphatics. By deriving non-dimensional Navier-Stokes equations for axi-symmetric flow though a cylindrical tube, as shown in section 3.1, we introduced coefficients into the system of equations whose range of values could be measured from the data set (Table 3.1). This allows us to know when the model is reasonable and under what periods of the contraction cycle it could break down. The main limitation of the final simplification is that the estimate is only reasonable for periods of flow in which

the magnitude of the fluid velocity is much greater than the magnitude of the wall velocity. Fortunately, this is true for most of the contraction cycle and really only breaks down during the period of flow reversal when the fluid velocity is near zero. Figure 3.7 was taken from the same data set as Figure 3.1. Note that while the assumption that Va<<Vp is true for most of the contraction cycle (i.e. those points that on the graph that are close to zero), there are periods in which the assumption breaks down and our method of calculating shear stress might break down as well. Because of the model used, the temporal cycle of wall shear stress has a pattern similar to the fluid velocity with the maximum shear stress of around 8 dynes/cm^2 occurring just after the systolic peak.

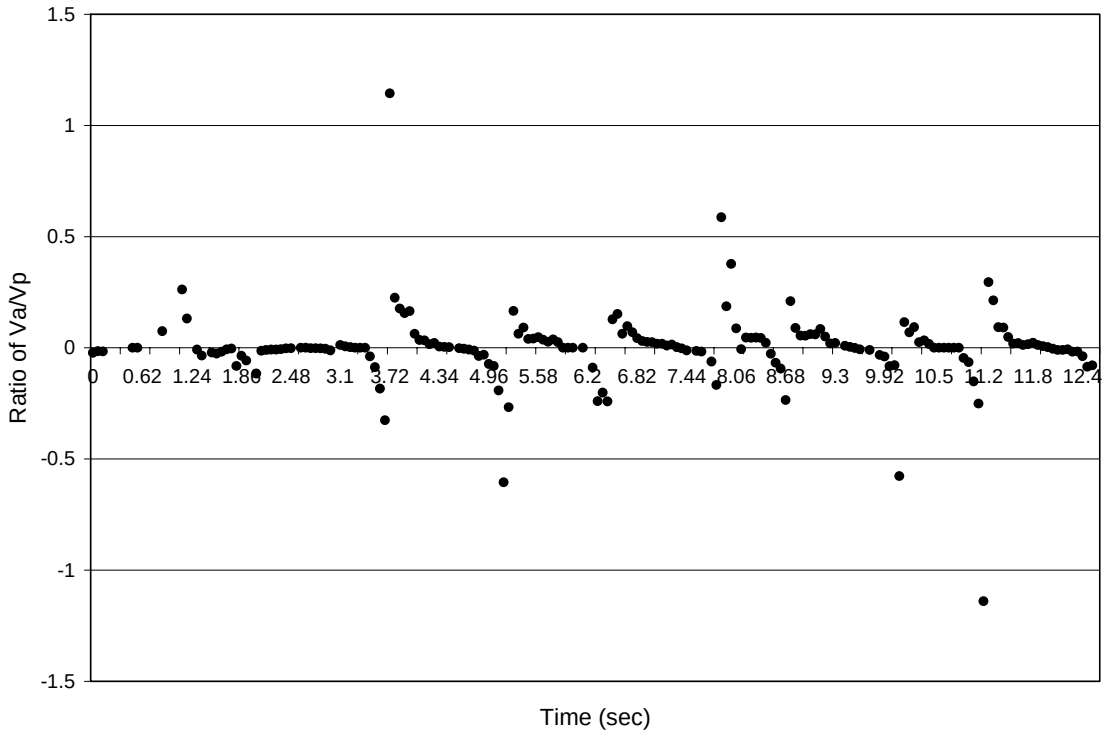

Figure 3.7: Ratio of the wall velocity (Va) to the lymphocyte velocity (Vp) for the data represented in Figure 3.1.

The other parameter that relies heavily on the assumption of Pouiselle flow is the volume flow rate. The flow rate is not actually measured but is calculated when the position and velocity of a single lymphocyte are applied to the Pouiselle flow model. The proximity of the mean volume flow rate to the volume ejection estimation, along with the observation that the mean volume flow rate is well correlated with the vessel radius and contraction velocity, seem to support that Pouiselle flow is indeed a reasonable model for estimating the volume flow rate for the majority of the contraction cycle.

3.3.3 Parameter averages for rat mesenteric lymphatics

Averages for the entire data set are summarized in Table 3.2. These averages represent data taken from seven rats over twenty-six different intervals of 30 seconds of raw flow data. Table 3.2 is an attempt to give a summary of the various phenomena observed throughout this study on each rat as well as to report overall averages. The average vessel size used was around 90 μm in diameter which is a reasonable average for rat mesenteric lymphatics. Maximum and average values for cell velocity, wall shear stress and the root mean squared (RMS) contraction velocity (an index of the strength and frequency of phasic contractions) are reported as a means of characterizing contractile activity. In one animal, maximum shear values were found to be around 10 dynes/cm^2, while the average maximum value was found to be apporoximately 6 dynes/cm^2. On average orthograde flow occurred 93% of the time. A comparison of the measured volume flow rate with the proposed volume flow rate, calculated as the

ejection flow rate, shows that on average the actual volume flow rate is less than (~72%) the ejection flow rate.

Table 3.2: Average values and mean standard errors of various parameters from seven different rats.

	Rat 1	**Rat 2**	**Rat 3**	**Rat 4**	**Rat 5**	**Rat 6**	**Rat 7**	**Average**
Avg Velocity, $\overline{V_p}$ (mm/sec)	0.35	1.01	1.51	1.02	1.15	0.43	0.55	0.87 ± 0.18
Avg Shear Stress, $\overline{\tau_w}$ (dynes/cm^2)	0.33	0.69	0.84	0.72	1.21	0.30	0.37	0.64 ± 0.14
Avg Diameter, $\overline{D}$ (μm)	77	92	125	112	66	97	70	91 ± 9.0
Average Volume Flow Rate, $\overline{Q}$ (μl/hr)	3.83	17.83	39.48	18.02	9.93	6.66	1.88	13.95 ± 5.27
Max Shear, $\tau_{w\max}$ (dynes/cm^2)	7.78	3.91	4.72	4.21	11.91	2.56	8.21	6.19 ± 1.33
Maximum Velocity, $V_{p\max}$ (mm/sec)	2.24	5.32	7.54	6.76	8.98	3.98	4.91	5.68 ± 0.93
Minimum Velocity, $V_{p\min}$ (mm/sec)	-0.70	-1.89	-1.99	-2.40	-0.64	-2.76	-1.19	-1.65 ± 0.34
RMS Contraction Velocity, V_{arms} (μm/sec)	22.94	52.70	69.53	51.77	27.86	39.40	38.19	43.2 ± 6.54
% Orthograde	98	97	94	89	98	82	90	92.5 ± 2.4
% Retrograde	2	3	6	11	2	18	10	7.5 ± 2.4
Ejection Flow (μl/hr)	7.31	21.54	43.87	29.17	7.09	18.74	8.24	19.42 ± 5.58

Of particular interest is the relationship between the RMS contraction velocity, the average radius, and the average volume flow rate for each imaging sequence as

shown in Figure 3.8 and Figure 3.9. From Figure 3.8 one can see that expressing the volume flow rate as a function of the square of the average vessel radius gives a correlation coefficient (R^2) value of 0.6102. If an additional variable, the RMS contraction velocity (an index of the strength of the phasic contractions), is introduced into the model the R^2 value improves to 0.7994 (Figure 3.9). In steady flow situations it is well known that the volume flow rate is directly proportional to the radius squared. However, in this case we have unsteady flow and thus the rate of contraction also plays a role in the promotion of flow.

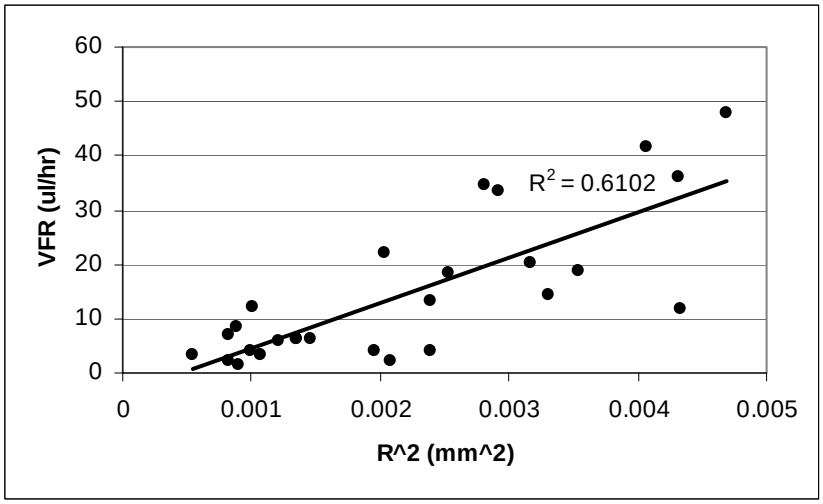

Figure 3.8: Relationship between the radius^2 and the volume flow rate. Data matched a linear fit with a correlation coefficient of 0.6102.

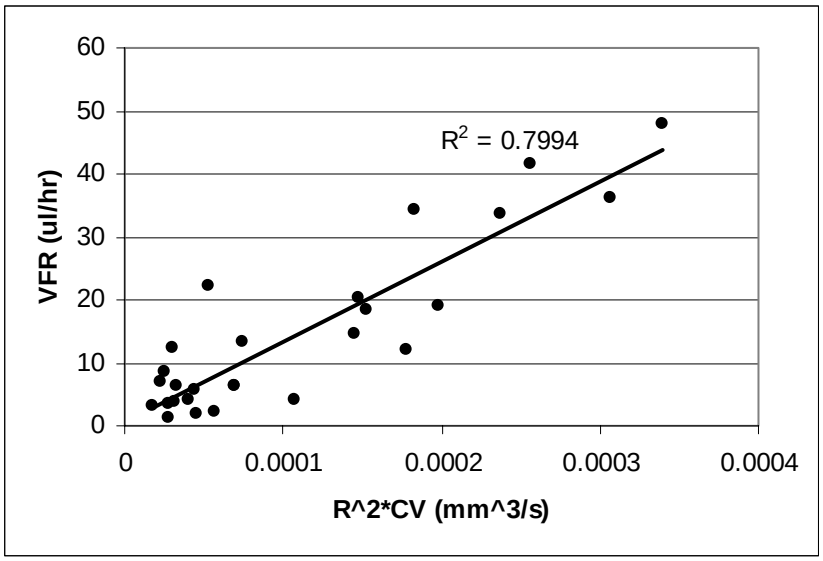

Figure 3.9: Relationship between the radius^2 multiplied by the RMS contraction velocity and the volume flow rate. The linear correlation statistic was improved to 0.7994.

Intuitively, it has long been thought that the intrinsic lymphatic pump plays a major role in the promotion of lymph flow through the lymphatic microcirculation [9]. This hypothesis is further supported by the evidence provided from Figure 3.8 and Figure 3.9. The results from Figure 3.8 should come as no surprise, since on average larger vessels are known to have larger volume flow rates (R^2=0.6102). This fit is improved (R^2=0.7994) when we take into account that pumping activity might also play an important role in increasing the volume flow rate (Figure 3.9). A larger RMS contraction velocity, which is essentially a measurement of the contractile activity of the vessel, does in fact increase the volume flow rate. It should be noted however, that under conditions in which a large pressure gradient already exists to promote flow, vessel contraction would actually inhibit flow [25]. In contrast, under conditions in

which no such pressure gradient is present or is very small, the active pump of the lymphatic vessel plays an important role in the promotion of lymph flow as evidenced by the fact that as pumping activity increases, the overall volume flow rate increases as well. Another way to investigate the effectiveness of the vessel contraction in promoting lymphatic flow is to compare the measured volume flow rate with the estimated volume ejection, both shown in Table 3.2. Since the estimated volume ejection was calculated with the assumption that all of the fluid displaced by the change in vessel volume would be ejected in the forward direction, one would expect that the actual volume flow rate would be slightly less than this value assuming there are no other pressure gradients. On average this seems to be the case (13.95 μl/hr < 19.42 μl/hr). The instances in which the actual volume flow rate is drastically smaller than the flow estimated from the ejection fraction may be an indication that the vessel is working against a pressure gradient upstream. For the one case in which the volume flow rate is greater than the ejection flow rate (Rat 5), it is likely that the vessel is experiencing a pressure gradient that promotes flow independent of the local contractions.

A few comments should be made here in regards to using the calculated percentages of orthograde and retrograde flow shown in Table 3.2 as a means of characterizing valve efficiency. For the most part, the valves were highly effective at preventing backflow into the upstream lymphangions; however, the effectiveness of the valves in preventing retrograde flow was shown to vary. For instance, the valves in Rat 6 were the least effective in preventing retrograde flow as it occurred 18% of the time. The reasons for this may be because this particular vessel was working against an

unusual pressure gradient, the valves may have been less effective, or there were multiple pacemakers and unusual contraction patterns, although we can really only speculate as to the exact cause at this point.

The estimation of wall shear stress was the main motivation behind this study, due to the questioned relevance of the pressure gradients applied in the flow-inhibition study cited throughout this chapter. Our fluids model was used to calculate the wall shear stresses and velocities applied in an original paper by Gashev, et. el [25], since only the axial pressure gradients were originally reported. Two wall shear stress parameters were estimated: 1) the wall shear stress resulting from the fluid flow due to the imposed axial pressure gradient, and 2) the wall shear stress resulting from the vessel contraction using the ejection volume estimation approach (Figure 3.10). As the transaxial pressure increases, the wall shear stress due to this pressure gradient goes up. The vessel appears to compensate for this by decreasing the frequency and amplitude of contraction and thus reducing the wall shear stress due to the phasic contraction.

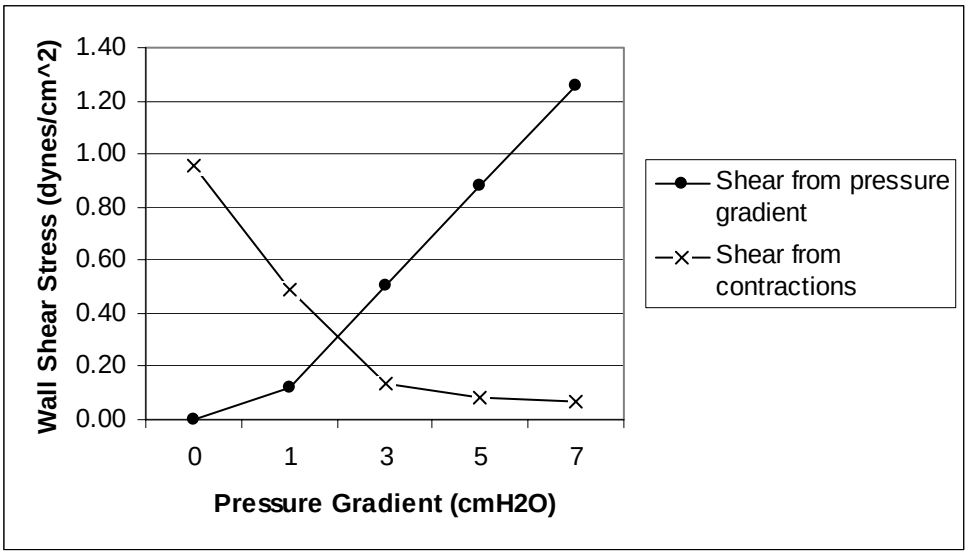

Figure 3.10: Wall shear stress estimates (dynes/cm^2) due to the imposed axial pressure gradients and phasic contractions calculated using current fluids model with previously reported isolated vessel experiments and plotted as a function of transaxial pressure gradient (cm H_2O).

This compensation seems to suggest that lymphatics have the capability of regulating wall shear stress, a capability of arterioles and venules that has been previously reported [27]. However, the average wall shear stresses that occur in the microlymphatics are significantly lower than those reported in the arterioles and venules [95] suggesting that the signaling mechanisms behind this shear stress dependent response in microlymphatics might be different or at least more sensitive than those that have been studied extensively in the microcirculation [27]. The wall shear stresses displayed in Figure 3.10 represent estimates using data from isolated lymphatic studies published previously and are in the same range as those that have now been observed and reported *in situ*, thus the magnitudes of imposed flows in the design of previous isolated lymphatic studies [25] appear physiologically relevant.

3.3.4 Lymphocyte flux data

Measuring the lymphocytes as markers of fluid flow provided another valuable piece of information regarding lymphatic function, an estimate of lymphocyte flux. Lymphatic vessels provide an important pathway in the trafficking of immune cells from the tissue spaces to the lymph nodes. Measurements of lymphocyte flux and density were taken for each of the seven rats represented here (Table 3.3). As noted in the table, there is a lot of variability between the number of lymphocytes present in each animal. The average lymphocyte flux in these vessels was 990 ± 260 cells/min with an average lymphocyte density of 12,000 ± 5,200 cells/μl.

Table 3.3: Values of lymphocyte density and lymphocyte flux for each of the seven rats represented in Table 3.2

	Lymphocyte Density (cells/μl)	**Lymphocyte flux (cells/min)**
Rat 1	2.20E+04	1.30E+03
Rat 2	1.23E+04	2.03E+03
Rat 3	3.26E+02	2.06E+02
Rat 4	3.65E+03	1.11E+03
Rat 5	2.00E+03	2.40E+02
Rat 6	8.57E+03	9.37E+02
Rat 7	3.55E+04	1.11E+03
Average	1.20E+04	9.90E+02
Standard Error	5.19E+03	2.57E+02

3.3.5 Volume loading experiments

To analyze the data from the volume loading experiments several different techniques were used. Since this data was collected much later than the initial physiology data just presented, the correlation algorithm which will be discussed in detail in Chapter IV had already been developed and verified. Therefore, the wall diameter was tracked using this method of post-processing; however, the number of lymphocytes available for tracking was very low in these experiments, especially after volume loading. This lack of lymphocytes prevented us from being able to use the correlation program for measuring the velocity, since it is highly dependent on a large number of particles in the field of view. Therefore, we used manual particle tracking as described earlier to measure the lymphocyte velocity. Each measurement (Table 3.4) corresponds to a one minute sequence of analyzed data. A total of 5 rats were tested (R1, R2, etc…) and flow sequences were recorded at three different time intervals: control before volume loading (C), five minutes after volume loading began (5), and ten minutes after volume loading began (10). The average lymphocyte velocity in the table represents the mean velocity of all lymphocytes tracked (at least 200) during the one minute interval.

Table 3.4: Changes in contractile dynamics and average lymphocyte velocities for 5 different rats at 3 different time periods each: control, 5 minutes after loading began, 10 minutes after loading began, X's denote period where no measurement could be made due to rarity of lymphocytes.

	Avg Diam (μm)	Max Diam (μm)	Min Diam (μm)	RMS CV (μm/s)	Avg Lymp Vel (mm/sec)
R1(C)	81.5	120.7	52.3	36.2	0.40
R1(5)	94.8	111.7	60.4	33.8	0.50
R1(10)	91.7	111.7	70.4	48.2	0.45
R2(C)	87.8	97.6	58.3	23.0	0.11
R2(5)	102.6	116.7	80.5	17.5	0.09
R2(10)	81.0	108.6	65.4	29.7	0.07
R3(C)	42.4	62.4	30.2	30.4	0.09
R3(5)	59.3	76.4	44.3	43.0	0.25
R3(10)	53.5	69.4	38.2	35.9	0.17
R4(C)	56.1	63.4	38.2	24.7	0.07
R4(5)	69.2	91.5	37.2	31.7	0.36
R4(10)	66.5	84.5	52.3	39.4	X
R5(C)	60.0	82.6	39.8	22.4	X
R5(5)	67.5	95.5	41.8	34.5	X
R5(10)	38.8	70.6	19.9	37.5	X

In order to be able to draw conclusions about the overall response of lymphatic flow and velocity to contraction, each data set had to be normalized to its control period to remove animal to animal variability (Table 3.5). From the normalized data it can be seen that the average diameter increased five minutes after volume loading as compared with the control (1.22 ± 0.05). After 10 minutes it seemed to return to its original state (1.03 ± 0.12) although it is hard to be certain since the standard error is so large. Maximum and minimum diameter increased 5 minutes after the control (1.19 ± 0.09 and 1.20 ± 0.11 respectively). RMS contraction velocity, which is a measure of contractile

activity, increased at 5 minutes and then again at 10 minutes after the control (1.19 ± 0.16 and 1.41 ± 0.10 respectively). Average lymph velocity also increases 5 minutes after control (2.61 ± 1.23). Data is missing for the average lymph velocity from four runs of data due to the very low lymphocyte concentrations in those sequences. In general lymphocyte density was found to diminish after volume loading.

Table 3.5: Data from Table 3.4 that has been normalized with the control period to remove animal to animal variability.

	Avg Diam (a.u.)	Max Diam (a.u.)	Min Diam (a.u.)	RMS CV (a.u.)	Avg Lymph Vel (a.u.)
R1(C)	1.00	1.00	1.00	1.00	1.00
R1(5)	1.16	0.93	1.15	0.93	1.23
R1(10)	1.13	0.93	1.35	1.33	1.11
R2(C)	1.00	1.00	1.00	1.00	1.00
R2(5)	1.17	1.20	1.38	0.76	0.82
R2(10)	0.92	1.11	1.12	1.29	0.63
R3(C)	1.00	1.00	1.00	1.00	1.00
R3(5)	1.40	1.23	1.47	1.41	2.88
R3(10)	1.26	1.11	1.27	1.18	2.00
R4(C)	1.00	1.00	1.00	1.00	1.00
R4(5)	1.24	1.44	0.97	1.28	5.52
R4(10)	1.19	1.33	1.37	1.60	X
R5(C)	1.00	1.00	1.00	1.00	X
R5(5)	1.13	1.16	1.05	1.54	X
R5(10)	0.65	0.86	0.50	1.67	X

Mean (control)		1	1	1	1	1
Mean (5 min)		1.22	1.19	1.20	1.19	2.61
Mean (10 min)		1.03	1.07	1.12	1.41	1.25

std error (control)		0	0	0	0	0
std error (5 min)		0.05	0.09	0.11	0.16	1.23
std error (10 min)		0.12	0.09	0.18	0.10	0.49

3.4 Concluding Remarks

Much work lies ahead of us if we desire to more fully understand the physical mechanisms and forces in place that both govern and influence lymphatic contractile regulation and lymphangiogenesis. However, without more detailed measurements of the lymph velocities and shear stresses that occur *in vivo*, it is difficult to establish the significance of the observed *in vitro* effects, whether by means of cell culture or isolated vessel models. The studies discussed here provide the measurements needed to establish the groundwork for the microlymphatic network, which should aid investigators in determining the necessary physical test conditions to create when investigating the specific signaling mechanisms and functional responses that these physical forces elicit.

CHAPTER IV

CORRELATION METHOD FOR PROCESSING LYMPHATIC IMAGES

The recent development of a high speed imaging system to measure lymphatic flow and estimate wall shear stress has now opened up a new area of research in lymphatic microcirculation [96]. The main difficulty with this system is the tedious post-processing required to analyze the large amount of data produced by high speed imaging (500 fps). To put this into perspective, the findings recently published by Dixon [97], which corresponded to data taken from 7 rats for a total of about 24 minutes or approximately 288,000 images, took over a year and a half to analyze. Not only is this expensive in terms of man hours, it is also difficult to perform various other flow-related studies when the results take so long to process. Pre-packaged particle tracking software produced spurious results due to the inherent low contrast of the imaging site. Contrast could be improved through the injection of fluorescent tracers; however, that would be undesirable given the influences such injections could have on tissue homeostasis. These limitations have led us to seek out an image analysis technique to calculate the fluid velocities automatically without having to introduce fluorescent tracers into the system.

Recently, Tsukada [53] reported on an image correlation method combined with a high speed imaging system that could measure the flow of erythrocytes in small capillaries (<50 μm in diameter). This method relies on measuring the displacement of a particular red cell distribution pattern between image frames through the use of the

correlation function. We have taken this method, adapted it, and integrated it into our high speed imaging system to simultaneously measure lymphatic flow and vessel diameter. With this innovation, an image sequence that would normally take over a week to analyze manually can be processed automatically with a high degree of accuracy in less than 30 minutes.

4.1 Materials and Methods

Since this correlation technique relies on the presence of particles to track their movement, only vessels with numerous lymphocytes were chosen to develop the algorithms for particle tracking. Considering that we had taken a large set of images using the *in situ* procedure described previously, no additional animal preparations were initially done. All code for the image correlation method was written in Matlab M-files and run in the command window.

4.1.1 Measuring lymph flow velocity

One of the main difficulties of automated image analysis of lymphocyte flow in lymphatic vessels is the poor contrast inherent to the images (Figure 4.1). In order to overcome this obstacle we took two sequential images separated by 2 ms and subtracted them from one another. This subtraction enhanced pixels in motion, while canceling out the motionless background. Given our sampling rate and magnification, the resulting image would only show particles moving greater than about 0.25 mm/sec, and would filter out the “motionless” background (motion less than 0.25 mm/sec). In our previous

work, we measured the motion artifact from vessel drift and the velocity of wall contractions to usually be well under 0.25 mm/sec.

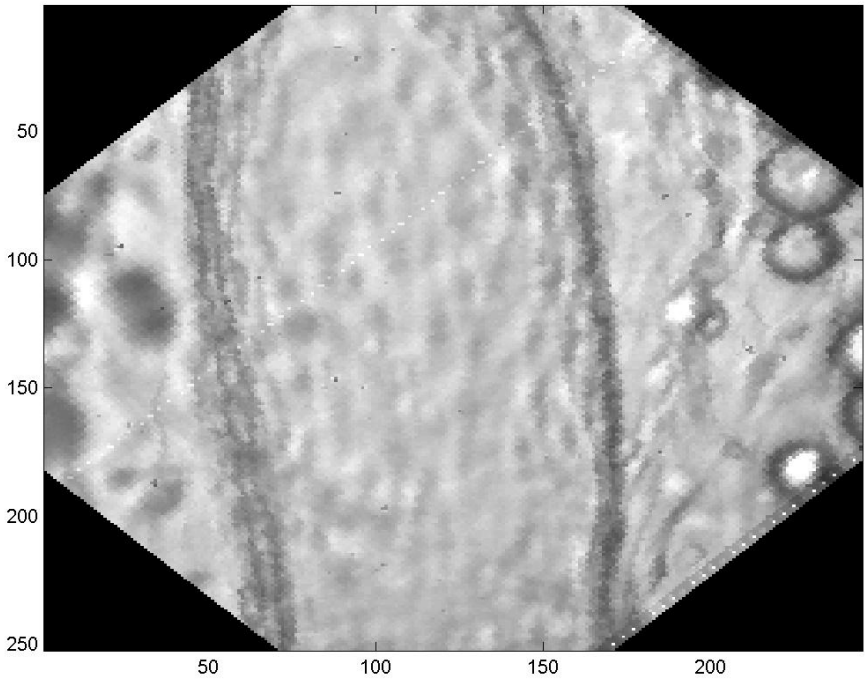

Figure 4.1: Image of a lymphatic vessel illustrating the poor contrast at the imaging site. There are actually several, 15 to be exact, lymphocytes present in this image, although they are very difficult to distinguish from the background unless you can see them move from frame to frame.

The subtraction described above was repeated with another pair of images and the two resultant images were then processed through a low pass filter to remove high frequency noise due to pixel to pixel variations. Each of these filtered images was then

used in the image correlation algorithm. A total of four raw images were used to calculate the fluid velocity as shown by the following equations (4.1 – 4.3):

$$\text{Picf} = \text{LPF}(\text{Pic1-Pic2}) \tag{4.1}$$

$$\text{Picg} = \text{LPF}(\text{Pic3-Pic4}) \tag{4.2}$$

$$\begin{aligned}\text{CCOR}(k,l) = &\left(\frac{1}{N}\sum_{m=0}^{N-1}\left(f_m(x,y)-\bar{f}\right)\left(g_m(x+k,y+l)-\bar{g}\right)\right)\\ &\times\left(\frac{1}{N}\sum_{m=0}^{N-1}\left(f_m(x,y)-\bar{f}\right)^2\frac{1}{N}\sum_{m=0}^{N-1}\left(g_m(x+k,y+l)-\bar{g}\right)^2\right)^{-1/2}\end{aligned} \tag{4.3}$$

In the above equations, Pic2 and Pic3 are separated by 4 ms, $f_m(x,y)$ corresponds to a given pixel within the window created in Picf, $g_m(x,y)$ corresponds to a given pixel in Picg, $\bar{f}$ is the mean of window f_m, and $\bar{g}$ is the mean of window g_m. LPF refers to the low pass filter used on the subtracted images. The window in image Picf was fixed, while the window in Picg was scanned across the picture to find the location of maximum correlation. The resultant window displacement, when combined with the known frame rate, gives a measure of fluid velocity (Figure 4.2).

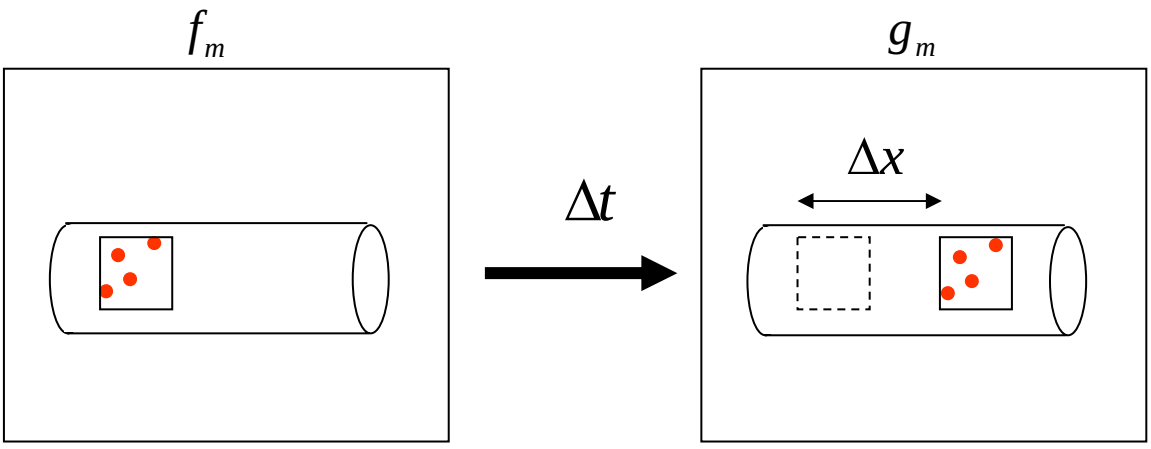

Figure 4.2: Illustration of the principle of the image correlation approach. Each image is taken at the same location separated by a small time interval. The displacement of the window corresponds to the movement of the fluid.

The main limitation found in using this approach with lymphatic vessels is that the particle densities are much lower than those found in the blood. Due to this limitation, we found that the best results were produced with a window size approaching at least half of the vessel diameter. All analysis was done in Matlab after capturing images with a high speed camera.

4.1.2 Measuring vessel diameter

The program was then modified to measure changes in vessel diameter. The program first provides an image for the user to select the left and right vessel wall on the image. The program then creates two reference windows around each of the selected locations. The displacements of these windows are measured by finding the maximum correlation in a sequential image as governed by Equation 4.3. From the coordinates of

these two windows, the vessel diameter can be measured through a simple subtraction (Figure 4.3). The displacement of the two windows averaged together gives information about motion artifact and overall image drift, which proves useful for improving the algorithm as described in the next section.

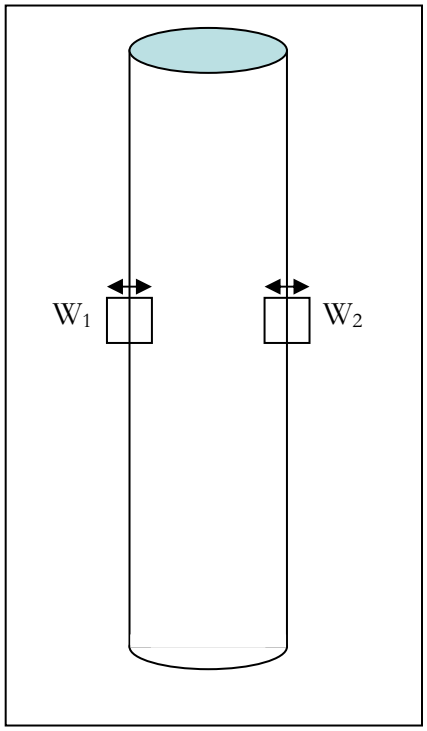

Figure 4.3: Two reference windows are created around each of the vessel walls in the same vertical location. Their displacements are tracked to measure changes in vessel diameter.

4.1.3 Optimizing the image correlation algorithm

After initial analysis, several improvements were made to the code. It was noted that the maximum correlation location was not always a good match and thus produced erroneous outliers in the velocity tracings. To improve this, a measure of relative correlation was introduced into the method by taking the ratio of the peak correlation

value with the average of its surrounding values (Figure 4.4 and Figure 4.5). As can be seen by visually comparing Figure 4.4 with Figure 4.5, the determined location of maximum correlation in Figure 4.4 is an acceptable match, while the determined location of maximum correlation in Figure 4.5 is just noise. Now, whenever an erroneous match is discovered, as in the example above, that value is replaced with an average of the velocities occurring before and after the event.

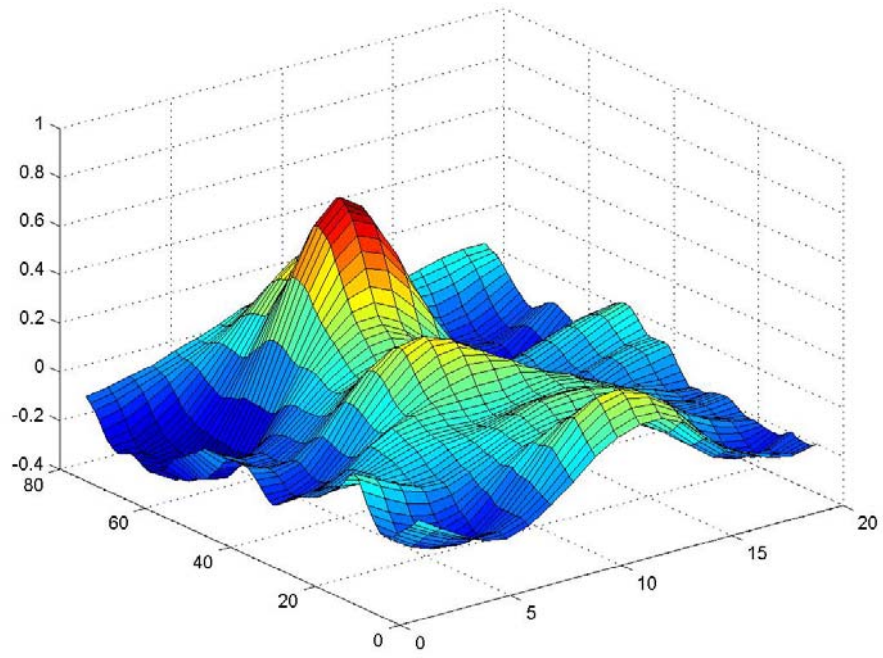

Figure 4.4: Correlation coefficient values for various window locations from Picg. Note the extent of the maximum as compared with the rest of the surface. This would be constituted as an acceptable match.

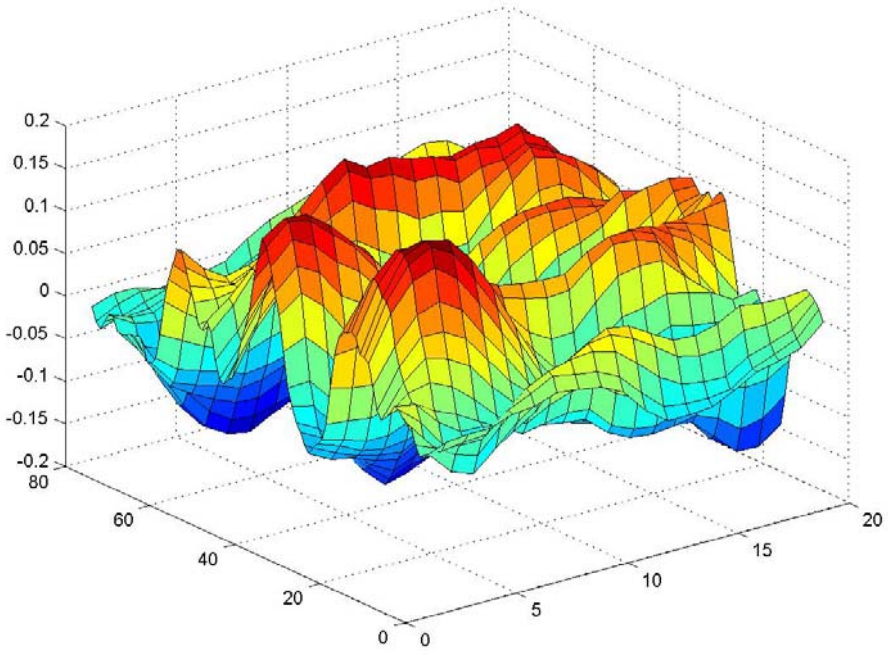

Figure 4.5: Correlation coefficient values for various window locations from Picg. Note the extent of the maximum as compared with the rest of the surface. This would be constituted as a poor match.

Another problem often encountered was that of motion artifact due to sudden movements by the animal or occasional intestinal motility at the imaging site. Since the magnification was so large, even the smallest movements could cause problems. Initially the velocity reference window created was not dynamic, but rather stayed in the same location for each given sequence during analysis. This made window matching difficult or even irrelevant if the window drifted partially or sometimes completely outside of the vessel. To correct this, the velocity calculations were implemented after the diameter measurements were made, so that the reference window could always be

placed in the center of the diameter. This also allowed us to change the width of the window to match the vessel's diameter (0.8*diameter), since as noted before a larger window size improves the chances of an acceptable match.

4.1.4 Increasing lymphocyte density

Since one of the main limitations of this technique is the necessity of high lymphocyte densities, a method was sought to increase this density naturally. It had been noted previously by others that after ingestion of lipids, the lipids are packaged into chylomicrons by the enterocytes of the small intestine and taken up into the lymphatics [98, 99]. In addition to this, lymphocyte concentration has been shown to increase temporarily after lipid absorption [54]. To harness this effect for improving our *in situ* conditions, we fed the rat a small amount of cream and waited approximately 20 minutes before beginning the *in situ* procedure. Doing this greatly enhanced the number of lymphocytes in our field of view (Figure 4.6); however, since the rat was no longer fasted, motion artifact through intestinal motility was greatly increased. The effects of this method are also only temporary and are therefore not useful after about an hour of imaging.

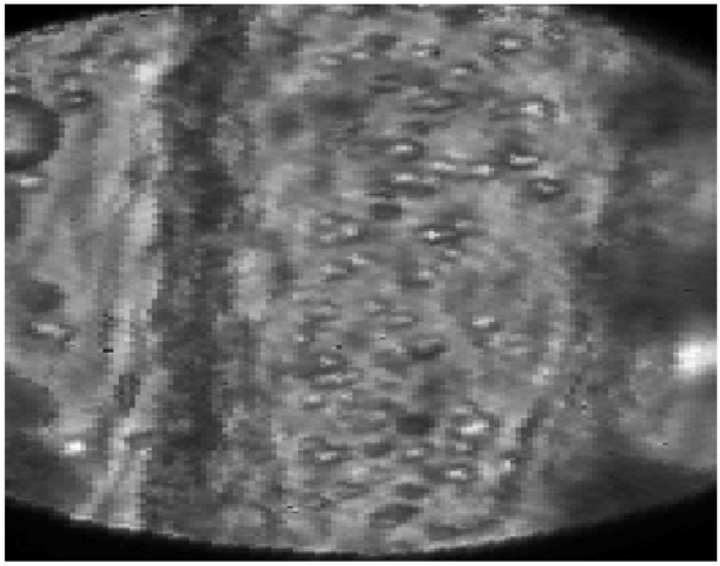

Figure 4.6: Mesenteric vessel of a rat approximately 45 minutes after being fed cream. Notice the increase in lymphocyte density as compared to Figure 4.1.

4.1.5 Isolated vessel protocol

We decided to perform further tests with the image correlation algorithm to see how well it would work with isolated vessels and to determine the actual velocities that occurred for various inlet and outlet pressures that were being applied. All animal procedures performed for this study were reviewed and approved by our institutional animal care and use committee, the Texas A&M University Laboratory Animal Care Committee. To isolate a mesenteric lymphatic, rats were euthanized with pentobarbital (120 mg/kg body weight IP). An abdominal incision was made to gain access to the mesenteric lymphatic vessels. A loop of the small intestine was exteriorized through the incision and gently positioned over a semicircular viewing pedestal on a Plexiglas preparation board. A lymphatic vessel was then carefully cleared of all surrounding

tissues using a dissecting microscope. Extreme caution was used to not grab or pinch the vessel at any time, thereby reducing the likelihood of damage. The area of interest was kept moist for the period of dissection using the standard Dulbecco's Phosphate-Buffered Saline (Invitrogen Corp. 14040-133). A mesenteric lymphatic vessel 1-2 cm long was dissected and used for experiments. Once the vessel was exteriorized, the lymphatic segment was transferred to an isolated vessel chamber (modified Living Systems Instrumentation single vessel chamber model CH/1) filled with room temperature albumin-physiological salt solution (APSS) (in mM: 145.0 NaCl, 4.7 KCl, 2.0 $CaCl_2$, 1.17 $MgSO_4$, 1.2 NaH_2PO_4, 5.0 Dextrose, 2.0 Sodium Pyruvate, 0.02 EDTA, 3.0 MOPS, and 10g/l bovine serum albumin) pH adjusted to 7.36 at 38^o C. The isolated segment was cannulated and tied onto two carefully matched glass pipettes (100-200 μm). Great care was used to prepare and select pairs of resistance-matched pipettes for these experiments. For each experiment we chose pairs of pipettes with matching diameters and tip lengths and we tested them to ensure that the difference between their measured electrical resistances did not exceed 10% [100]. The pipettes were filled with a 0.97 μm polystyrene microsphere suspension diluted into an APSS solution at a ratio of 1:500. Microspheres were needed to act as the particles that the correlation algorithm would track. The inflow and outflow pipettes were connected to independently adjustable pressure reservoirs filled with APSS. Care was taken to ensure that there were no air bubbles in the tubing or in the pipettes. Once the vessel was cannulated, a slight positive transmural pressure (2-3 cm H_2O) was applied to it to detect leaks and to ensure that the vessel was undamaged and untwisted. The vessel was set to its

approximate *in situ* length and positioned just above the glass coverslip comprising the chamber bottom. The vessel chamber was then transferred to the stage of a microscope. The vessel was set to an equilibration transmural pressure of 3 cm H_2O and warmed to 38^{o} C during 15-20 minutes. Once tone and spontaneous contractions were observed, the segments of data were recorded with the high speed camera (Dalstar64K1M, 1M fps 245x245, CCD camera) at various inflow and outflow pressures. We waited five minutes between each recording sequence to allow for the previous data set to be saved to the hard drive and to give the vessel time to equilibrate to the new pressures.

4.2 Results and Discussion

4.2.1 *In situ* experiments

A sequence of data, represented in Table 3.2, was taken from Rat 6 and processed through the developed correlation algorithm (Figure 4.7). As one can see from the figure, the program successfully picked out fluctuations in velocity; however, there are numerous segments of data that appear to be noise. The standard error of prediction for this case sequence was 0.8479 mm/sec. While one could easily remove the points classified as "noise" after comparing them with the manually tracked data, a method was sought to consistently improve the noise level without having to use the manual data analysis. To do this, several improvements to the correlation algorithm were made, as mentioned in the materials an methods section (4.1.3).

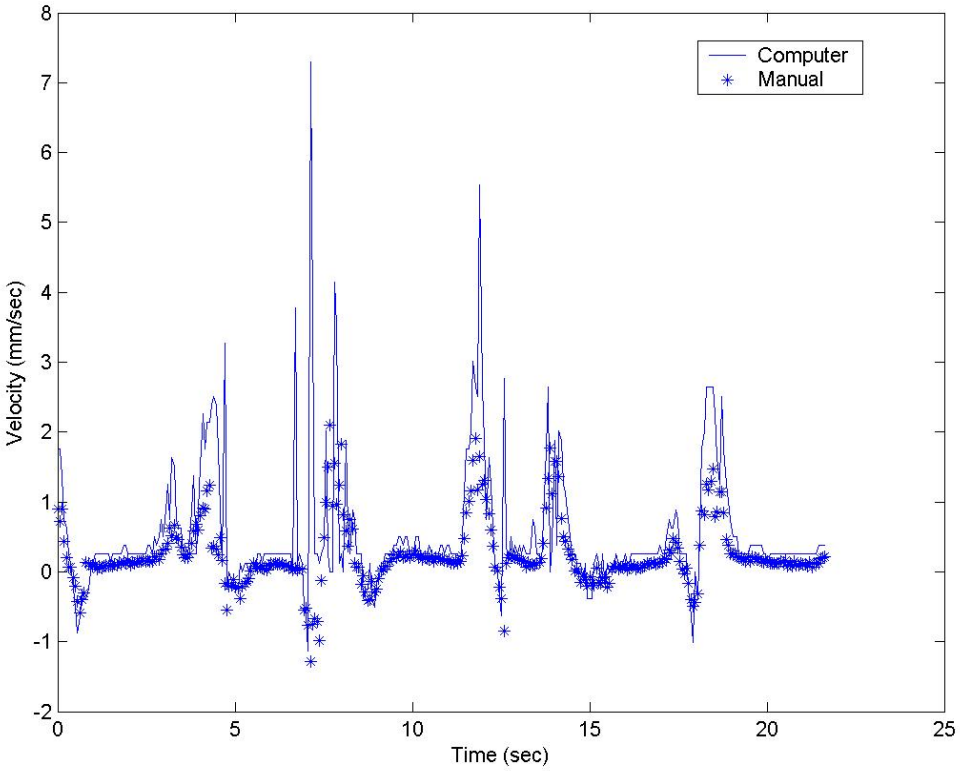

Figure 4.7: Comparison of spatially averaged velocity calculated from manually tracked data with that of the correlation algorithm. The standard error of prediction was 0.8479 mm/sec.

As described in the materials and methods section (4.1.3), one other modification that was made to improve the lymphocyte velocity measurements was to create a method for removing "bad" data points by comparing the correlation coefficient at the best fit with the correlation coefficients spatially surrounding that fit. This, in conjunction with the dynamic reference window, improved the data dramatically (Figure 4.8).

One question that arises from this is whether or not the displacement of the reference window found by the program is actually a measure of spatially averaged

velocity ($\overline{V}$) (assuming Poiseuille flow $\overline{V}$ would be half of the maximum velocity (V_{max})). This should be the case if there is an even distribution of lymphocytes across the radius of the vessel. However, if there are more lymphocytes in the center of the vessel than near the wall, the displacement of the window would approach the center velocity (i.e. V_{max}) instead (Figure 4.9).

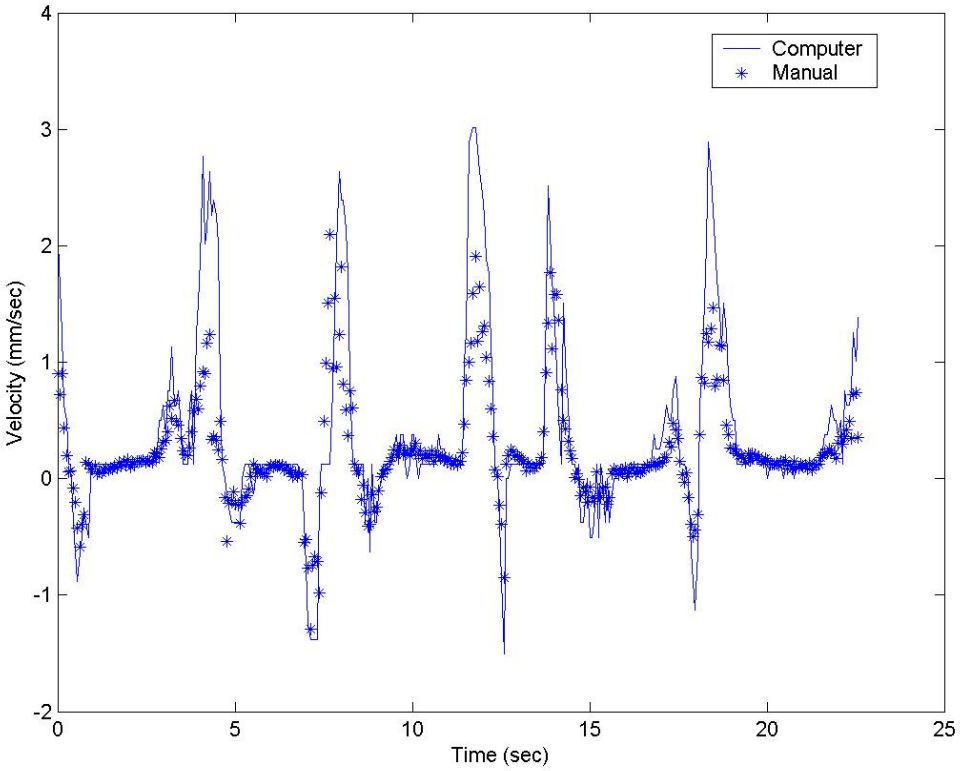

Figure 4.8: Comparison of spatially averaged velocity calculated from manually tracked data with that calculated by the correlation algorithm after modifications were made to improve the algorithm. The standard error of prediction is 0.5009 mm/sec.

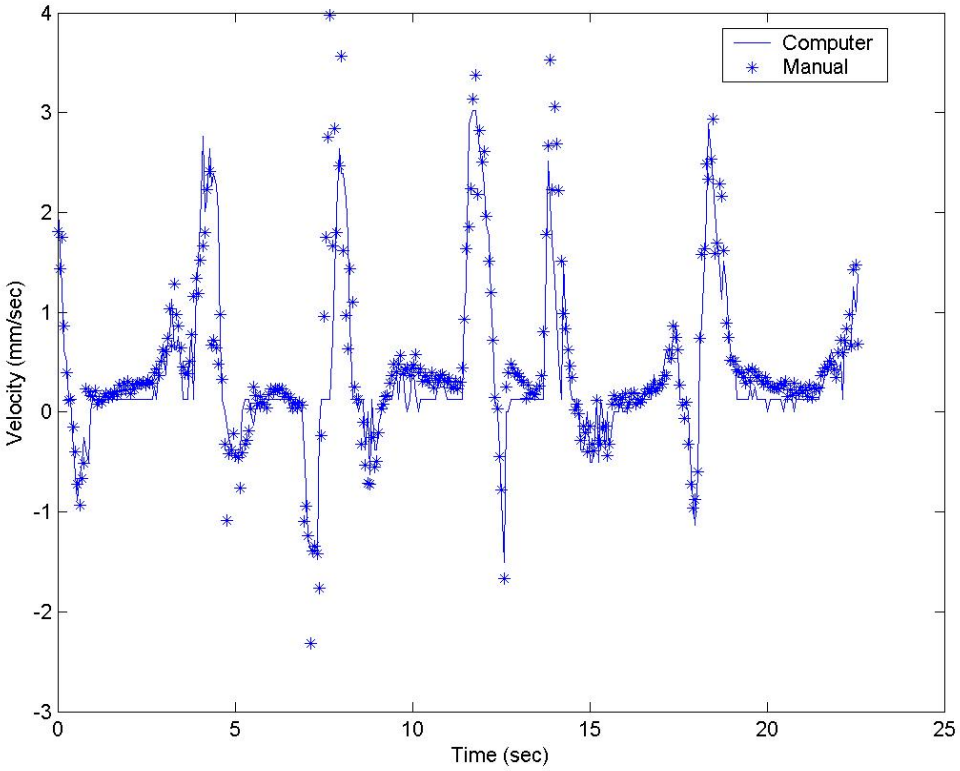

Figure 4.9: Comparison of maximum velocity calculated from manually tracked data with that calculated by the correlation algorithm after modifications were made to improve the algorithm. The standard error of prediction is 0.4850 mm/sec.

Of course, in order for V_{max} to be the best match, all of the tracked lymphocytes would have to be in the center, which is unlikely to be the case if you have more than one lymphocyte located in a given cross section of the vessel. It seems logical then, that the physical representation of the velocity calculated by the correlation algorithm is larger than $\overline{V}$ (since particles tend to locate themselves near the center) and lower than V_{max} (since all of the particles cannot flow through the center). To see if this is the case for this particular set of data, a program was written in Matlab to vary the velocities

calculated from the manually tracked data from $\overline{V}$ to V_{max}, while keeping the correlation tracked velocities the same, and find the minimum standard error of prediction for the correlation method (Figure 4.10). For this particular case the best fit occurred at $V^* = 0.55V_{max} + 0.45\overline{V}$ (Figure 4.11).

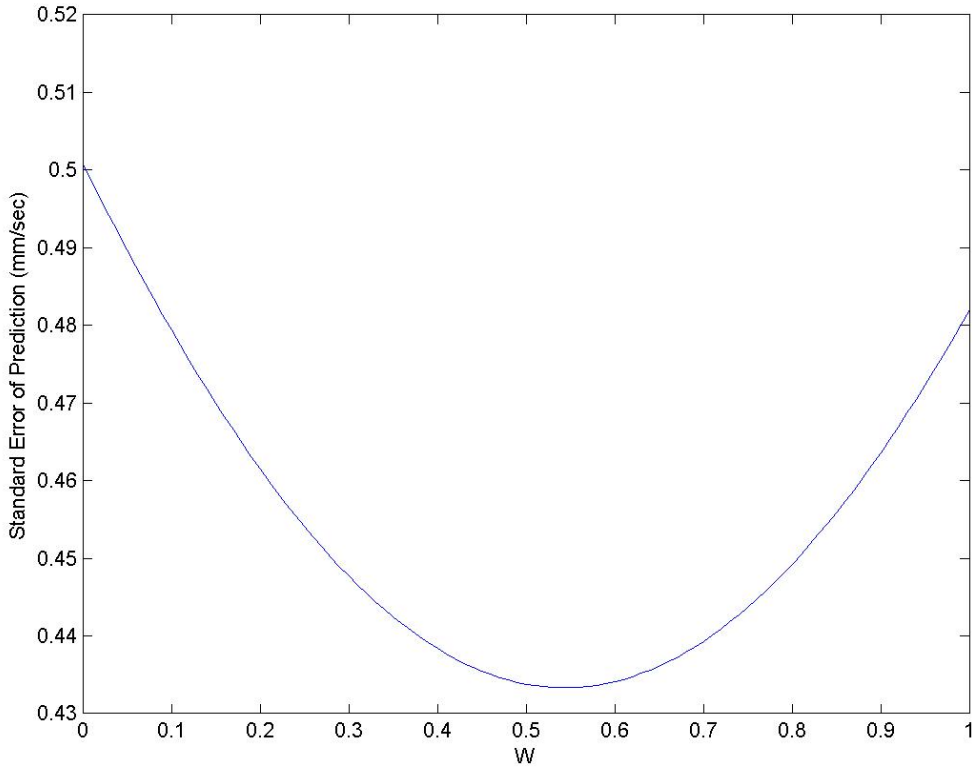

Figure 4.10: The standard error of prediction as the manually tracked velocity is varied from $\overline{V}$ to V_{max} where W on the x-axis is represented by the equation $V^* = W \times V_{max} + (1-W)\overline{V}$.

When the program is being run on a data set where there is no manually tracked data to which it can be compared, at least as of now there is no way as of now to tell whether the velocities being measured are closer to the spatially averaged velocity or the maximum particle velocity as this will depend on the radial distribution of the total number of particles. In Chapter V, I have laid out some future work that could be done to take the spatial distribution of lymphocytes into account.

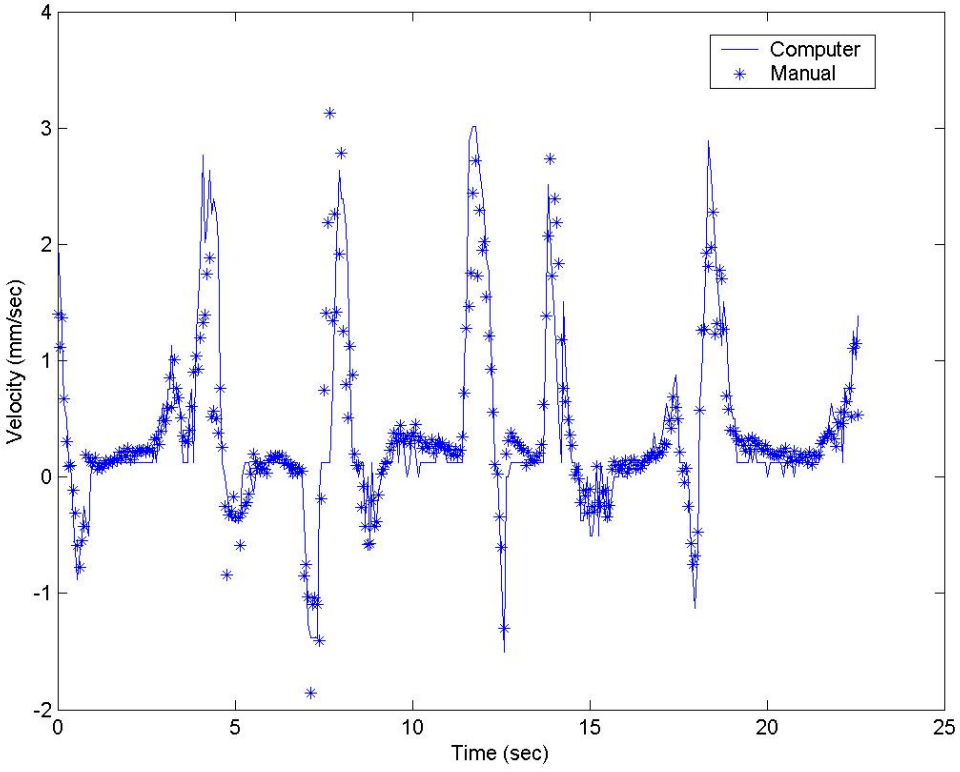

Figure 4.11: Comparison of the optimized velocity ($V^* = W \times V_{\max} + (1-W)\overline{V}$) calculated from manually tracked data with that calculated by the correlation algorithm. The standard error of prediction is 0.4333 mm/sec.

After optimizing and finalizing the algorithm on this particular set of data, we wanted to test it on other *in situ* data runs. A few sequences of data were chosen that had a large enough lymphocyte density to ensure that there were multiple lymphocytes in the field of view at every time interval during the sequence. This limited the number of manually tracked data sets that could be used and thus compared to the correlation method, but each of them represents a different vessel and rat so as to establish the robustness of the program provided there are enough lymphocytes available (Figure 4.12 and Figure 4.13). I have tried to represent two extreme situations here, with Figure 4.12 illustrating a vessel with several rapid changes in velocity and Figure 4.13 exemplifying a vessel that experienced just a few spontaneous contractions and thus not much velocity fluctuation.

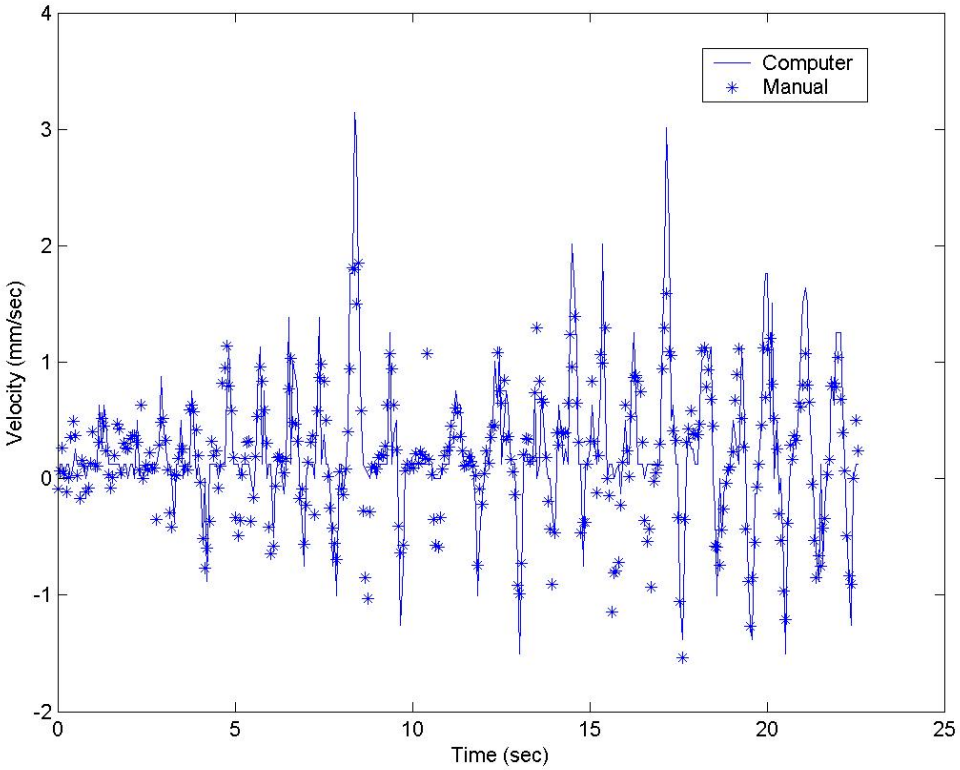

Figure 4.12: Another data sequence comparing the velocities calculated by the correlation algorithm with $\overline{V}$ calculated from the manually tracked data. The standard error of prediction is 0.3894 mm/sec.

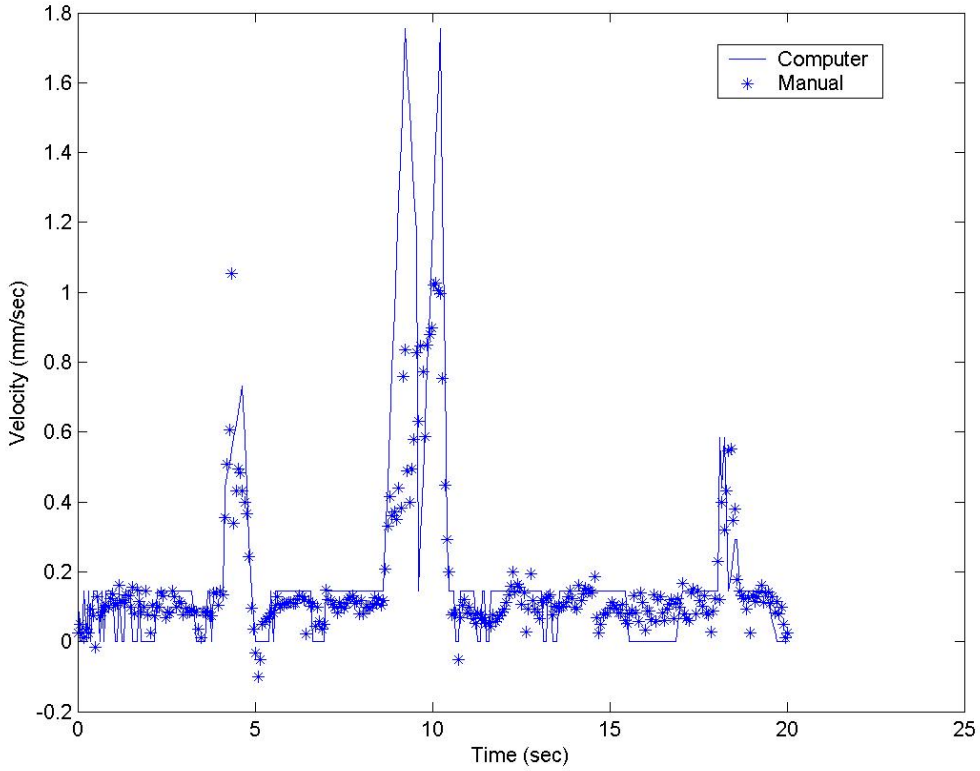

Figure 4.13: Another data sequence comparing the velocities calculated by the correlation algorithm with $\overline{V}$ calculated from the manually tracked data. The standard error of prediction is 0.2005 mm/sec.

Given that V_p is the predicted velocity determined by the correlation algorithm, the equation used for finding the standard error or prediction is:

$$(4.4) \quad e = \sqrt{\frac{1}{n}\sum_{k=0}^{n}\left(\overline{V}(k) - V_p(k)\right)^2}$$

One should be able to see from this equation that the best achievable standard error of prediction is determined by the resolution of the system. The smallest discernable shift in the correlation window is one pixel. If this value is divided by the time interval

between the image sets used in the correlation algorithm (8 ms), then the velocity resolution of the system is 125 pixels/sec. While the corresponding actual resolution varies with the magnification used, it is typically around .125 mm/sec; therefore, a standard error of prediction of approximately .200 mm/sec is actually getting fairly close to the resolution of the current system. The resolution could be improved by increasing the time interval between the image sets used by the correlation program; however, this would decrease the maximum detectable velocity of the system. Eight milliseconds seems to be an optimal time interval between image sets.

It was also suggested that the program could be improved by altering the shape of the second velocity window to fit the assumed Poiseuille flow distribution. This alteration could be done by finding an initial guess of the velocity using two square windows and then deforming the second window by an amount proportional to that guess. The program could then reiterate this procedure to give you a better guess and could continue either a fixed number of times or until you converge on some solution. While the code to do this was written and has been included in Appendix IV, the results it produced were actually noisier than those produced using the square window. I think the main reason for this noise was due to the "particles" size being around 5-7 pixels so that if the window was shifted based upon the radial location of each pixel, then the expected shape of the lymphocytes were actually distorted, which does not actually happen physically.

As stated before mesenteric lymphatic vessels undergo drift in the imaging field due to various forms of motion artifact. This drift can have a huge impact on the

original method used above for measuring velocity since the reference window created in Pic f was static. If the window drifted outside of the vessel or even partially out of the vessel, the results were seriously altered. The main way to correct for this was to take into consideration the spatial location of each of the vessel walls so as to always postion the reference window in the center of the vessel. In doing this, not only did we improve the algorithm, but our algorithm allowed us to track movements in the vessel diameter as well (Figure 4.14). The main discrepancies between the manually tracked diameters and those determined according to the algorithm are more than likely due to inconsistencies in where the user measured in each image. Fortunately, the correlation algorithm is completely consistent in where it measures vessel diameter each time. The accuracy of the diameters determined from the correlation algorithm can be verified through visual inspection by overlaying the computer's projection of the wall with the image itself (Figure 4.15).

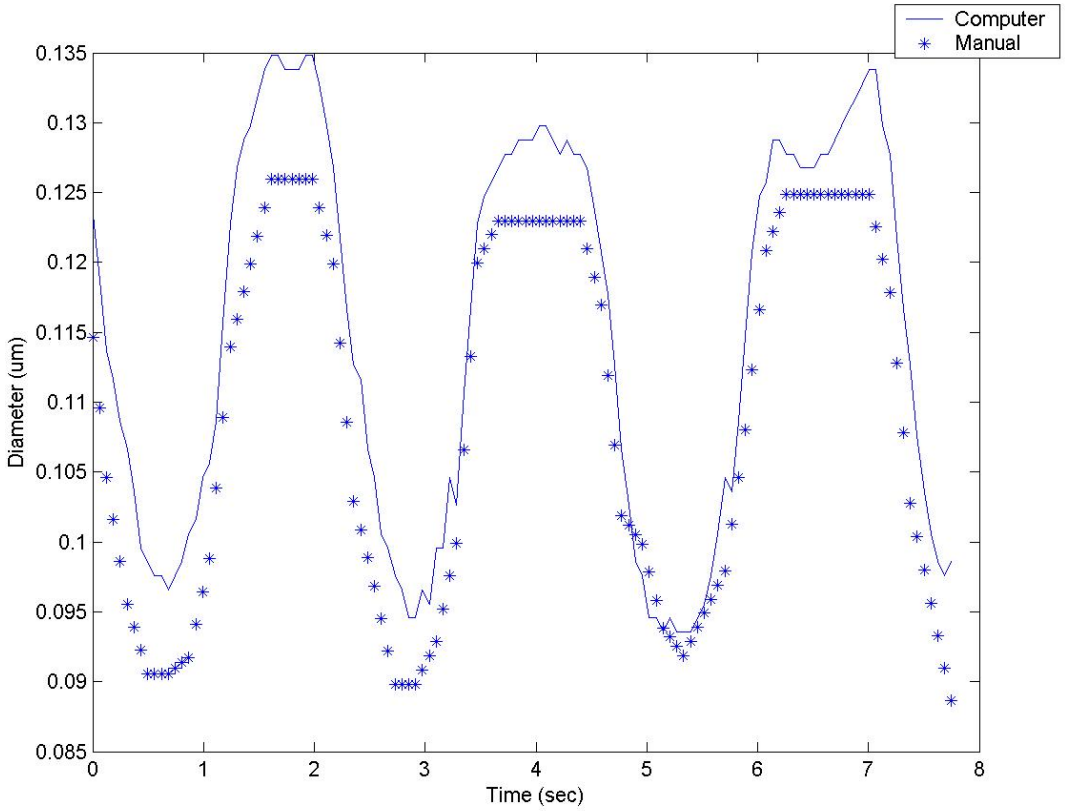

Figure 4.14: Diameter tracings calculated by the correlation algorithm compared with those calculated from the manually tracked data. The standard error of prediction is 6.8 μm.

While it cannot be shown visually here, a movie was actually created that shows an animated version of Figure 4.15 with the computer tracking the variations in vessel diameter. It should be noted, however, that when there are fat cells overlapping the vessel, something that can occur quite often with mesenteric vessels, the user can "work around" the fat cells, while the program cannot always distinguish between the edge of a fat cell and the edge of the vessel wall. One should also be aware that it makes a difference where the vessel wall is measured. The vessel is not exactly a straight tube,

and sometimes the vessel contracts more strongly in some portions than in others (Figure 4.16).

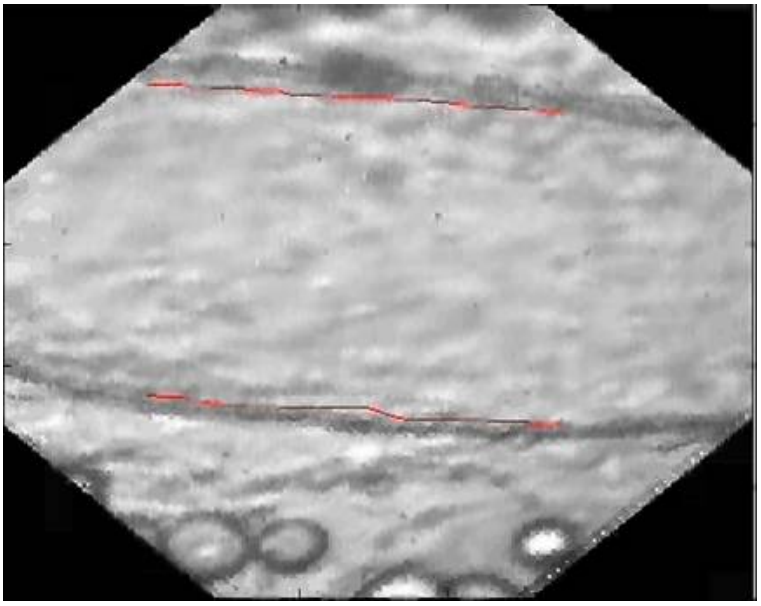

Figure 4.15: Image correlation was used to track the wall at multiple locations and fit them together with a line. This image represents a snapshot of a movie showing the program's ability to continuously and accurately track wall movement.

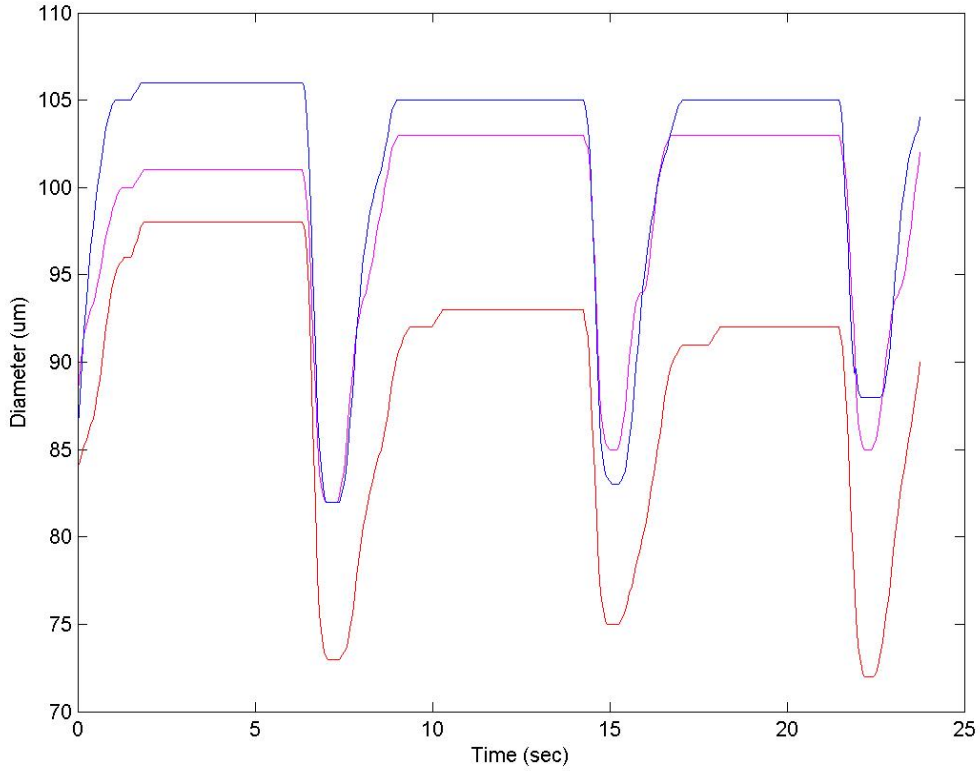

Figure 4.16: Diameter measurements taken at three different locations of the vessel (top, middle, and bottom). In this case the vessel narrows as you go from top to bottom, and the vessel also contracts more strongly at the bottom.

4.2.2 Increasing lymphocyte density through lipid absorption

As mentioned in section 4.2.4, after we had tested the program on the original *in situ* experiments, we decided to run the algorithm on data sets where we had tried to increase the lymphocyte concentration by feeding the rats some cream before surgery. The best way to illustrate the advantage of having a large lymphocyte density is to compare the results of a rat that has been fed cream and thus has more lymphocytes with one that has a low density (Figure 4.17 and Figure 4.18).

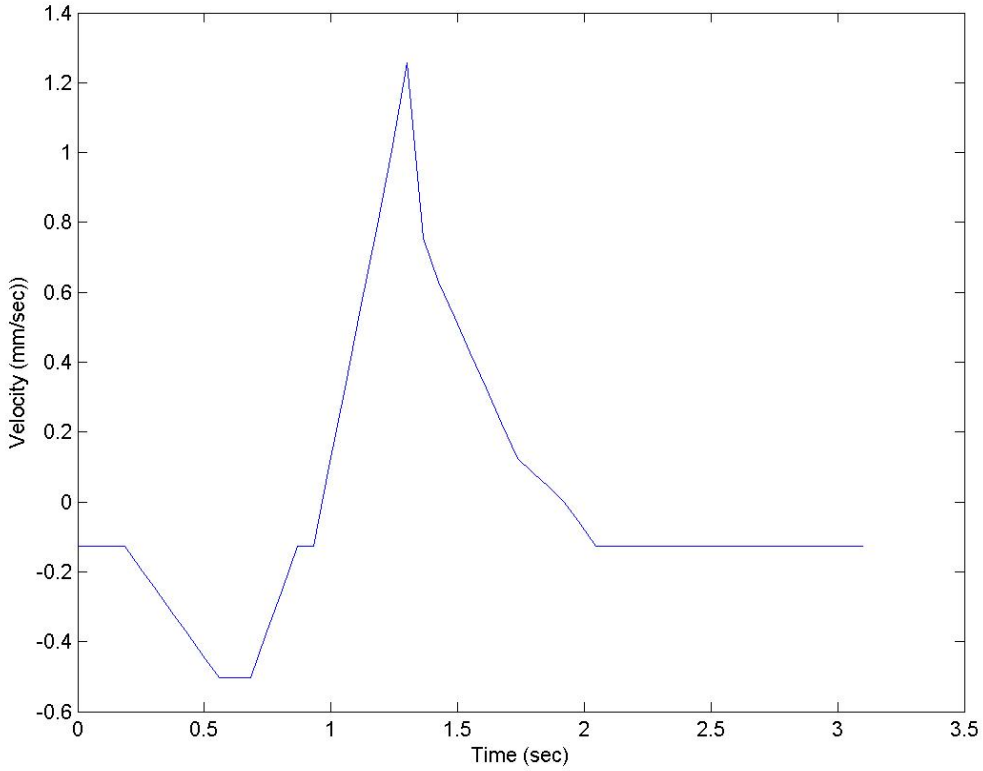

Figure 4.17: A 3 second portion of a velocity fluctuation measured with the image correlation method for a "lipid enhanced" rat with a large lymphocyte density.

Figure 4.17 shows a 3 second interval of data where the correlation program could continuously measure the velocity throughout the time interval with very little noise. Figure 4.18 was generated by the correlation program using the data set represented at approximately time t = 4 sec in Figure 2.11. While it is not evident from Figure 2.11, the lymphocyte density is fairly low for this particular sequence. The spikes from t = 1.5 sec to 2.5 sec in Figure 4.18 do not represent fluctuations in fluid flow, but are rather periods during the flow in which there are no lymphocytes in the correlation window. Therefore, the best match found by the program is at the site of the original window,

which gives a velocity of 0 mm/sec, when in fact the fluid is moving at a much higher speed.

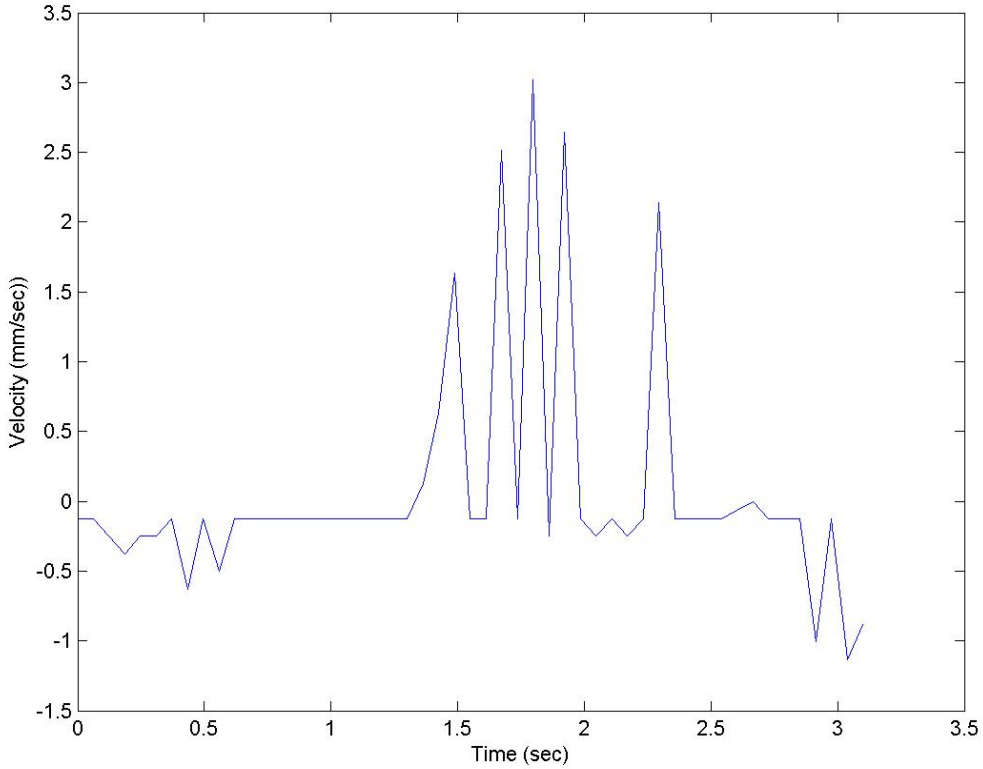

Figure 4.18: A 3 second portion of a velocity fluctuation (from Figure 2.11 at ~ t = 4 sec) measured with the image correlation method, lymphocyte density was very low.

4.2.3 Using the image correlation method with isolated vessels

Preliminary tests on isolated vessels demonstrated the capability of the correlation algorithm to measure flows being applied under various input and output pressures, provided one can seed the media flowing through the vessel with particles that are at least ~ 1 micron in diameter (Table 4.1). Outflow, P(out), and inflow P(in) pressures are reported in cmH_2O.

Table 4.1: Measurement of contraction and flow parameters as calculated by the correlation program for various pressure gradients for two different experiments (1 & 2).

	P(in)	P(out)	Avg Vel (mm/sec)	Max Vel (mm/sec)	Avg Diam (μm)	Max Diam (μm)	Min Diam (μm)	RMS CV (μm/s)	# contract
1	5	5	0.22	10.11	158.5	169.7	94.4	106.3	3.50
	3	3	0.66	14.05	141.1	165.2	77.5	127.5	5.50
	1	1	0.61	12.36	83.2	107.9	53.9	52.2	3.00
	7.5	2.5	7.21	24.16	159.2	171.9	114.6	76.4	4.00
	6.5	3.5	8.46	28.09	134.8	160.7	98.9	77.6	6.25
	5.5	4.5	3.74	19.66	145.5	165.2	112.4	62.8	4.50
	4.5	5.5	0.60	6.74	97.7	140.5	75.3	39.0	4.50
2	5	5	0.30	5.62	133.4	143.8	103.4	59.3	6.00
	3	3	0.36	5.62	133.4	137.1	109.0	39.9	3.00
	1	1	0.05	3.93	121.1	128.1	95.5	31.3	2.00
	7.5	2.5	1.08	5.06	149.3	159.6	119.1	49.7	5.00
	6.5	3.5	0.38	2.81	154.7	161.8	119.1	43.4	2.75
	5.5	4.5	0.20	3.93	158.8	164.0	113.5	29.4	1.00
	4.5	5.5	-0.14	0.56	142.8	157.3	106.7	53.5	4.50

The overall responses measured agreed with those found in the literature [25, 45]. For instance, in Experiment 2 contractile activity increased with increasing transmural pressure as measured by the RMS contraction velocity (59.3, 39.9, and 31.3 μm/s). Diameter increases with transmural pressure as expected for both Experiment 1 and 2. Velocity was also shown to increase, as expected, with increasing pressure gradient (0.20, 0.38, 1.08 mm/sec). However, when one compares the velocity ranges from Experiment 1 and 2, it can be seen that they are drastically different even when the diameters are similar. This is most likely due to our inability to ensure that the inflow and outflow resistance do not fluctuate from experiment to experiment. The primary source of this fluctuation is due to the microspheres aggregating and clogging the outflow pipette tip. The main difficulty encountered in these experiments was that the

microspheres themselves seemed to illicit a physiologic response to the lymphatic system. The microspheres were also affected by the APSS solution in which they were placed. Specifically, they began to clump together over time and their surfaces began to appear "sticky". Initially we tried 5 μm particles due to their similarity in size to lymphocytes; however, these particles immediately clogged the pipette tip, which was around 50 μm in diameter. This occurred due to the fairly high density of microspheres needed to ensure successful tracking and due to the "sticky" effect that we had observed. We tried various sizes of microspheres and the 0.95 micron diameter spheres were the only ones that did not clog the pipette tip. At first we were unsure if this size would work with the correlation program since they were smaller than the resolution of our image (1 μm ~ 1 pixel). When they began to aggregate together, the groups were the ideal size to allow for tracking and yet still prevent clogging (~3-4 μm). On several occasions we observed the particles sticking to the valve leaflets and thus increasing the flow resistance, which probably explains some of the variability that we saw when comparing the two data sets with one another. It is also highly likely that the microspheres are damaging the endothelial cells of the vessel, since in many cases the vessel stopped contracting under conditions that would normally enhance contraction. While the program will work quite well for tracking these microspheres in isolated vessels, if this method is to be used in physiologic studies with isolated vessels, there needs to be a way to better minimize the effects of the seeded particle on the vessels themselves.

4.3 Concluding Remarks

Through various experiments I have demonstrated the capability of image correlation approaches to measure fluctuations in diameter of contracting mesenteric lymphatics. While there are many well established approaches for measuring the diameter of vessels [101-103], it was advantageous to measure them through our image correlation program. This ensured that our measurements could be used to optimize our ability to track lymph flow within the image correlation program by temporally adjusting the correlation window according to the vessel contractions. The program has proven to be quite robust at detecting temporal fluctuations in lymph flow. For all the cases that it was tested, the actual velocity appears to be somewhere between the spatially averaged velocity and the maximum velocity, although its exact value presumably depends on the radial distribution of the lymphocytes. If one wanted to obtain measurements to be used in more detailed fluids modeling, this program would not provide the sufficient accuracy necessary to do so. We have provided, however, a large database of quantitative measurements of flow in Chapter III should one need more accurate measurements for further fluid dynamics modeling. This methodology will work quite well for future physiological studies, provided that the main parameter of interest is measuring temporal fluctuations in flow before and after various conditions are imposed on the vessel.

CHAPTER V

CONCLUSION AND FUTURE WORK

The role of lymphatic vessel contraction in the promotion of lymph flow in mesenteric lymphatics was investigated in this research. While vessel contraction had been studied quite extensively in the past, measurements quantifying the velocity fluctuations that occur throughout the entire contraction cycle had not been made. This lack of data was partly due to the large dynamic range of velocities that we found to occur in mesenteric lymphatics using our high-speed microscopy system: from -2 mm/sec to 10 mm/sec. In the past, standard video microscopy had not been capable of measuring these speeds due to the large magnifications necessary to observe these smaller vessels (~100 μm in diameter). Knowing these velocity ranges not only improved our understanding of each individual lymphangion's role in promoting lymph flow, but it also has provided the background necessary to pursue flow studies in isolated vessels and in cell culture models. For example, it had previously been shown that imposed flow produced an inhibition of the lymphatic intrinsic pump; however, it was not known for certain whether the velocities applied to the isolated vessels in this study represented the actual velocities that would occur *in vivo.* Until these velocities could be verified, the conclusions of such experiments would always be in question.

Of course, ultimately it is not velocity itself that produces this inhibition, but rather the sensitivity of the endothelial cells lining the vessel wall to wall shear stress. By taking into account other parameters while measuring the lymphocyte velocity, such

as vessel diameter, contraction velocity, and the distance between valves, it was verified that Poiseuille flow was a reasonable model for estimating shear stress for a majority of the contraction cycle. These estimations of shear stress will be very important for investigators to take into consideration in their future studies on shear dependent responses *in vitro* or in isolated vessels. The process of verifying the Poiseuille model has also demonstrated the need for more extensive modeling if accurate quantifications of shear stress for every moment in the contraction cycle are needed. In brief, the model breaks down when the vessel wall velocity approaches the same order of magnitude as the lymphocyte velocity. While this scenario only occurs approximately 20% of the time in mesenteric lymphatics, more extensive modeling could potentially provide useful information for studying shear stress in low flow situations where the vessel contraction has been shown to be very active in isolated vessels.

One of the main difficulties encountered in quantifying lymph velocity in these experiments was the tedious manual lymphocyte tracking procedure used to process the thousands of images generated by the high speed microscopy system and to produce only a few minutes worth of data. It was very important to meticulously process the images in the initial studies in order to ensure that the velocities were calculated as accurately as possible, since they were intended to provide a framework for future studies with isolated vessels and with cell culture models. This method of processing is not , however, ideal for most physiological studies, since it takes so long to acquire the final data from each experiment. Multiple image processing software packages were tested with the image sets; however, they all produced spurious results due to the

inherent low contrast at the imaging site. While introduction of fluorescent particles into the animal could have enhanced this contrast, it was undesirable to use foreign particles with a system that is so closely tied to the immune system. A method was therefore sought that would be able to automatically extract information about lymph flow from a sequence of images using the contrast inherent to those image. This goal was obtained through the development of an image correlation program. By using this program to measure vessel wall location first, the algorithm was also able to compensate for motion artifact and to process sections of images where particle velocities were known to occur (i.e. inside of the vessel walls). It was demonstrated that the velocities the program calculates fall somewhere between the spatially averaged velocity of a Poiseuille flow model and the peak center velocity. As to which value is best represented, it most likely depends on the radial distribution of lymphocytes in the vessel. If the majority of the lymphocytes are flowing through the center of the vessel, then the program-generated velocity more closely approaches the peak velocity; however, if the lymphocyte density is very large, necessitating that the lymphocytes be more evenly distributed across the radius, then the program-generated velocity approaches the spatially averaged velocity. Future work could be done to quantify this dependence and to develop a method for automatically determining lymphocyte distribution, so that a calibration algorithm could be written into the program to compensate for it.

In its current state, however, this image correlation program should work quite well for future physiological studies, provided that the main parameter of interest is the temporal fluctuation in flow before and after various conditions are imposed on the

lymphatic vessel. This algorithm could also be modified and implemented to provide real time measurements of flow fluctuations, which could be useful for numerous physiological studies. In conclusion, this research has provided quantitative measurements of lymphocyte velocity and of various other parameters, has resulted in estimations of wall shear stress that have proven to be reasonable for a majority of the contraction cycle, has produced a correlation algorithm capable of measuring velocity fluctuations with an accuracy of approximately 0.4 mm/sec, and has generated a solid framework upon which future studies in lymphatics can build.

REFERENCES

[1] A. C. Guyton, *Textbook of Medical Physiology*, 9 ed. Philadelphia: W.B. Saunders Company, 1996.

[2] A. R. Hargens and B. W. Zweifach, "Contractile stimuli in collecting lymph vessels," *American Journal of Physiology*, vol. 233, pp. H57-H65, 1977.

[3] N. L. Harvey, R. S. Srinivasan, M. E. Dillard, N. C. Johnson, M. H. Witte, K. Boyd, M. W. Sleeman, and G. Oliver, "Lymphatic vascular defects promoted by Prox1 haploinsufficiency cause adult-onset obesity," *Nat Genet*, vol. 37, pp. 1072-81, 2005.

[4] R. Smith, "Lymphatic contractility. A possible intrinsic mechanism of lymphatic vessels for the transport of lymph.," *Journal of Experimental Medicine*, vol. 90, pp. 497-509, 1949.

[5] T. Campbell and T. Heath, "Intrinsic contractility of lymphatics in sheep and in dogs.," *Quarterly J Exptl Physiol*, vol. 58, pp. 207-217, 1973.

[6] S. Armenio, F. Cetta, G. Tanzini, C. Guercia, and F. Burroni, "Spontaneous contractility of the lymphatic vessels in man," *Angiologia*, vol. 33, pp. 325-7, 1981.

[7] J. B. Kinmonth and G. W. Taylor, "Spontaneous rhythmic contractility in human lymphatics.," *J Physiol*, vol. 133, pp. 3P, 1956.

[8] W. L. Olszewski and A. Engeset, "Intrinsic contractility of pre-nodal lymph vessels and lymph-flow in human leg," *American Journal of Physiology*, vol. 239, pp. H775-H783, 1980.

[9] G. W. Schmidschonbein, "Microlymphatics and lymph-flow," *Physiological Reviews*, vol. 70, pp. 987-1028, 1990.

[10] T. Ohhashi, T. Azuma, and M. Sakaguchi, "Active and passive mechanical characteristics of bovine mesenteric lymphatics," *American Journal of Physiology*, vol. 239, pp. H88-95, 1980.

[11] G. W. Schmid-Schonbein, "Mechanisms causing initial lymphatics to expand and compress to promote lymph flow.," *Arch Histol Cytol*, vol. 53 Suppl, pp. 107-14, 1990.

[12] M. Muthuchamy, A. Gashev, N. Boswell, N. Dawson, and D. Zawieja, "Molecular and functional analyses of the contractile apparatus in lymphatic muscle," *Faseb Journal*, vol. 17, pp. -, 2003.

[13] M. Takada, "The ultrastructure of lymphatic valves in rabbits and mice.," *Amer J Anatomy*, vol. 32, pp. 207-217, 1971.

[14] M. Papp, S. Viragh, and G. Ungvary, "Structure of cutaneous lymphatics propelling lymph.," *Acta Med Acad Sci Hung*, vol. 32, pp. 311-20, 1975.

[15] G. W. Schmid-Schonbein, "Microlymphatics and Lymph Flow," *Physiological Reviews*, vol. 70, pp. 987-1028, 1990.

[16] T. Ohhashi, "Comparison of viscoelastic properties of walls and functional characteristics of valves in lymphatic and venous vessels," *Lymphology*, vol. 20, pp. 219-23, 1987.

[17] D. C. Zawieja, K. L. Davis, R. Schuster, W. M. Hinds, and H. J. Granger, "Distribution, propagation, and coordination of contractile activity in lymphatics," *American Journal of Physiology*, vol. 264, pp. H1283-H1291, 1993.

[18] J. Zhang, H. W. Li, and R. J. Xiu, "The role of microlymphatic valve in the propagation of spontaneous rhythmical lymphatic motion in rat," *Clinical Hemorheology and Microcirculation*, vol. 23, pp. 349-353, 2000.

[19] K. Nakamura and T. Yamamoto, "Morphology of smooth muscle cells in the rat thoracic duct. A scanning and transmission electron-microscope study.," *Cell Tissue Res*, vol. 251, pp. 243-8, 1988.

[20] S. Baez, "Flow properties of lymph - a microcirculation study," in *Flow Properties of Blood and other Biological Systems*. New York: Pergamon Press, 1960.

[21] M. Fischer, U. Costanzo, U. Hoffmann, A. Bollinger, and U. K. Franzeck, "Flow velocity of cutaneous lymphatic capillaries in patients with primary lymphedema," *International Journal of Microcirculation-Clinical and Experimental*, vol. 17, pp. 143-149, 1997.

[22] M. Fischer, U. K. Franzeck, I. Herrig, U. Costanzo, S. Wen, M. Schiesser, U. Hoffmann, and A. Bollinger, "Flow velocity of single lymphatic capillaries in human skin," *American Journal of Physiology-Heart and Circulatory Physiology*, vol. 39, pp. H358-H363, 1996.

[23] A. J. Leu, D. A. Berk, F. Yuan, and R. K. Jain, "Flow velocity in the superficial lymphatic network of the mouse tail," *American Journal of Physiology-Heart and Circulatory Physiology*, vol. 36, pp. H1507-H1513, 1994.

[24] J. N. Benoit, D. C. Zawieja, A. H. Goodman, and H. J. Granger, "Characterization of intact mesenteric lymphatic pump and its responsiveness to acute edemagenic stress," *American Journal of Physiology*, vol. 257, pp. H2059-H2069, 1989.

[25] A. A. Gashev, M. J. Davis, and D. C. Zawieja, "Inhibition of the active lymph pump by flow in rat mesenteric lymphatics and thoracic duct," *Journal of Physiology-London*, vol. 540, pp. 1023-1037, 2002.

[26] P. F. Davies, "Mechanical sensing mechanisms: shear stress and endothelial cells," *J Vasc Surg*, vol. 13, pp. 729-31, 1991.

[27] P. F. Davies, "Flow-mediated endothelial mechanotransduction," *Physiological Reviews*, vol. 75, pp. 519-560, 1995.

[28] P. F. Davies, A. Robotewskyj, M. L. Griem, R. O. Dull, and D. C. Polacek, "Hemodynamic forces and vascular cell communication in arteries," *Arch Pathol Lab Med*, vol. 116, pp. 1301-6, 1992.

[29] P. F. Davies and S. C. Tripathi, "Mechanical stress mechanisms and the cell. An endothelial paradigm," *Circ Res*, vol. 72, pp. 239-45, 1993.

[30] A. M. Malek, G. H. Gibbons, V. J. Dzau, and S. Izumo, "Fluid shear-stress differentially modulates expression of genes encoding basic fibroblast growth-factor and platelet-derived growth factor-B chain in vascular endothelium," *Journal of Clinical Investigation*, vol. 92, pp. 2013-2021, 1993.

[31] A. A. Biewener and J. E. A. Bertram, "Structural response of growing bone to exercise and disuse," *Journal of Applied Physiology*, vol. 76, pp. 946-955, 1994.

[32] M. Liu, A. K. Tanswell, and M. Post, "Mechanical force-induced signal transduction in lung cells," *Am J Physiol*, vol. 277, pp. L667-83, 1999.

[33] H. R. Wirtz and L. G. Dobbs, "The effects of mechanical forces on lung functions," *Respir Physiol*, vol. 119, pp. 1-17, 2000.

[34] E. H. Burger and J. Klein-Nulend, "Microgravity and bone cell mechanosensitivity," *Bone*, vol. 22, pp. 127S-130S, 1998.

[35] M. V. Hillsley and J. A. Frangos, "Bone tissue engineering: the role of interstitial fluid flow," *Biotechnol Bioeng*, vol. 43, pp. 573-81, 1994.

[36] K. John and A. I. Barakat, "Modulation of ATP/ADP concentration at the endothelial surface by shear stress: effect of flow-induced ATP release," *Annals of Biomedical Engineering*, vol. 29, pp. 740-751, 2001.

[37] N. P. Reddy, "Lymph circulation - physiology, pharmacology, and biomechanics," *Crc Critical Reviews in Biomedical Engineering*, vol. 14, pp. 45-91, 1986.

[38] Y. Shirasawa, F. Ikomi, and T. Ohhashi, "Physiological roles of endogenous nitric oxide in lymphatic pump activity of rat mesentery *in vivo*," *American Journal of Physiology-Gastrointestinal and Liver Physiology*, vol. 278, pp. G551-G556, 2000.

[39] H. Sakai, F. Ikomi, and T. Ohhashi, "Effects of endothelin on spontaneous contractions in lymph vessels," *American Journal of Physiology-Heart and Circulatory Physiology*, vol. 277, pp. H459-H466, 1999.

[40] R. Mizuno, A. Koller, and G. Kaley, "Regulation of the vasomotor activity of lymph microvessels by nitric oxide and prostaglandins," *American Journal of Physiology-Regulatory Integrative and Comparative Physiology*, vol. 43, pp. R790-R796, 1998.

[41] A. Koller, R. Mizuno, and G. Kaley, "Flow reduces the amplitude and increases the frequency of lymphatic vasomotion: role of endothelial prostanoids," *American Journal of Physiology-Regulatory Integrative and Comparative Physiology*, vol. 277, pp. R1683-R1689, 1999.

[42] P. Y. von der Weid, J. Zhao, and D. F. Ven Helden, "Nitric oxide decreases pacemaker activity in lymphatic vessels of guinea pig mesentery," *American Journal of Physiology-Heart and Circulatory Physiology*, vol. 280, pp. H2707-H2716, 2001.

[43] R. Mizuno, G. Dornyei, A. Koller, and G. Kaley, "Myogenic responses of isolated lymphatics: modulation by endothelium," *Microcirculation*, vol. 4, pp. 413-20., 1997.

[44] N. G. Mchale and I. C. Roddie, "Effect of transmural pressure on pumping activity in isolated bovine lymphatic vessels," *Journal of Physiology-London*, vol. 261, pp. 255-269, 1976.

[45] A. A. Gashev, M. J. Davis, M. D. Delp, and D. C. Zawieja, "Regional variations of contractile activity in isolated rat lymphatics," *Microcirculation*, vol. 11, pp. 477-492, 2004.

[46] K. C. Boardman and M. A. Swartz, "Interstitial flow as a guide for lymphangiogenesis," *Circ Res*, vol. 92, pp. 801-8, 2003.

[47] C. L. Helm, M. E. Fleury, A. H. Zisch, F. Boschetti, and M. A. Swartz, "Synergy between interstitial flow and VEGF directs capillary morphogenesis in vitro through a gradient amplification mechanism," *Proc Natl Acad Sci U S A*, vol. 102, pp. 15779-84, 2005.

[48] C. P. Ng, C. L. Helm, and M. A. Swartz, "Interstitial flow differentially stimulates blood and lymphatic endothelial cell morphogenesis *in vitro*," *Microvasc Res*, vol. 68, pp. 258-64, 2004.

[49] X. P. Li, M. Su, C. A. West, C. F. He, S. J. Swanson, T. W. Secomb, and S. J. Mentzer, "Effect of shear stress on efferent lymph-derived lymphocytes in contact with activated endothelial monolayers," *In Vitro Cellular & Developmental Biology-Animal*, vol. 37, pp. 599-605, 2001.

[50] B. Fagrell, A. Fronek, and M. Intaglietta, "Microscope-television system for studying flow velocity in human-skin capillaries," *American Journal of Physiology*, vol. 233, pp. H318-H321, 1977.

[51] G. Saintemarie, F. S. Peng, and C. Belisle, "Overall architecture and pattern of lymph-flow in the rat lymph-node," *American Journal of Anatomy*, vol. 164, pp. 275-309, 1982.

[52] T. O. Neild, "Measurement of arteriole diameter changes by analysis of television images," *Blood Vessels*, vol. 26, pp. 48-52, 1989.

[53] K. Tsukada, H. Minamitani, E. Sekizuka, and C. Oshio, "Image correlation method for measuring blood flow velocity in microcirculation: correlation 'window' simulation and in vivo image analysis," *Physiological Measurement*, vol. 21, pp. 459-471, 2000.

[54] S. Miura, E. Sekizuka, H. Nagata, C. Oshio, H. Minamitani, M. Suematsu, M. Suzuki, Y. Hamada, K. Kobayashi, H. Asakura, and et al., "Increased lymphocyte transport by lipid absorption in rat mesenteric lymphatics," *American Journal of Physiology*, vol. 253, pp. G596-600, 1987.

[55] E. I. Galanzha, V. V. Tuchin, and V. P. Zharov, "*In vivo* integrated flow image cytometry and lymph/blood vessels dynamic microscopy," *Journal of Biomedical Optics*, vol. 10, pp. -, 2005.

[56] A. Bollinger, K. Jager, F. Sgier, and J. Seglias, "Fluorescence microlymphography," *Circulation*, vol. 64, pp. 1195-200, 1981.

[57] A. Bollinger, "Microlymphatics of human skin," *International Journal of Microcirculation: Clinical & Experimental*, vol. 12, pp. 1-15, 1993.

[58] D. A. Berk, M. A. Swartz, A. J. Leu, and R. K. Jain, "Transport in lymphatic capillaries .2. Microscopic velocity measurement with fluorescence photobleaching," *American Journal of Physiology-Heart and Circulatory Physiology*, vol. 39, pp. H330-H337, 1996.

[59] M. A. Swartz, D. A. Berk, and R. K. Jain, "Transport in lymphatic capillaries .1. Macroscopic measurements using residence time distribution theory," *American Journal of Physiology-Heart and Circulatory Physiology*, vol. 39, pp. H324-H329, 1996.

[60] H. Mishina, T. Asakura, and S. Nagai, "Laser doppler microscope," *Optics Communications*, vol. 11, pp. 99-102, 1974.

[61] G. E. Nilsson, T. Tenland, and P. A. Oberg, "Evaluation of a laser dopler flowmeter for measurement of tissue blood flow," *Ieee Transactions on Biomedical Engineering*, vol. 27, pp. 597-604, 1980.

[62] R. Bonner and R. Nossal, "Model for Laser doppler Measurements of Blood-Flow in Tissue," *Applied Optics*, vol. 20, pp. 2097-2107, 1981.

[63] J. S. Cole and C. J. Hartley, "The pulsed doppler coronary artery catheter preliminary report of a new technique for measuring rapid changes in coronary artery flow velocity in man," *Circulation*, vol. 56, pp. 18-25, 1977.

[64] Benchimo.A, K. B. Desser, and J. L. Gartlan, "Bidirectional Blood-Flow Velocity in Cardiac Chambers and Great Vessels Studied with doppler ultrasonic flowmeter," *American Journal of Medicine*, vol. 52, pp. 467-&, 1972.

[65] R. H. Mohiaddin, P. J. Kilner, S. Rees, and D. B. Longmore, "Magnetic-resonance volume flow and jet velocity mapping in aortic coarctation," *Journal of the American College of Cardiology*, vol. 22, pp. 1515-1521, 1993.

[66] S. J. Tang, M. L. Gordon, V. X. D. Yang, M. E. Faughnan, M. Cirocco, B. Qi, E. S. Yue, G. Gardiner, G. Haber, P. Kortan, G. Kandel, A. Vitkin, B. C. Wilson, and N. E. Marcon, "*In vivo* color doppler optical coherence tomography of mucocutaneous telangiectases in hereditary hemorrhagic telangiectasia," *Gastroenterology*, vol. 124, pp. A17-a17, 2003.

[67] S. Yazdanfar, A. M. Rollins, and J. A. Izatt, "In vivo imaging of human retinal flow dynamics by color doppler optical coherence tomography," *Archives of Ophthalmology*, vol. 121, pp. 235-239, 2003.

[68] G. V. Oliveira, D. Chinkes, C. Mitchell, G. Oliveras, H. K. Hawkins, and D. N. Herndon, "Objective assessment of burn scar vascularity, erythema, pliability, thickness, and planimetry," *Dermatologic Surgery*, vol. 31, pp. 48-58, 2005.

[69] C. L. Riordan, M. McDonough, J. M. Davidson, R. Corley, C. Perlov, R. Barton, J. Guy, and L. B. Nanney, "Noncontact laser doppler imaging in burn depth analysis of the extremities," *Journal of Burn Care & Rehabilitation*, vol. 24, pp. 177-186, 2003.

[70] R. Bray, K. Forrester, C. Leonard, R. McArthur, J. Tulip, and R. Lindsay, "Laser doppler imaging of burn scars: a comparison of wavelength and scanning methods," *Burns*, vol. 29, pp. 199-206, 2003.

[71] W. R. Schiller, R. L. Garren, R. C. Bay, M. H. Ruddell, G. A. Holloway, A. Mohty, and C. A. Luekens, "Laser doppler evaluation of burned hands predicts need for surgical grafting," *Journal of Trauma-Injury Infection and Critical Care*, vol. 43, pp. 35-39, 1997.

[72] A. Berger, H. G. Machens, and P. Mailaender, "Approaches to postoperative blood flow monitoring after free tissue transfer. Which is the best?," *International Angiology*, vol. 14, pp. 288-296, 1995.

[73] S. Langer, P. Biberthaler, A. G. Harris, H. U. Steinau, and K. Messmer, "*In vivo* monitoring of microvessels in skin flaps: Introduction of a novel technique," *Microsurgery*, vol. 21, pp. 317-324, 2001.

[74] J. R. Payette, E. Kohlenberg, L. Leonardi, A. Pabbies, P. Kerr, K. Z. Liu, and M. G. Sowa, "Assessment of skin flaps using optically based methods for measuring blood flow and oxygenation," *Plastic and Reconstructive Surgery*, vol. 115, pp. 539-546, 2005.

[75] J. M. Jones, A. K. Gamperl, A. P. Farrell, and D. P. Toews, "Direct measurement of flow from the posterior lymph hearts of hydrated and dehydrated toads (Bufo marinus)," *Journal of Experimental Biology*, vol. 200, pp. 1695-1702, 1997.

[76] V. X. D. Yang, M. L. Gordon, S. J. Tang, N. E. Marcon, G. Gardiner, B. Qi, S. Bisland, E. Seng-Yue, S. Lo, J. Pekar, B. C. Wilson, and I. A. Vitkin, "High speed, wide velocity dynamic range doppler optical coherence tomography (Part III): *in vivo* endoscopic imaging of blood flow in the rat and human gastrointestinal tracts," *Optics Express*, vol. 11, pp. 2416-2424, 2003.

[77] J. A. Izatt, M. D. Kulkami, S. Yazdanfar, J. K. Barton, and A. J. Welch, "*In vivo* bidirectional color doppler flow imaging of picoliter blood volumes using optical coherence tomograghy," *Optics Letters*, vol. 22, pp. 1439-1441, 1997.

[78] H. W. Ren, K. M. Brecke, Z. H. Ding, Y. H. Zhao, J. S. Nelson, and Z. P. Chen, "Imaging and quantifying transverse flow velocity with the doppler bandwidth in a phase-resolved functional optical coherence tomography," *Optics Letters*, vol. 27, pp. 409-411, 2002.

[79] B. H. Park, M. C. Pierce, B. Cense, and J. F. de Boer, "Real-time multi-functional optical coherence tomography," *Optics Express*, vol. 11, pp. 782-793, 2003.

[80] R. A. Leitgeb, W. Drexler, A. Unterhuber, B. Hermann, T. Bajraszewski, T. Le, A. Stingl, and A. F. Fercher, "Ultrahigh resolution fourier domain optical coherence tomography," *Optics Express*, vol. 12, pp. 2156-2165, 2004.

[81] A. F. Fercher, M. Peukert, and E. Roth, "Visualization and measurement of retinal blood-flow by means of laser speckle photography," *Optical Engineering*, vol. 25, pp. 731-735, 1986.

[82] H. Fujii, T. Asakura, K. Nohira, Y. Shintomi, and T. Ohura, "Blood-flow observed by time-varying laser speckle," *Optics Letters*, vol. 10, pp. 104-106, 1985.

[83] J. D. Briers, "Optical filtering techniques to enhance speckle contrast variations in single-exposure laser speckle photography," *Optik*, vol. 63, pp. 265-276, 1983.

[84] J. D. Briers and A. F. Fercher, "Retinal blood-flow visualization by means of laser speckle photography," *Investigative Ophthalmology & Visual Science*, vol. 22, pp. 255-259, 1982.

[85] Y. Aizu, H. Ambar, T. Yamamoto, and T. Asakura, "Measurements of flow velocity in a microscopic region using dynamic laser speckles based on the photon-correlation," *Optics Communications*, vol. 72, pp. 269-273, 1989.

[86] Y. Aizu and T. Asakura, "Bio-speckle phenomena and their application to the evaluation of blood-flow," *Optics and Laser Technology*, vol. 23, pp. 205-219, 1991.

[87] I. V. Fedosov, E. I. Galanzha, A. V. Solov'eva, and V. V. Tuchin, "Laser monitoring of the flow velocity in lymphatic microvessels based on a spatiotemporal correlation of the dynamic speckle fields," *Technical Physics Letters*, vol. 28, pp. 690-692, 2002.

[88] S. S. UlYanov, V. V. Tuchin, A. A. Bednov, G. E. Brill, and E. I. Zakharova, "The application of speckle interferometry for the monitoring of blood and

lymph flow in microvessels," *Lasers in Medical Science*, vol. 11, pp. 97-107, 1996.

[89] I. V. Fedosov, V. V. Tuchin, E. I. Galartzha, A. V. Solov'eva, and T. V. Stepanova, "Recording of lymph flow dynamics in microvessels using correlation properties of scattered coherent radiation," *Quantum Electronics*, vol. 32, pp. 970-974, 2002.

[90] W. Svensson, D. M. Glass, D. Bradley, and A. M. Peters, "Measurement of lymphatic function with technetium-99m-labelled polyclonal immunoglobulin," *European Journal of Nuclear Medicine*, vol. 26, pp. 504-510, 1999.

[91] C. L. Witte, M. H. Witte, E. C. Unger, W. H. Williams, M. J. Bernas, G. C. McNeill, and A. M. Stazzone, "Advances in imaging of lymph flow disorders," *Radiographics*, vol. 20, pp. 1697-1719, 2000.

[92] S. Cliff, A. J. Bedlow, A. W. B. Stanton, and P. S. Mortimer, "An *in vivo* study of the microlymphatics in psoriasis using fluorescence microlymphography," *British Journal of Dermatology*, vol. 140, pp. 61-66, 1999.

[93] O. Sorensen, A. Engeset, W. Olszewski, and T. Lindmo, "High-sensitivity optical lymph flow-meter.," *Lymphology*, vol. 15, pp. 29-31, 1982.

[94] P. A. Duffy, D. N. Granger, and A. E. Taylor, "Intestinal secretion induced by volume expansion in dog," *Gastroenterology*, vol. 75, pp. 413-418, 1978.

[95] H. H. Lipowsky, "Microvascular rheology and hemodynamics," *Microcirculation*, vol. 12, pp. 5-15, 2005.

[96] J. B. Dixon, D. C. Zawieja, A. A. Gashev, and G. L. Coté, "Measuring microlymphatic flow using fast video microscopy," *Journal of Biomedical Optics*, vol. 10, pp. 064016-1 to 064016-7, 2005.

[97] J. B. Dixon, J. Moore Jr., G. L. Coté, A. A. Gashev, and D. C. Zawieja, "Fluid velocity and wall shear stress in contracting mesenteric rat lymphatics *in situ*," *Microcirculation*, vol. in review, 2006.

[98] P. Tso and J. A. Balint, "Formation and transport of chylomicrons by enterocytes to the lymphatics," *Am. J. Physiol.*, vol. 250, pp. G715-G726, 1986.

[99] P. Tso, V. Pitts, and D. N. Granger, "Role of lymph flow in intestinal chylomicron transport," *Am J Physiol*, vol. 249, pp. G21-8., 1985.

[100] L. Kuo, W. M. Chilian, and M. J. Davis, "Coronary arteriolar myogenic response is independent of endothelium," *Circulation Research*, vol. 66, pp. 860-6., 1990.

[101] A. V. Clough, G. S. Krenz, M. Owens, A. Altinawi, C. A. Dawson, and J. H. Linehan, "An algorithm for angiographic estimation of blood-vessel diameter," *Journal of Applied Physiology*, vol. 71, pp. 2050-2058, 1991.

[102] S. Y. Molloi, A. Ersahin, W. W. Roeck, and O. Nalcioglu, "Absolute cross-sectional area measurements in quantitative coronary arteriography by dual-energy dsa," *Investigative Radiology*, vol. 26, pp. 119-127, 1991.

[103] C. Uyama, Y. Kita, and S. Matsusita, "Optimal sampling interval and edge-detection algorithm for measurement of blood-vessel diameter on a cineangiogram," *Investigative Radiology*, vol. 28, pp. 1128-1133, 1993.

APPENDIX I

PROTOCOL FOR PREPARATION OF APSS

PREPARATION OF APSS (ALBUMIN-PHYSIOLOGICAL SALT SOLUTION)

Salt	Chemical MW	Molarity (mM)	Amount per 1 liter	Amount per 2 liters
NaCl	58.44	145.000	8.47 g/l	16.94 g/2 l
KCl	74.56	4.700	0.35 g/l	0.7 g/2 l
$CaCl_2$ ($CaCl_2$*$2H_2O$)	110.99 (147.02)	2.000	0.22 g/l (0.29 g/l)	0.44 g/2 l (0.58 g/2 l)
$MgSO_4$ ($MgSO_4$*$7H_2O$)	120.37 (246.48)	1.170	0.14 g/l (0.29 g/l)	0.28 g/2 l (0.58 g/ 2 l)
NaH_2PO_4 (NaH_2PO_4*H_2O)	119.98 (137.99)	1.200	0.14 g/l (0.16 g/l)	0.28 g/2 l (0.32 g/ 2 l)
Dextrose	180.16	5.000	0.9 g/l	1.8 g/ 2 l
Sodium Pyruvate	100 mM solution	2.000	20 ml/l	40 ml/ 2 l
EDTA (EDTA*$2H_2O$)	292.25 (372.2)	0.020	0.0058 g/l (0.0074 g/l)	0.0116 g/ 2 l (0.0148 g/ 2 l)
MOPS	209.2	3.000	0.628 g/l	1.256 g/ 2 l

1. Fill 1 liter volumetric flask with 0.8 liters of RO H_2O or 2 liters flask with 1.6 liters of RO H_2O.
2. Add all above ingredients (for 1 liter or for 2 liters) while mixing and wait them to be dissolved.
3. Add 10 g/liter or 20 g/2 liters of Bovine Serum Albumin (96% minimum) to solution and mix until all BSA goes into solution.
4. Adjust volume to 1 or to 2 liters by RO H_2O.
5. pH all to 7.4 at room temperature.
6. Filter all (for more that one day storage or for use for vessels perfusion with vessels bigger that 0.5 mm in diameter).
7. Keep refrigerated and tightly closed.
8. Check pH and adjust if needed to 7.4 at the 38° C before use.

APPENDIX II

DIAMETER AND VELOCITY TRACINGS FOR EACH RAT

Rat 1

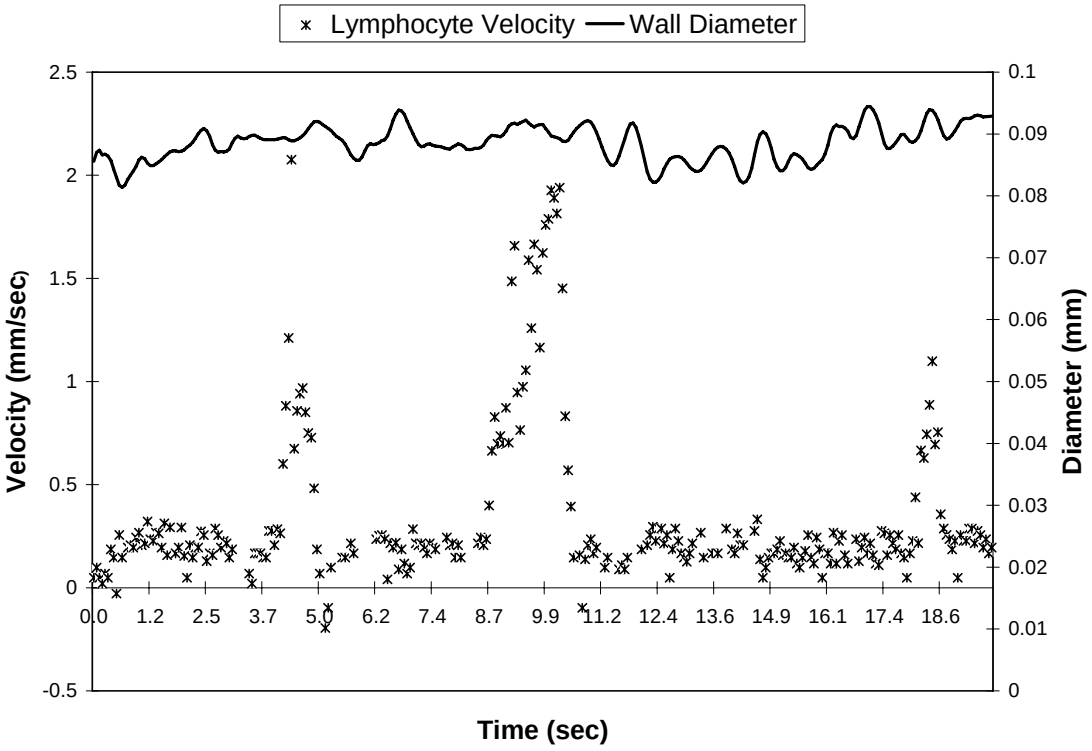
Lymphocyte Velocity
Wall Diameter
Velocity (mm/sec)
Diameter (mm)
Time (sec)
2.5
2
1.5
1
0.5
0
-0.5
0.1
0.09
0.08
0.07
0.06
0.05
0.04
0.03
0.02
0.01
0
0.0
1.2
2.5
3.7
5.0
6.2
7.4
8.7
9.9
11.2
12.4
13.6
14.9
16.1
17.4
18.6

Rat 1

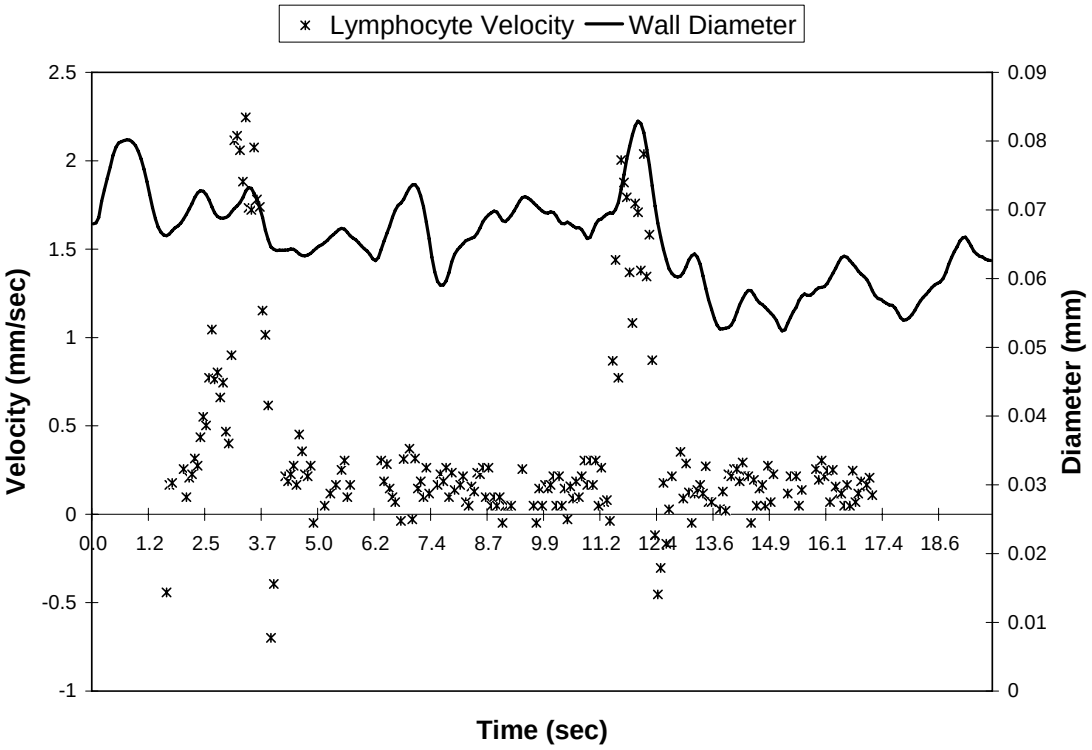
Lymphocyte Velocity
Wall Diameter
Velocity (mm/sec)
Diameter (mm)
Time (sec)
2.5
2
1.5
1
0.5
0
-0.5
-1
0.09
0.08
0.07
0.06
0.05
0.04
0.03
0.02
0.01
0
0.0
1.2
2.5
3.7
5.0
6.2
7.4
8.7
9.9
11.2
12.4
13.6
14.9
16.1
17.4
18.6

Rat 2

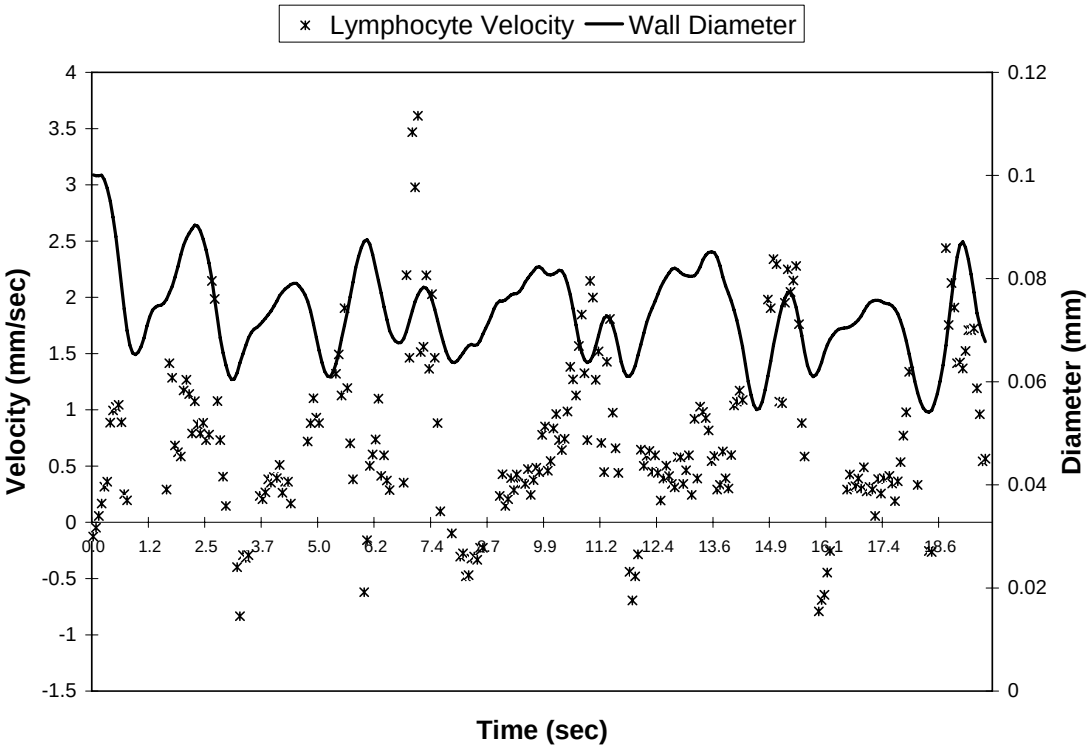
Lymphocyte Velocity
Wall Diameter
Velocity (mm/sec)
Diameter (mm)
Time (sec)
4
3.5
3
2.5
2
1.5
1
0.5
0
-0.5
-1
-1.5
0.12
0.1
0.08
0.06
0.04
0.02
0
0.0
1.2
2.5
3.7
5.0
6.2
7.4
8.7
9.9
11.2
12.4
13.6
14.9
16.1
17.4
18.6

Rat2

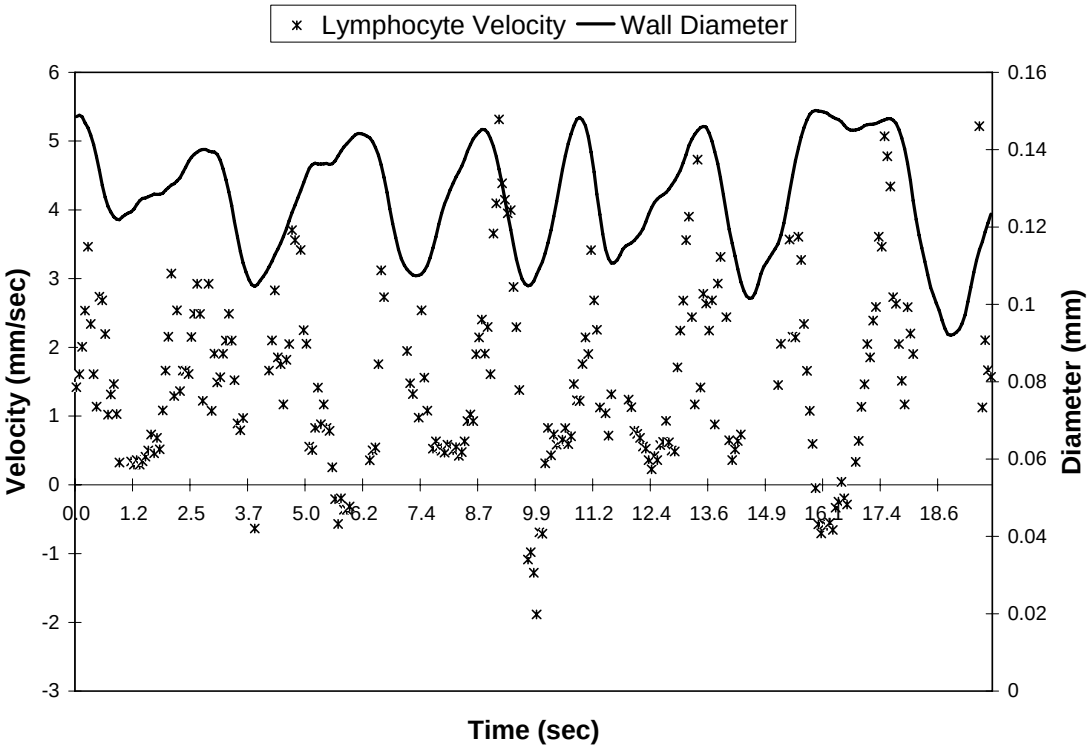
Lymphocyte Velocity
Wall Diameter
Velocity (mm/sec)
Diameter (mm)
Time (sec)
6
5
4
3
2
1
0
-1
-2
-3
0.16
0.14
0.12
0.1
0.08
0.06
0.04
0.02
0
0.0
1.2
2.5
3.7
5.0
6.2
7.4
8.7
9.9
11.2
12.4
13.6
14.9
16.1
17.4
18.6

Rat 2

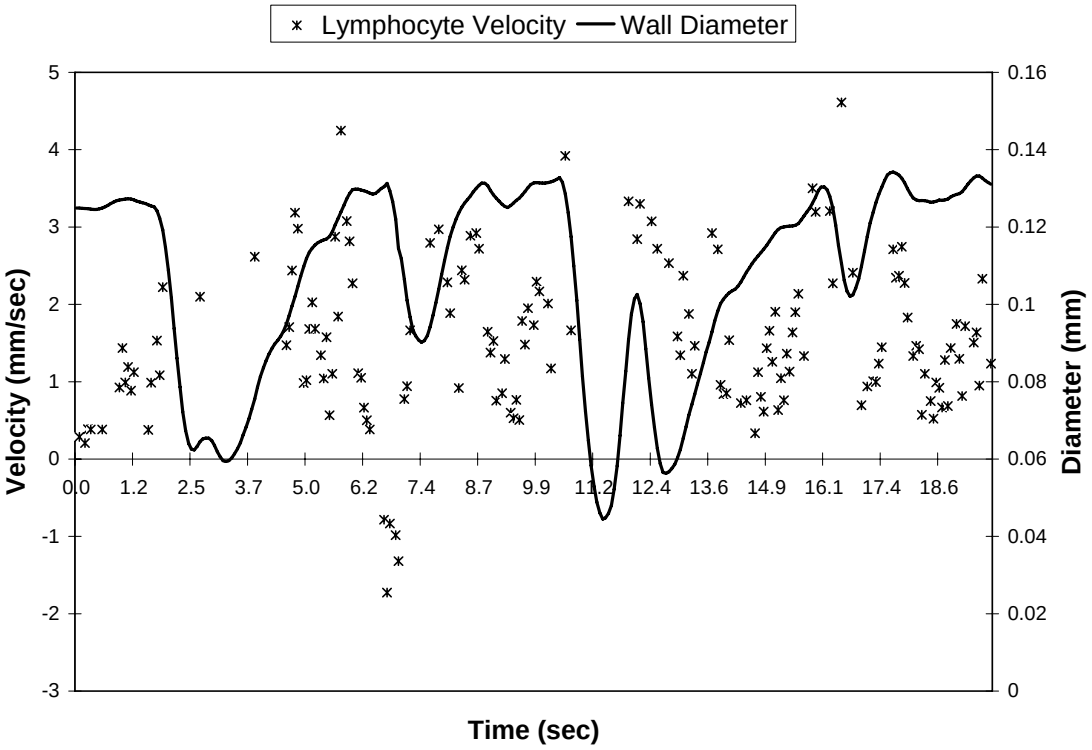
Lymphocyte Velocity
Wall Diameter
Velocity (mm/sec)
Diameter (mm)
Time (sec)
5
4
3
2
1
0
-1
-2
-3
0.16
0.14
0.12
0.1
0.08
0.06
0.04
0.02
0
0.0
1.2
2.5
3.7
5.0
6.2
7.4
8.7
9.9
11.2
12.4
13.6
14.9
16.1
17.4
18.6

Rat 2

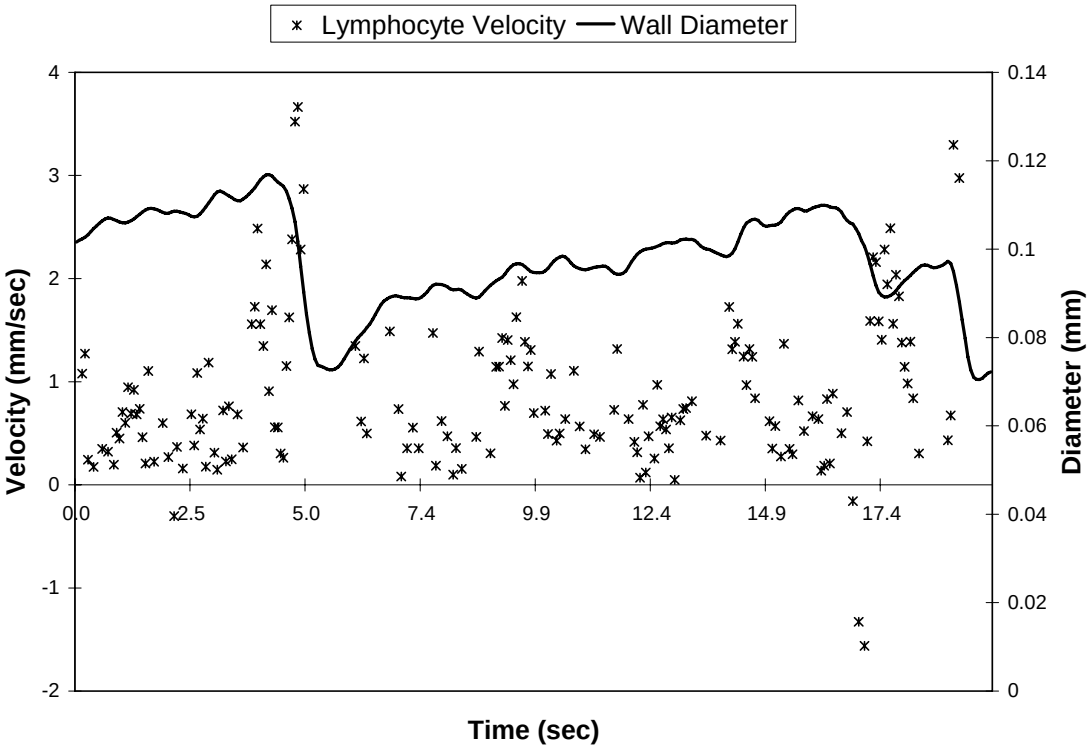
Lymphocyte Velocity
Wall Diameter
Velocity (mm/sec)
Diameter (mm)
Time (sec)
4
3
2
1
0
-1
-2
0.14
0.12
0.1
0.08
0.06
0.04
0.02
0
0.0
2.5
5.0
7.4
9.9
12.4
14.9
17.4

Rat 2

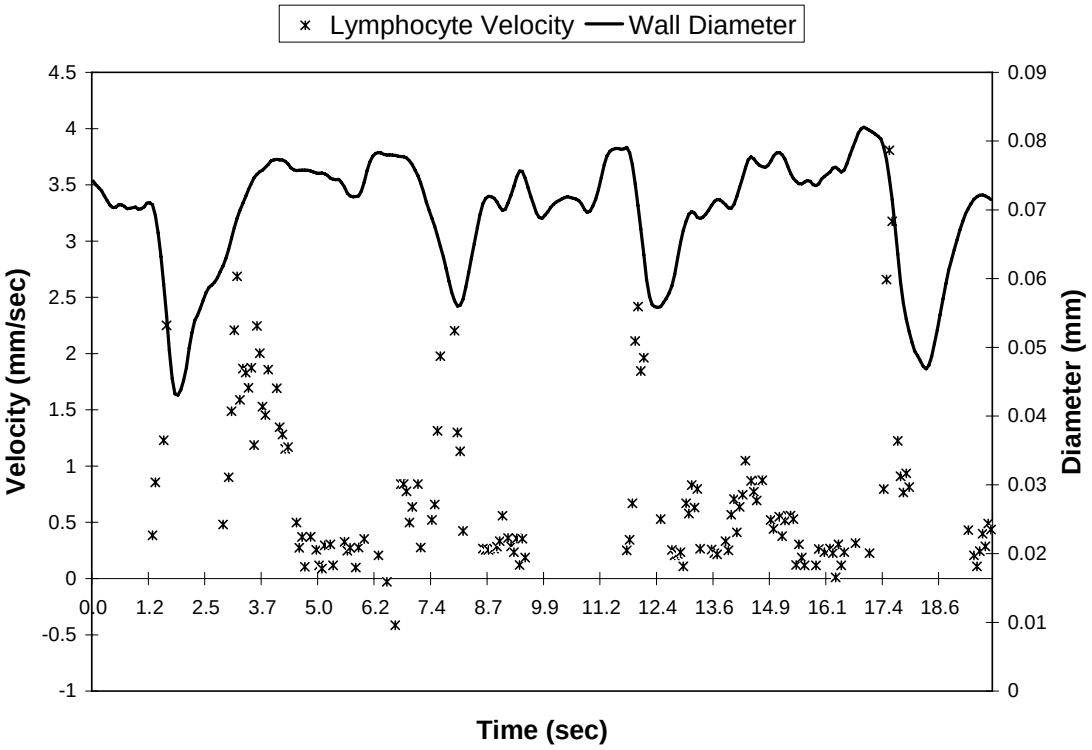
Lymphocyte Velocity
Wall Diameter
Velocity (mm/sec)
Diameter (mm)
Time (sec)
4.5
4
3.5
3
2.5
2
1.5
1
0.5
0
-0.5
-1
0.09
0.08
0.07
0.06
0.05
0.04
0.03
0.02
0.01
0
0.0
1.2
2.5
3.7
5.0
6.2
7.4
8.7
9.9
11.2
12.4
13.6
14.9
16.1
17.4
18.6

Rat 2

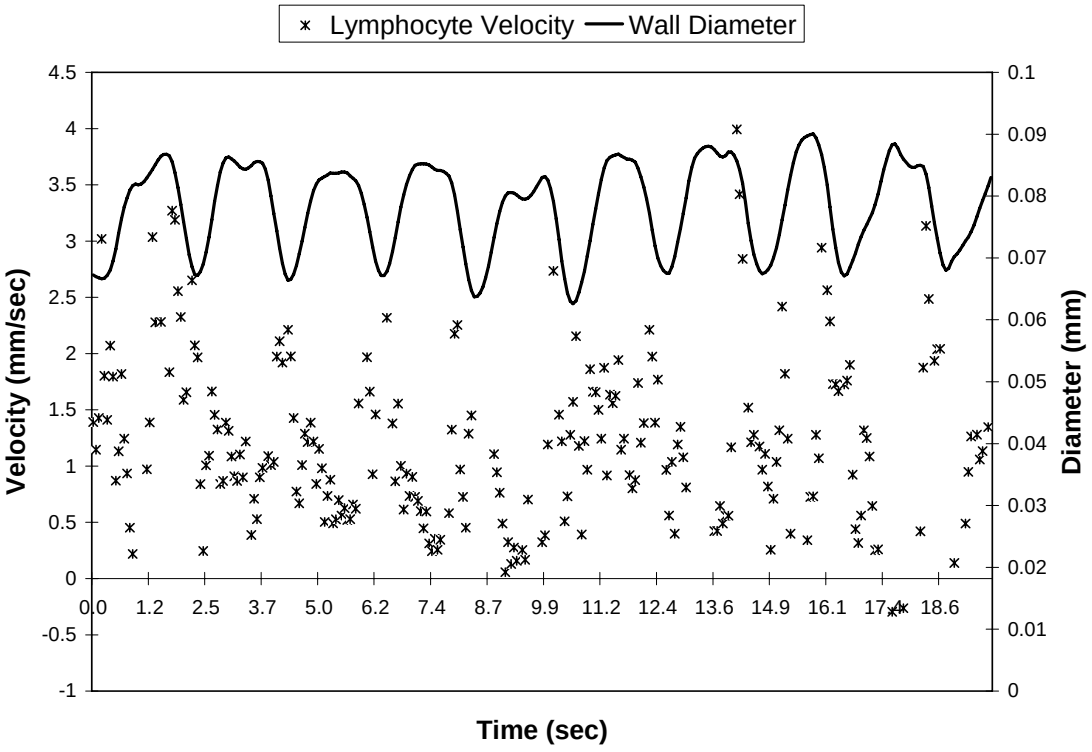
Lymphocyte Velocity
Wall Diameter
Velocity (mm/sec)
Diameter (mm)
Time (sec)
4.5
4
3.5
3
2.5
2
1.5
1
0.5
0
-0.5
-1
0.1
0.09
0.08
0.07
0.06
0.05
0.04
0.03
0.02
0.01
0
0.0
1.2
2.5
3.7
5.0
6.2
7.4
8.7
9.9
11.2
12.4
13.6
14.9
16.1
17.4
18.6

Rat 3

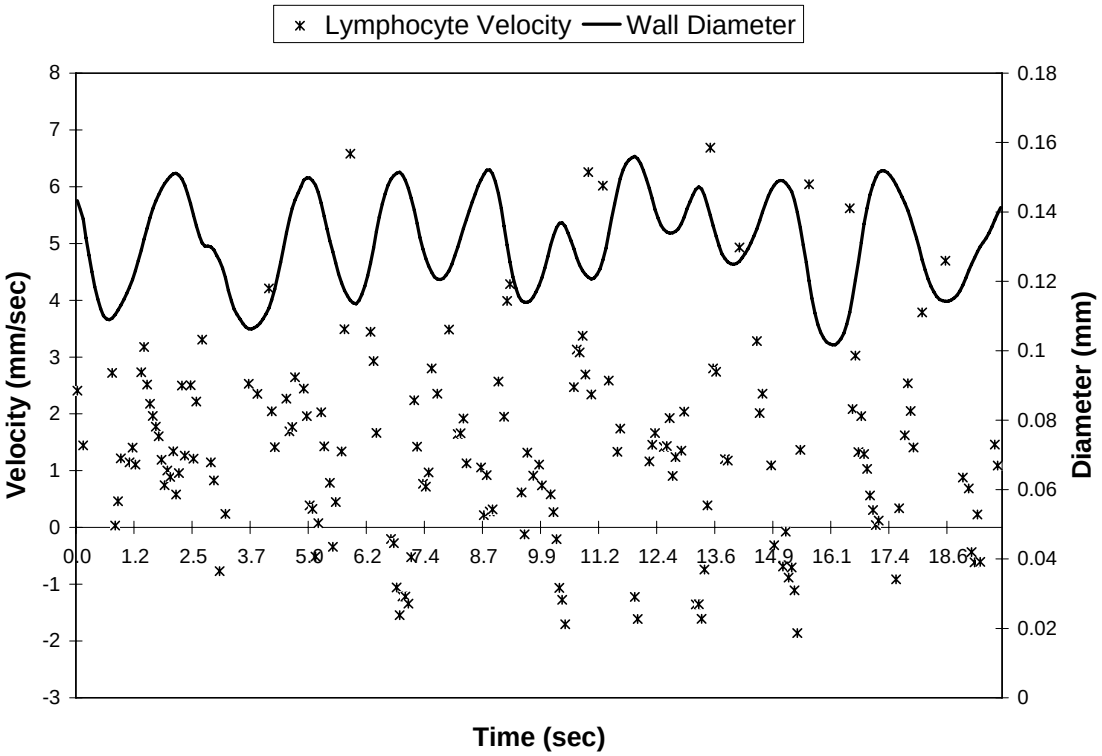
Lymphocyte Velocity
Wall Diameter
Velocity (mm/sec)
Diameter (mm)
Time (sec)
8
7
6
5
4
3
2
1
0
-1
-2
-3
0.18
0.16
0.14
0.12
0.1
0.08
0.06
0.04
0.02
0
0.0
1.2
2.5
3.7
5.0
6.2
7.4
8.7
9.9
11.2
12.4
13.6
14.9
16.1
17.4
18.6

Rat 3

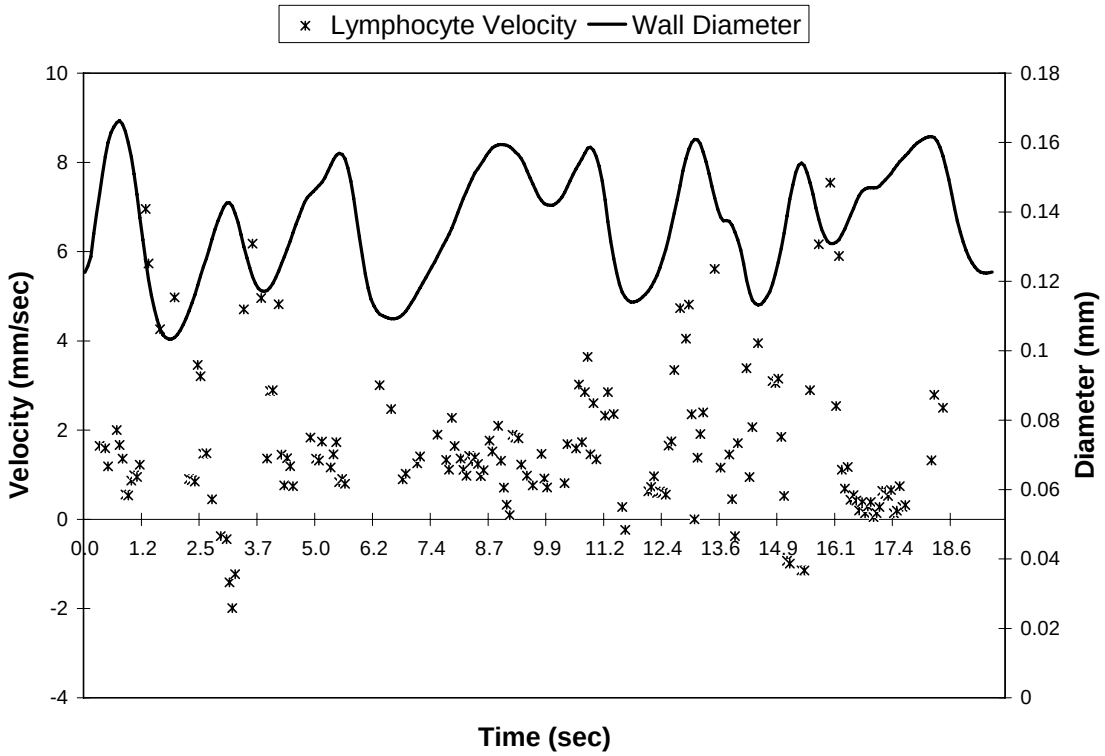
Lymphocyte Velocity
Wall Diameter
Velocity (mm/sec)
Diameter (mm)
Time (sec)
10
8
6
4
2
0
-2
-4
0.18
0.16
0.14
0.12
0.1
0.08
0.06
0.04
0.02
0
0.0
1.2
2.5
3.7
5.0
6.2
7.4
8.7
9.9
11.2
12.4
13.6
14.9
16.1
17.4
18.6

Rat 3

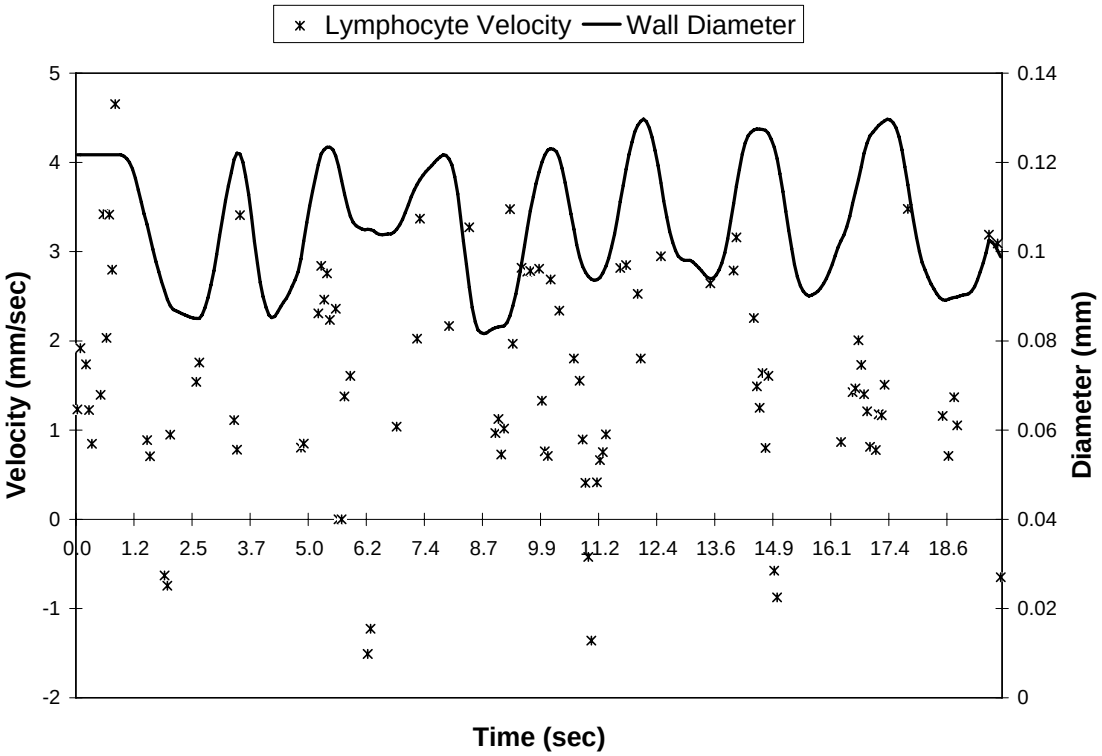
Lymphocyte Velocity
Wall Diameter
Velocity (mm/sec)
Diameter (mm)
Time (sec)
5
4
3
2
1
0
-1
-2
0.14
0.12
0.1
0.08
0.06
0.04
0.02
0
0.0
1.2
2.5
3.7
5.0
6.2
7.4
8.7
9.9
11.2
12.4
13.6
14.9
16.1
17.4
18.6

Rat 4

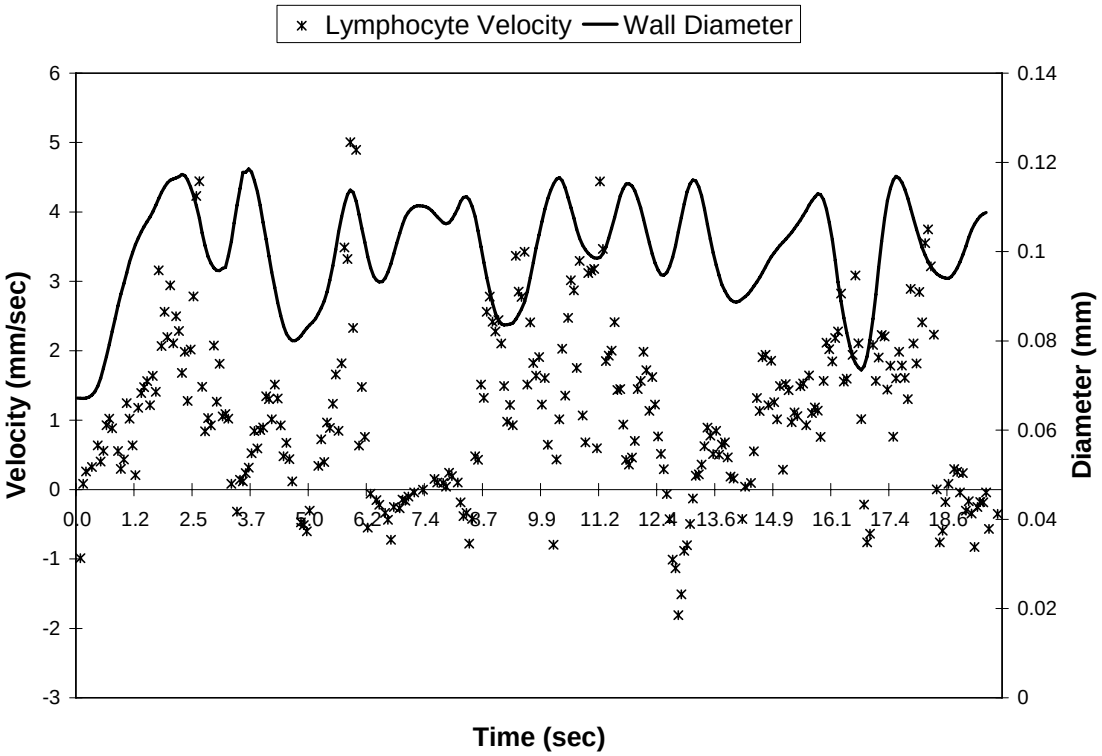
Lymphocyte Velocity
Wall Diameter
Velocity (mm/sec)
Diameter (mm)
Time (sec)
6
5
4
3
2
1
0
-1
-2
-3
0.14
0.12
0.1
0.08
0.06
0.04
0.02
0
0.0
1.2
2.5
3.7
5.0
6.2
7.4
8.7
9.9
11.2
12.4
13.6
14.9
16.1
17.4
18.6

Rat 4

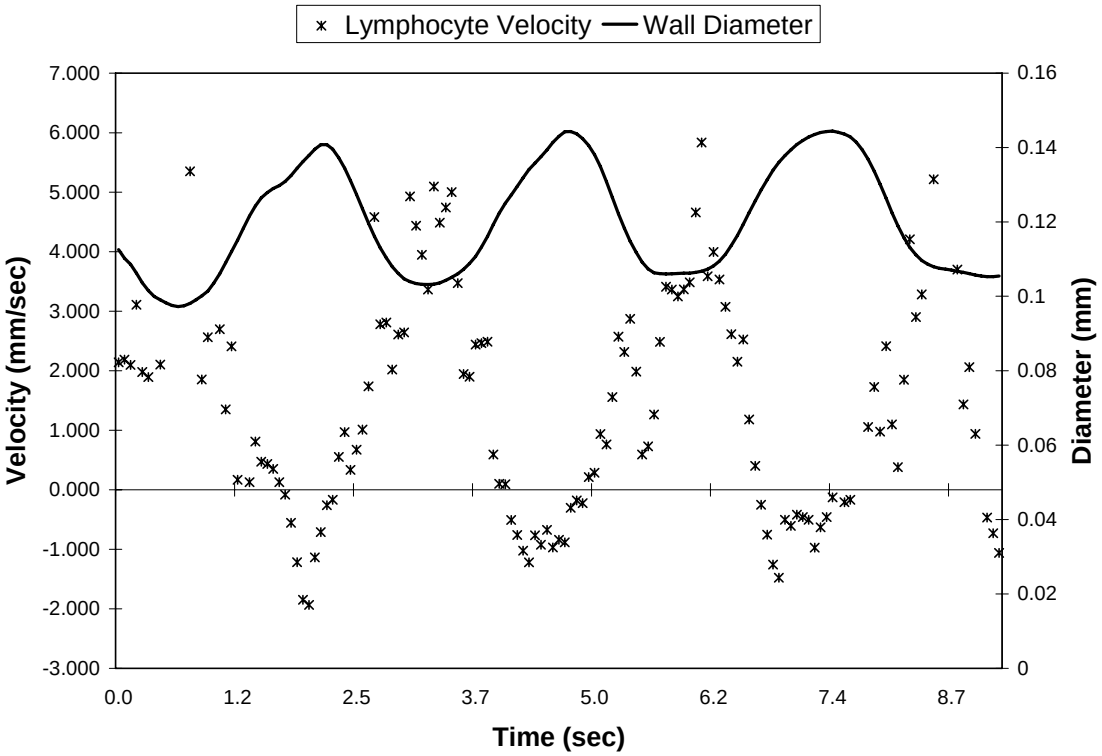
Lymphocyte Velocity
Wall Diameter
Velocity (mm/sec)
Diameter (mm)
Time (sec)
7.000
6.000
5.000
4.000
3.000
2.000
1.000
0.000
-1.000
-2.000
-3.000
0.16
0.14
0.12
0.1
0.08
0.06
0.04
0.02
0
0.0
1.2
2.5
3.7
5.0
6.2
7.4
8.7

Rat 4

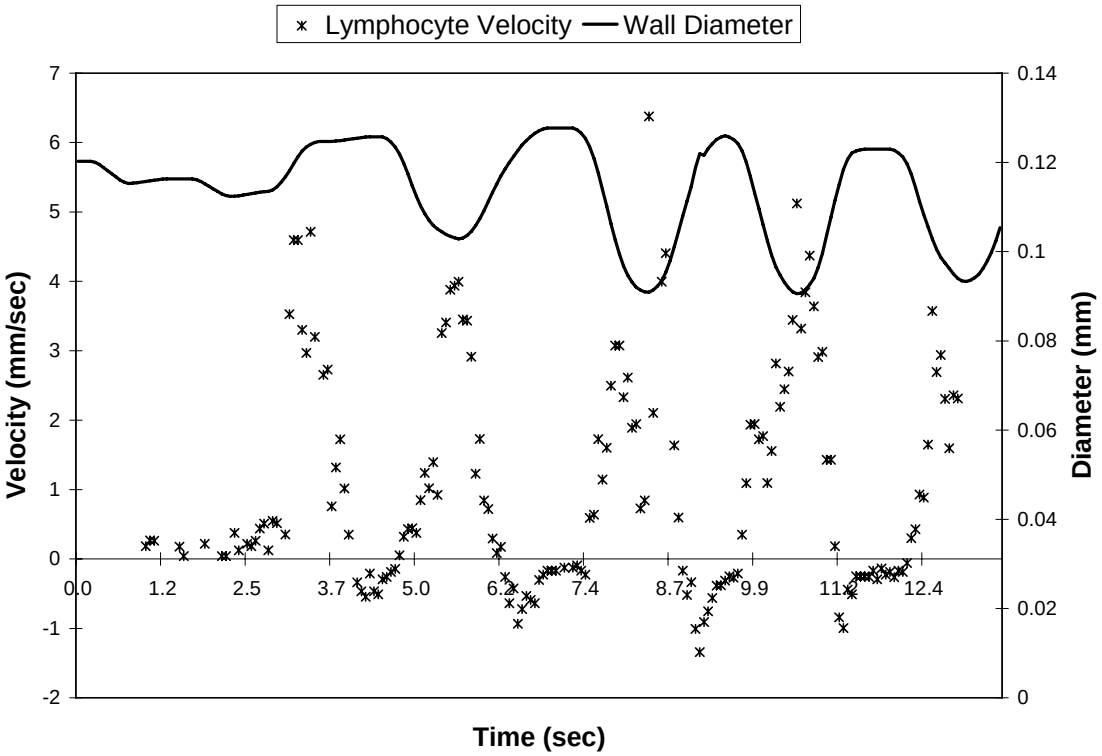
Lymphocyte Velocity
Wall Diameter
Velocity (mm/sec)
Diameter (mm)
Time (sec)
7
6
5
4
3
2
1
0
-1
-2
0.14
0.12
0.1
0.08
0.06
0.04
0.02
0
0.0
1.2
2.5
3.7
5.0
6.2
7.4
8.7
9.9
11.
12.4

Rat 4

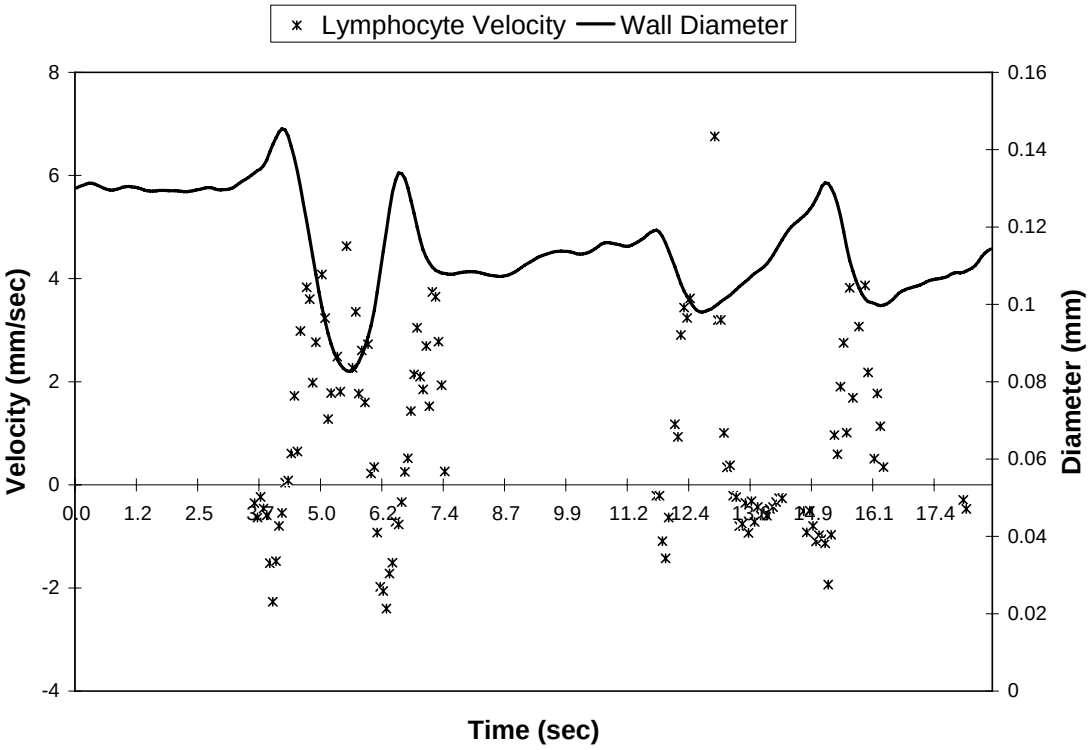
Lymphocyte Velocity
Wall Diameter
Velocity (mm/sec)
Diameter (mm)
Time (sec)
8
6
4
2
0
-2
-4
0.16
0.14
0.12
0.1
0.08
0.06
0.04
0.02
0
0.0
1.2
2.5
3.7
5.0
6.2
7.4
8.7
9.9
11.2
12.4
13.6
14.9
16.1
17.4

Rat 5

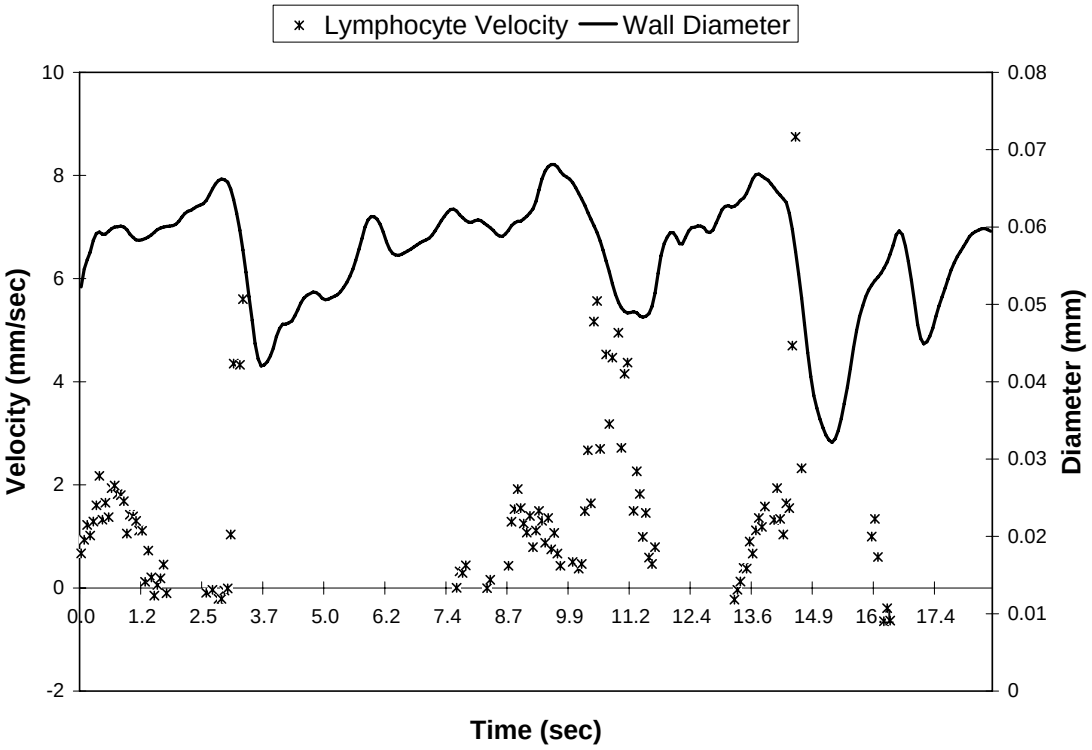
Lymphocyte Velocity
Wall Diameter
Velocity (mm/sec)
Diameter (mm)
Time (sec)
10
8
6
4
2
0
-2
0.08
0.07
0.06
0.05
0.04
0.03
0.02
0.01
0
0.0
1.2
2.5
3.7
5.0
6.2
7.4
8.7
9.9
11.2
12.4
13.6
14.9
16.1
17.4

Rat 5

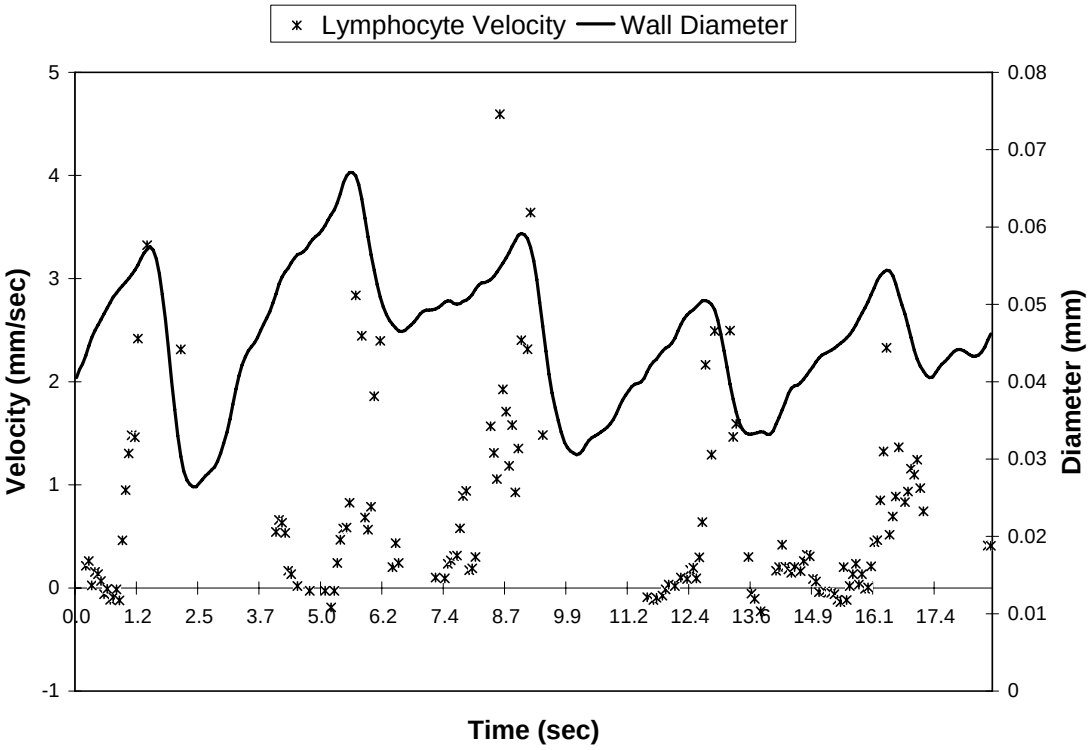
Lymphocyte Velocity
Wall Diameter
Velocity (mm/sec)
Diameter (mm)
Time (sec)
5
4
3
2
1
0
-1
0.08
0.07
0.06
0.05
0.04
0.03
0.02
0.01
0
0.0
1.2
2.5
3.7
5.0
6.2
7.4
8.7
9.9
11.2
12.4
13.6
14.9
16.1
17.4

Rat 5

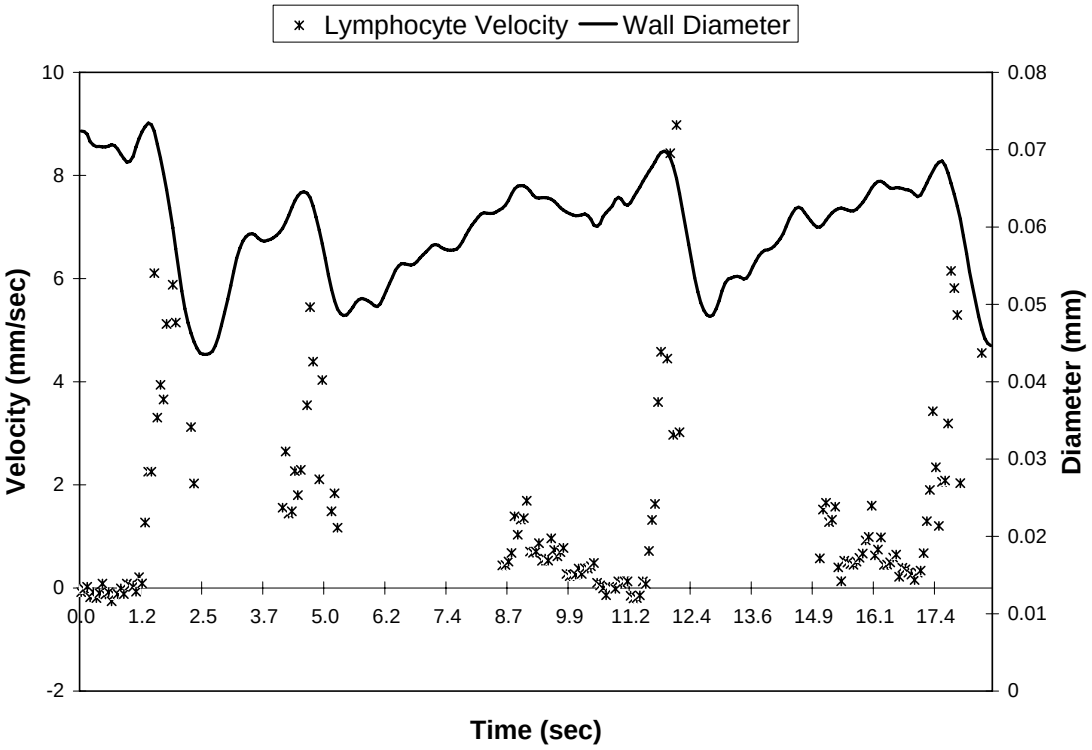
Lymphocyte Velocity
Wall Diameter
Velocity (mm/sec)
Diameter (mm)
Time (sec)
10
8
6
4
2
0
-2
0.08
0.07
0.06
0.05
0.04
0.03
0.02
0.01
0
0.0
1.2
2.5
3.7
5.0
6.2
7.4
8.7
9.9
11.2
12.4
13.6
14.9
16.1
17.4

Rat 5

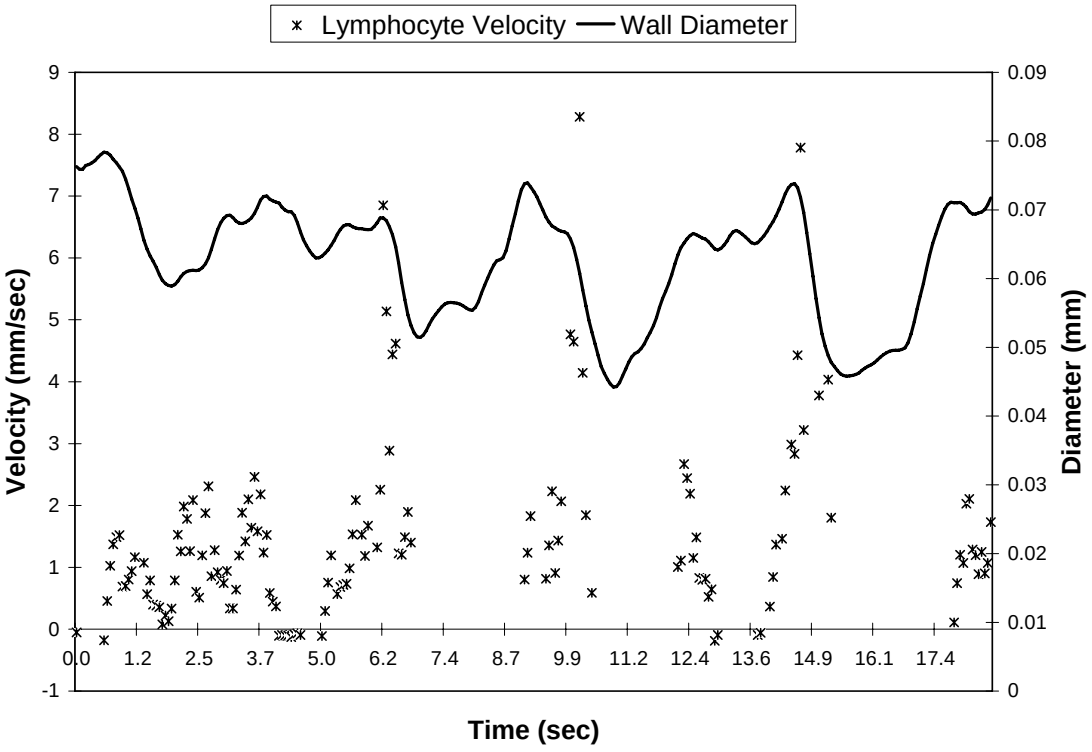
Lymphocyte Velocity
Wall Diameter
Velocity (mm/sec)
Diameter (mm)
Time (sec)
9
8
7
6
5
4
3
2
1
0
-1
0.09
0.08
0.07
0.06
0.05
0.04
0.03
0.02
0.01
0
0.0
1.2
2.5
3.7
5.0
6.2
7.4
8.7
9.9
11.2
12.4
13.6
14.9
16.1
17.4

Rat 5

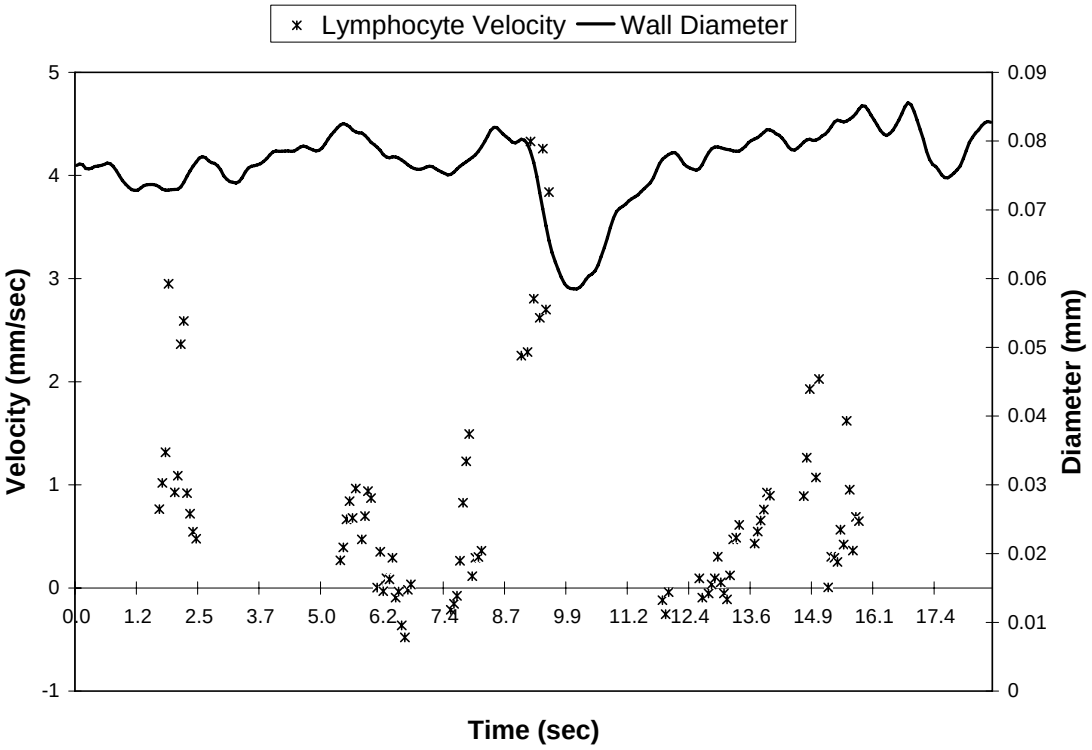
Lymphocyte Velocity
Wall Diameter
Velocity (mm/sec)
Diameter (mm)
Time (sec)
5
4
3
2
1
0
-1
0.09
0.08
0.07
0.06
0.05
0.04
0.03
0.02
0.01
0
0.0
1.2
2.5
3.7
5.0
6.2
7.4
8.7
9.9
11.2
12.4
13.6
14.9
16.1
17.4

Rat 5

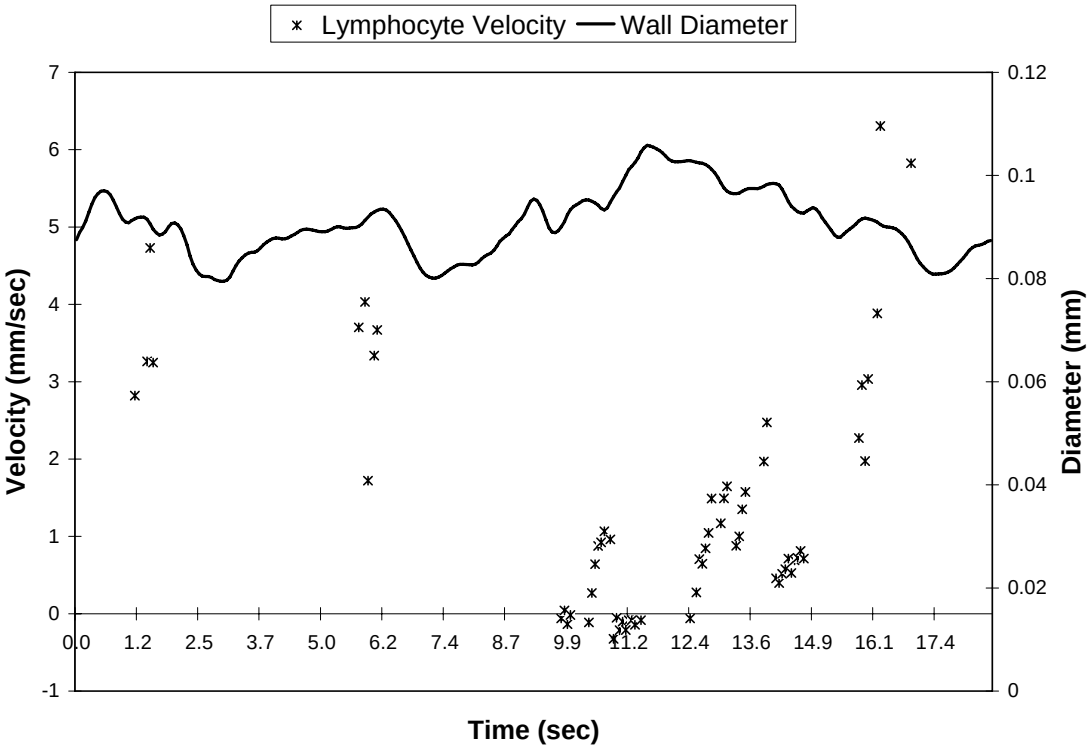
Lymphocyte Velocity
Wall Diameter
Velocity (mm/sec)
Diameter (mm)
Time (sec)
7
6
5
4
3
2
1
0
-1
0.12
0.1
0.08
0.06
0.04
0.02
0
0.0
1.2
2.5
3.7
5.0
6.2
7.4
8.7
9.9
11.2
12.4
13.6
14.9
16.1
17.4

Rat 6

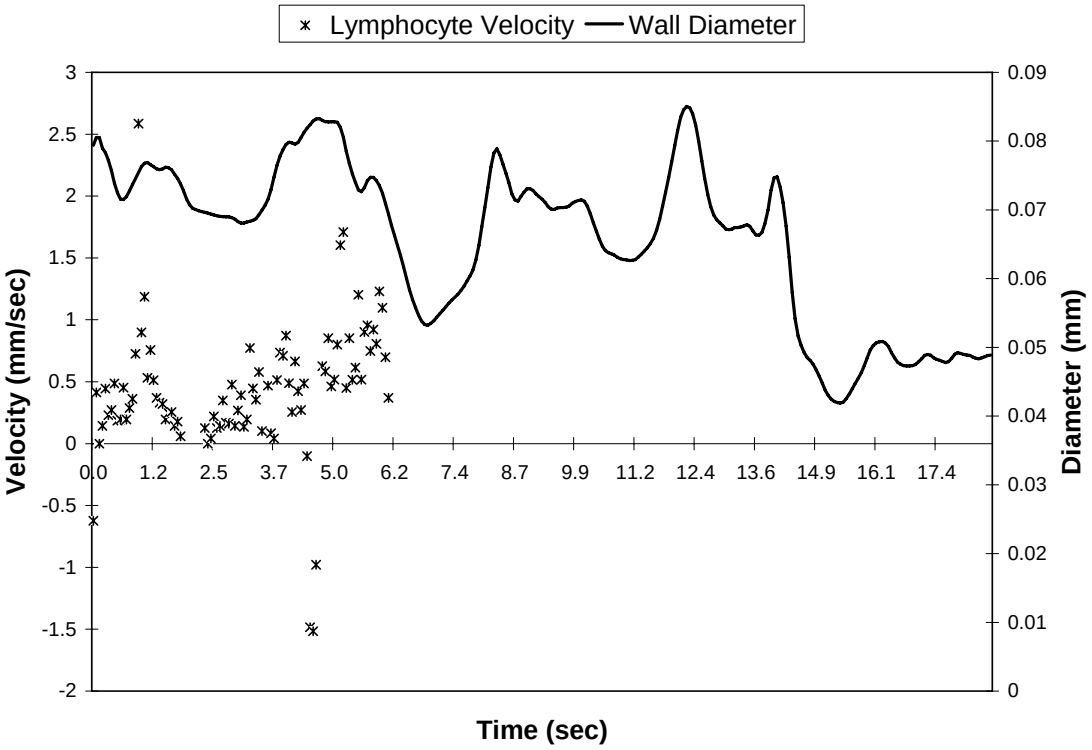
Lymphocyte Velocity
Wall Diameter
Velocity (mm/sec)
Diameter (mm)
Time (sec)
3
2.5
2
1.5
1
0.5
0
-0.5
-1
-1.5
-2
0.09
0.08
0.07
0.06
0.05
0.04
0.03
0.02
0.01
0
0.0
1.2
2.5
3.7
5.0
6.2
7.4
8.7
9.9
11.2
12.4
13.6
14.9
16.1
17.4

Rat 6

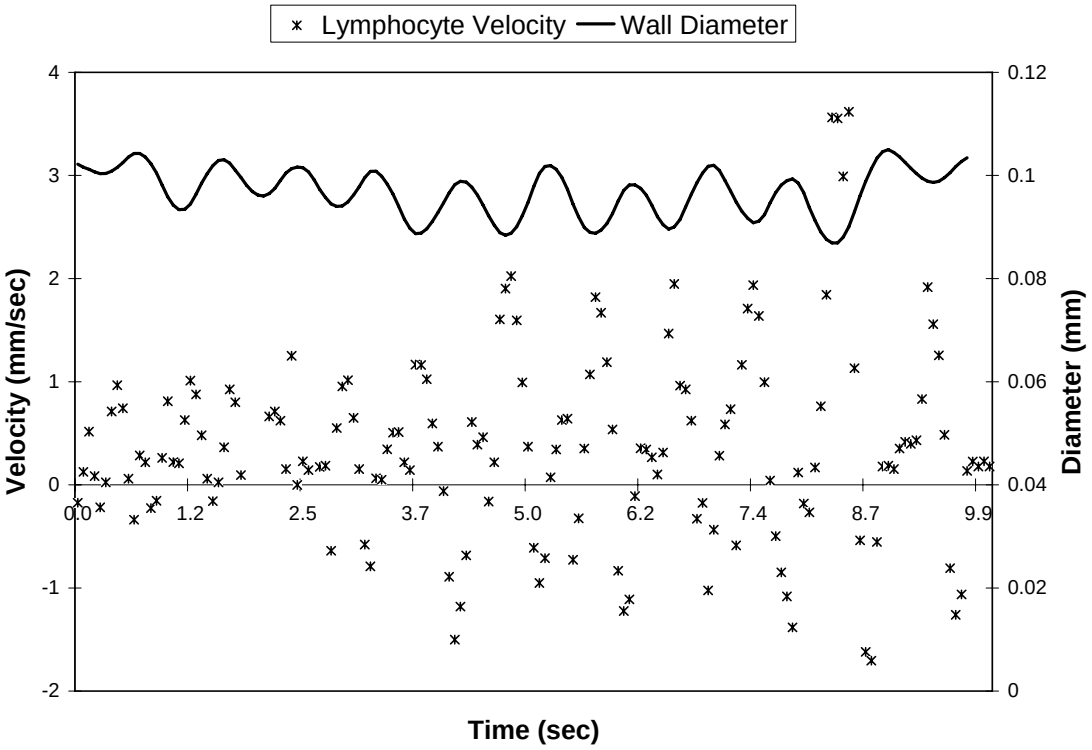
Lymphocyte Velocity
Wall Diameter
Velocity (mm/sec)
Diameter (mm)
Time (sec)
4
3
2
1
0
-1
-2
0.12
0.1
0.08
0.06
0.04
0.02
0
0.0
1.2
2.5
3.7
5.0
6.2
7.4
8.7
9.9

Rat 6

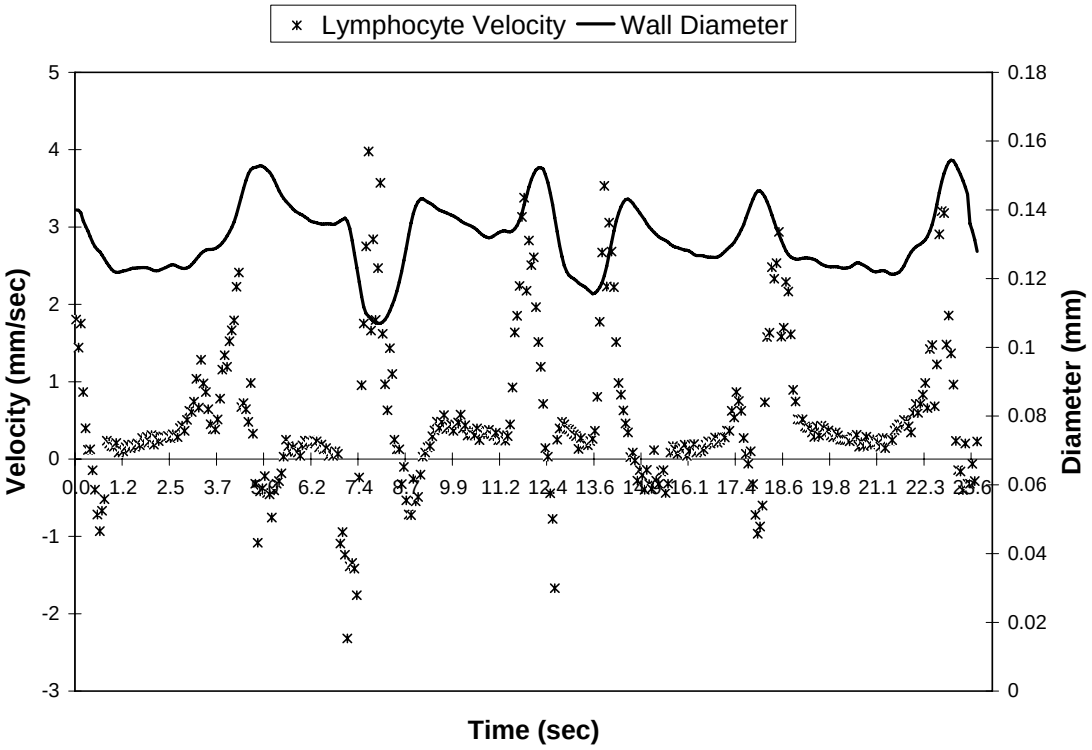
Lymphocyte Velocity
Wall Diameter
Velocity (mm/sec)
Diameter (mm)
Time (sec)
5
4
3
2
1
0
-1
-2
-3
0.18
0.16
0.14
0.12
0.1
0.08
0.06
0.04
0.02
0
0.0
1.2
2.5
3.7
6.2
7.4
9.9
11.2
12.4
13.6
16.1
17.4
18.6
19.8
21.1
22.3

Rat 7

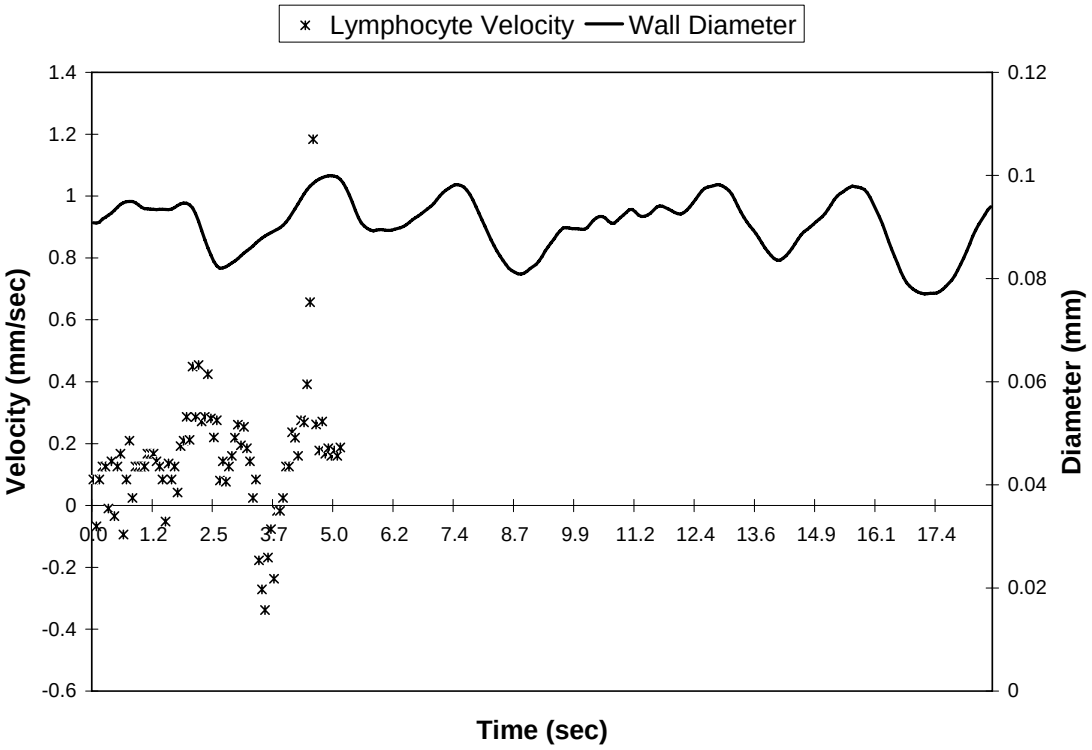
Lymphocyte Velocity
Wall Diameter
Velocity (mm/sec)
Diameter (mm)
Time (sec)
1.4
1.2
1
0.8
0.6
0.4
0.2
0
-0.2
-0.4
-0.6
0.12
0.1
0.08
0.06
0.04
0.02
0
0.0
1.2
2.5
3.7
5.0
6.2
7.4
8.7
9.9
11.2
12.4
13.6
14.9
16.1
17.4

Rat 7

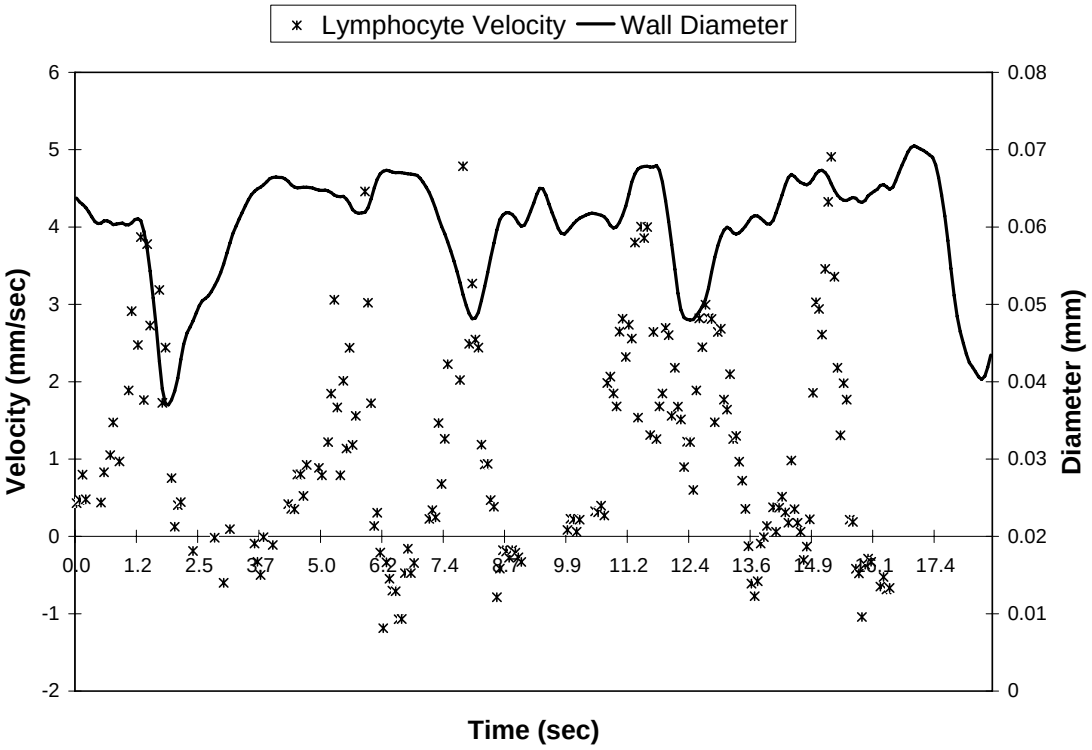
Lymphocyte Velocity
Wall Diameter
Velocity (mm/sec)
Diameter (mm)
Time (sec)
6
5
4
3
2
1
0
-1
-2
0.08
0.07
0.06
0.05
0.04
0.03
0.02
0.01
0
0.0
1.2
2.5
3.7
5.0
6.2
7.4
8.7
9.9
11.2
12.4
13.6
14.9
16.1
17.4

Rat 7

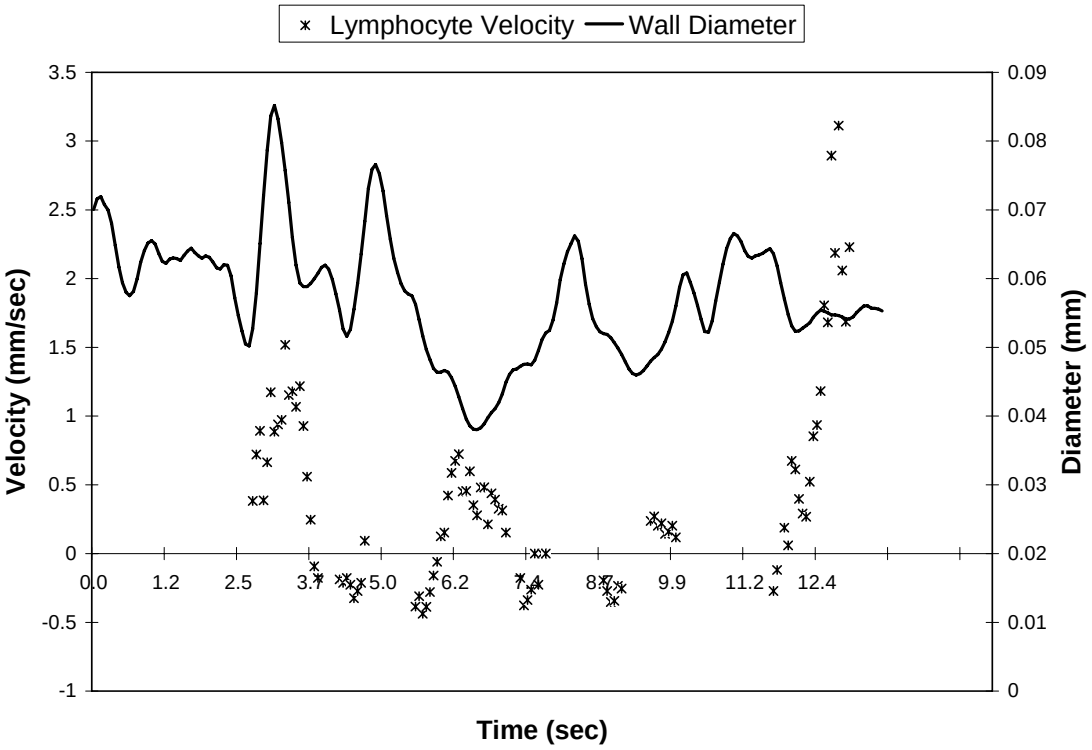
Lymphocyte Velocity
Wall Diameter
Velocity (mm/sec)
Diameter (mm)
Time (sec)
3.5
3
2.5
2
1.5
1
0.5
0
-0.5
-1
0.09
0.08
0.07
0.06
0.05
0.04
0.03
0.02
0.01
0
0.0
1.2
2.5
3.7
5.0
6.2
7.4
8.7
9.9
11.2
12.4

APPENDIX III

DOCUMENTED MATLAB CODE

```
%Imagecorrelationwall
%This program calculates and saves the coordinates of the left and
right
%wall at a selected location.
%It must be run before the Imagecorrelation can be run

%To process an entire sequence of data, you must run the code in the
following %order: imagecorrelationwall, imagecorrelation, filterdata

clear;

rotangle=-40;     %amount to rotate image to ensure vessel is vertical,
user                    %user will have to determine this by evaluating
image
cd 'D:\Rat9\Run2'; %sets the directory to the location of your images

i=2;
if i < 10
        a = 'lymph000';
        c = '.tif';
    elseif i <100
        a = 'lymph00';
        c = '.tif';
    elseif i <1000
        a = 'lymph0';
        c = '.tif';
    else
        a = 'lymph';
        c = '.tif';
    end
f = num2str(i);
t = strcat(a,f,c);
Pic2=double(imread(t)'); %initializes the image that will be assigned
to Pic1
Pic2=imrotate(Pic2,rotangle);
figure; imagesc(Pic2); colormap 'gray';
pixval(1,'on');
[y1(1),x1,P] = impixel; %prompts user to select left wall with mouse
[y2(1),x2,P] = impixel; %prompts user to select right wall with mouse
pixval('off');
X=1;
while i<6500
    Pic1=Pic2; %sets Pic1 to the Pic2 image that was used in the
previous iteration
    i=i+17
    X=X+1;
    if i < 10
        a = 'lymph000';
        c = '.tif';
    elseif i <100
        a = 'lymph00';
        c = '.tif';
    elseif i <1000
        a = 'lymph0';
```

```
        c = '.tif';
    else
        a = 'lymph';
        c = '.tif';
    end
    f = num2str(i);
    t = strcat(a,f,c);
    Pic2=double(imread(t)');
    Pic2=imrotate(Pic2,rotangle);
    fwin=Pic1(x1-4:x1+4,y1(X-1)-7:y1(X-1)+7);
    fbar=mean(mean(fwin));
    a=1;
    for l=(y1(X-1)-7):1:(y1(X-1)+7)
        gwin=Pic2(x1-4:x1+4,l-7:l+7);
        gbar=mean(mean(gwin));
        num1=(fwin-fbar).*(gwin-gbar);
        num1=sum(sum(num1));
        num2=(fwin-fbar).^2;
        num2=sum(sum(num2));
        num3=(gwin-gbar).^2;
        num3=sum(sum(num3));
        ccorr(a)=num1/sqrt(num2*num3);
        a=a+1;
    end

[Y,I]=max(ccorr);
corvall(X)=Y;
if Y>0.8 %rejects poor matches and keeps the window location the same
if             %condition fails
    y1(X)=y1(X-1)-8+I; %assigns left window location to place of max
correlation
else y1(X)=y1(X-1);
end


fwin=Pic1(x1-4:x1+4,y2(X-1)-7:y2(X-1)+7);
fbar=mean(mean(fwin));

    a=1;
    for l=(y2(X-1)-7):1:(y2(X-1)+7)
        gwin=Pic2(x1-4:x1+4,l-7:l+7);
        gbar=mean(mean(gwin));
        num1=(fwin-fbar).*(gwin-gbar);
        num1=sum(sum(num1));
        num2=(fwin-fbar).^2;
        num2=sum(sum(num2));
        num3=(gwin-gbar).^2;
        num3=sum(sum(num3));
        ccorr(a)=num1/sqrt(num2*num3);
        a=a+1;
    end
[Y,I]=max(ccorr);
corvalr(X)=Y;
```

```
if Y>0.8 %rejects poor matches and keeps the window location the same
if             %condition fails

    y2(X)=y2(X-1)-8+I;  %assigns right window location to place of max
                              %correlation
else y2(X)=y2(X-1);
end
end
diam=(y2-y1);     %this variable must be saved by the user after
running as                    %diameter.mat
cent=(y2+y1)/2;   %this variable must be saved by the user as
center.mat
```

```
%Imagecorrelation
clear;
load run2diameter;
load run2center;  %imports diameter in pixels and pixel location of the
center                  %of the vessel

cd 'D:\Rat9\Run2'; %sets the directory to the location of your images

rotangle=-40;     %amount to rotate image to ensure vessel is vertical,
user                    %user will have to determine this by evaluating
image
xi=110;     %makes vertical location of the reference window in the
center
for X=1:365 %iterates through each of the 365 sets of 17 images
for Q=1:4   %chooses 4 image pairings within a set of 17
i=(X-1)*17+Q %determines image # to load
if i < 10 %determines format of file string
        a = 'lymph000';
        c = '.tif';
    elseif i <100
        a = 'lymph00';
        c = '.tif';
    elseif i <1000
        a = 'lymph0';
        c = '.tif';
    else
        a = 'lymph';
        c = '.tif';
    end
f = num2str(i);
t = strcat(a,f,c);
Pic1=double(imread(t)); %reads first image

i=i+2; %iterates to an image 2 frames later for subtraction
if i < 10
        a = 'lymph000';
        c = '.tif';
    elseif i <100
        a = 'lymph00';
        c = '.tif';
    elseif i <1000
        a = 'lymph0';
        c = '.tif';
    else
        a = 'lymph';
        c = '.tif';
    end
f = num2str(i);
t = strcat(a,f,c);
Pic1b=double(imread(t));

i=i+2; %iterates to an image 2 frames later for 2nd image set
if i < 10
        a = 'lymph000';
```

```
        c = '.tif';
    elseif i <100
        a = 'lymph00';
        c = '.tif';
    elseif i <1000
        a = 'lymph0';
        c = '.tif';
    else
        a = 'lymph';
        c = '.tif';
    end
f = num2str(i);
t = strcat(a,f,c);
Pic2=double(imread(t));
i=i+2; % iterates 2 images later for subtraction of image forming 2nd
set
if i < 10
        a = 'lymph000';
        c = '.tif';
    elseif i <100
        a = 'lymph00';
        c = '.tif';
    elseif i <1000
        a = 'lymph0';
        c = '.tif';
    else
        a = 'lymph';
        c = '.tif';
    end
f = num2str(i);
t = strcat(a,f,c);
Pic2b=double(imread(t));

Pic1=(Pic1-Pic1b)';     %assumes the image read is in the horizontal
position,
                        % ' switches it to vertical, forms subtracted
image pair
Pic2=(Pic2-Pic2b)';     % forms 2nd subtracted image pair
Pic1=medfilt2(Pic1, [5 5]); %applies low pass filter to remove
pixilation noise
Pic2=medfilt2(Pic2, [5 5]);
Pic1=imrotate(Pic1,rotangle); %rotates image by amount specified
earlier
Pic2=imrotate(Pic2,rotangle);

fwin=Pic1(xi-15:xi+15,(cent(X)-diam(X)/2+5):(cent(X)+diam(X)/2-5));
%horizontal window size is set as a function of the diameter
% and the center of the vessel

fbar=mean(mean(fwin));
a=0;
for k=xi-50:xi+50 %scans the window vertically to measure fluid
displacement
    a=a+1;
```

```
    b=0;
    for l=cent(X)-6:cent(X)+6 %scans the window horizontally to
compensate for                              %image shifting due to motion
artifact
        b=b+1;
        gwin=Pic2(k-15:k+15,(l-diam(X)/2+5):(l+diam(X)/2-5));
%gwin window size must be identical to fwin
        gbar=mean(mean(gwin));
        num1=(fwin-fbar).*(gwin-gbar);
        num1=sum(sum(num1))/400;
        num2=(fwin-fbar).^2;
        num2=sum(sum(num2))/400;
        num3=(gwin-gbar).^2;
        num3=sum(sum(num3))/400;
        Data(X,Q).ccorr(a,b)=num1/sqrt(num2*num3);
%saves all the correlation images in file Data(X,Q)to be processed by
%processcorr and filterdata

end %for l

end %for k

end %for Q
end %for X
```

```
% Processcor
% the image correlation program must be run first and the variable Data
must be % in the workspace
% this program need not be executed as it is a subprogram used by
filterdata
% the main difference between this program and Processcor2 is that
Processcor2
% averages all 4 runs in a 17 image set, while this one chooses the
best of
% the four

clear temp1 temp2 maxval corval num i j bestps bestcv bestps2

for x=1:365
    for y=1:4
        [temp1, temp2]=max(Data(x,y).ccorr');
        [maxval(x,y),maxloc(x,y)]=max(temp1);
        %chooses the best match of each of the 4 pairings in a set of
17 images
        corval(x,y)=maxval(x,y)./mean(mean(abs(Data(x,y).ccorr)));
        %calculates relative correlation coeff
    end
    [num,i(x)]=max(corval(x,:));  %chooses the best of the 4
    [num,j(x)]=max(maxval(x,:));
    bestps(x)=maxloc(x,i(x)); %based on relative CC
    bestcv(x)=corval(x,i(x));
    bestps2(x)=maxloc(x,j(x)); %based on absolute CC
end
% figure;
% plot(bestps);
```

```
% Processcor2
% the image correlation program must be run first and the variable Data
must be % in the workspace
% this program need not be executed as it is a subprogram used by
filterdata
% the main difference between this program and Processcor is that this
one
% averages all 4 runs in a 17 image set, while Processcor chooses the
best of
% the four

clear temp1 temp2 maxval corval bestps bestcv tempdata

for x=1:365
    tempdata(x).ccorr=Data(x,1).ccorr;
    for y=1:4
        tempdata(x).ccorr=tempdata(x).ccorr+Data(x,y).ccorr;
        %sums each of the 4 pairings into a single correlation matrix
for each      %of the 17 image sets
    end
    tempdata(x).ccorr=tempdata(x).ccorr/4; %computes the average
    [temp1,temp2]=max(tempdata(x).ccorr');
      %finds the column in which the maximum correlation value is
contained
    [maxval(x),bestps(x)]=max(temp1);
    %finds the row in which the maximum correlation window is contained
    corval(x)=maxval(x)/mean(mean(abs(tempdata(x).ccorr)));
    %calculates the relative correlation coefficient
end
% figure;
% plot(bestps);
bestcv=corval;
```

```
% Filter data – the last program to be run in the sequence


Processcor2; %calls the subprogram can be Processcor2 or 1 see
documentation for
             %difference

velocity=(bestps-51)*0.001005814/.008;
%0.00100518 is dimension per pixel in mm, depends on optical settings

err=sqrt(mean((manualv'-velocity).^2))

cutoff=5.0; %sets the value the corr coeff must be to be a good match
found=0;
y=1;
while found==0 %searches for the first good fit
    if bestcv(y)<cutoff
        y=y+1;
    else
        found=1;
    end
end
found=0;
z=365;
while found==0  %searches for the last good fit
    if bestcv(z)<cutoff
        z=z-1;
    else
        found=1;
    end
end
for x=y:z  %looks at all values between first and last good fits
        if bestcv(x)<cutoff

%is it’s a poor match this sequence of if then statements search the
data to
%find the closest good matches before and after and user linear
interpolation to
%replace the bad match

            findlower=0;
            findupper=0;
            a=1;
            while findlower==0
            if and(bestcv(x-a)<cutoff,(x-a)>0)
                a=a+1;
            else
                findlower=1;
                lownum=x-a;
            end %if
            end %while findlower
            a=1;
            while findupper==0
            if and(bestcv(x+a)<cutoff,(x+a)<350)
```

```
                a=a+1;
            else
                findupper=1;
                highnum=x+a;
            end %if
            end %while fundupper
            bestps(x)=bestps(lownum)+(bestps(highnum)-
bestps(lownum))/(highnum-lownum)*(x-lownum);
        else
            bestps(x)=bestps(x); %accepts good matches
        end %if best
    end
    %figure;
    %plot(smooth(bestps));
    %hold;
%     plot(bestps, 'r');
mean(bestps)
mean(bestcv)
velocity=(bestps-51)*0.001005814/.008;
%0.00100518 is dimension per pixel in mm, depends on optical settings

err=sqrt(mean((manualv'-velocity).^2))
%calculates the standard error of prediction assuming you already have
a vector
%of manually recorded values in the workspace saved as manualv
```

```
%Findbestfit
%this program weighs the manually tracked data from spatially averaged
velocity
%to max velocity and calculates the error of this weighing as compared
with the
%correlation program

for x=0:100

weight=.01*x;
fitvel=manualv*weight+sav*(1-weight);
% figure; plot(fitvel, '*');
% hold;
% plot(velocity);

err(x+1)=sqrt(mean((fitvel'-velocity).^2));
end;
```

```
%Makemovie
%this program makes a movie from a sequence of lymphatic images

x=0;
figure;
colormap 'gray';
for i=0*17:17:365*17
    x=x+1;
    if i < 10
        a = 'rat000';
        c = '.tif';
    elseif i <100
        a = 'rat00';
        c = '.tif';
    elseif i <1000
        a = 'rat0';
        c = '.tif';
    else
        a = 'rat';
        c = '.tif';
    end
    f = num2str(i);
    t = strcat(a,f,c);
    Pic(x).picture=double(imread(t)');
    imagesc(Pic(x).picture);
    F(x)=getframe;
end
```

```
%Imagecorrelationwinchage
%clear;
%This program changes the second window to fit that of a parabolic flow
profile.
%It was tested on Rat9Run3
%Last modified 8/11/05

for X=3:3 %Number of velocities you want to calculate
    cd 'c:\corrtest';
Vnew=0; %initialize
V(X)=0; %initialize
i=(X-1)*17+1
if i < 10
        a = 'lymph000';
        c = '.tif';
    elseif i <100
        a = 'lymph00';
        c = '.tif';
    elseif i <1000
        a = 'lymph0';
        c = '.tif';
    else
        a = 'lymph';
        c = '.tif';
    end
f = num2str(i);
t = strcat(a,f,c);
Pic1=double(imread(t));
i=i+2; %Loads an image to images later to subtract from the original
if i < 10
        a = 'lymph000';
        c = '.tif';
    elseif i <100
        a = 'lymph00';
        c = '.tif';
    elseif i <1000
        a = 'lymph0';
        c = '.tif';
    else
        a = 'lymph';
        c = '.tif';
    end
f = num2str(i);
t = strcat(a,f,c);
Pic1b=double(imread(t));
i=i+2;
if i < 10
        a = 'lymph000';
        c = '.tif';
    elseif i <100
        a = 'lymph00';
        c = '.tif';
    elseif i <1000
        a = 'lymph0';
```

```
        c = '.tif';
    else
        a = 'lymph';
        c = '.tif';
    end
f = num2str(i);
t = strcat(a,f,c);
Pic2=double(imread(t));
i=i+2; %Loads an image to images later to subtract from the original
if i < 10
        a = 'lymph000';
        c = '.tif';
    elseif i <100
        a = 'lymph00';
        c = '.tif';
    elseif i <1000
        a = 'lymph0';
        c = '.tif';
    else
        a = 'lymph';
        c = '.tif';
    end
f = num2str(i);
t = strcat(a,f,c);
Pic2b=double(imread(t));
Pic1=Pic1-Pic1b;
Pic2=Pic2-Pic2b; %Pic2 is seperated by 2*framerate from Pic1
Pic1=medfilt2(Pic1, [5 5]); %smooths out pixel noise
Pic2=medfilt2(Pic2, [5 5]);
fwin=Pic1(x1-15:x1+15,y1(X)+15:y2(X)-15);
%sets the window on Pic1, y1&y2 are the left and right wall edges which
are %found by running Imagecorrelationwall
fbar=mean(mean(fwin));
count=0; %initialize
while and(or(abs(Vnew-V(X))>0,count<1),count<6)
%condition ensures that loop is run from 1 to 6 times and quits if it
produces a %reduntant value
V(X)=Vnew; %assigns previously found value to V(X)
count=count+1;
Pic2disp=Pic2; %Pic2disp will be the Pic2 image shifted to compensate
for the
              %velocity distribution
p2davg=mean(mean(Pic2disp));
for k=y1(X)+15:y2(X)-15
    disp=round(-1.5*V(X)*(1-((k-(y1(X)+y2(X))/2)/((y1(X)+y2(X))/2-
y1(X)))^2)); %calculates the disp based on measured V(X), was not sure
if V(X) was centerline %or average velocity, so used the mean of the
two instead
    for l=1:252
        if and((disp+l)<=252,(disp+l)>=1)
        %can't displace beyond the image border
            Pic2disp(l,k)=Pic2disp(l+disp,k);
        else
```

```
            Pic2disp(l,k)=p2davg; %assigns a background value to
references beyond the image edge
        end %if
    end %for l
end %for k
    for k=51:200
    %this nested loop moves the second window around and calculates the
    %correlation
        a=k-50;
        for l=-4:4
        b=l+5;
        gwin=Pic2disp(k-15:k+15,y1(X)+15+l:y2(X)-15+l);
        gbar=mean(mean(gwin));
        num1=(fwin-fbar).*(gwin-gbar);
        num1=sum(sum(num1))/400;
        num2=(fwin-fbar).^2;
        num2=sum(sum(num2))/400;
        num3=(gwin-gbar).^2;
        num3=sum(sum(num3))/400;
        ccorr(a,b)=num1/sqrt(num2*num3);
        end %for l
    end %for k
[corvec,I]=max(ccorr'); %finds all of the maximums in the radial
direction
[Y,J]=max(corvec); %finds the maximum in the flow direction
Vnew=Vnew+(x1-J-50)
%x1 is the center of window f, J+50 is the center of window g
end %while loop
pixshift(X)=Vnew;
corval(X)=Y;
relcorval(X)=Y/mean(corvec);
%finds the max correlation in the flow direction relative to the other
max
%correlations in the radial direction
end %for X=1:350
```

APPENDIX IV

ANIMAL USE PROTOCOL: NUMBER 2004-238

Funding Source: _____ Protocol Number: _____(Assigned by ULACC)
Routing Agency:_____ Revised 8/04

TEXAS A&M UNIVERSITY
Research/Teaching Proposals Involving Animal Subjects

Research investigators and class instructors are entrusted with an essential role in assuring the humane care and use of animals. In activities you conduct or that are conducted under your supervision, you have a direct and continuing responsibility to ensure that animals are adequately cared for and used in a humane fashion. Investigators and instructors must ensure that discomfort, pain or injury to the animals is avoided or minimized, consistent with sound experimental/teaching design; that no more animals are used than are necessary to reach sound scientific conclusions or to teach the class; and that, when appropriate, animals are painlessly sacrificed in accordance with methods of euthanasia approved by the Panel on Euthanasia of the American Veterinary Medical Association. Forms and requirements for approval by the Institutional Biosafety Committee (IBC) can be accessed through the ULACC web page (http://animal.tamu.edu).

Please check below if your research/teaching protocol involves any of the following:
___ Decapitation or cervical dislocation without anesthesia [*Provide rationale in Section II.E*]
___ Death (without appropriate euthanasia) as an experimental endpoint [*Complete Section III.D.4*]
___ More than momentary pain and distress not relieved by anesthesia and/or analgesics
_x_ Surgery [*Complete Attachment 1: Surgical Procedures*]
__ Multiple major survival surgery [*Provide rationale in Attachment 1]*
___ Use of adjuvants or antibody production [*Complete Attachment 2: Antibody Production*]
___ Use of hazardous chemicals (including chemical carcinogens) or radioactive materials *[Complete Attachment 3 for each]*
___ Use of recombinant DNA or genetically altered materials *[Provide IBC Approval]*
___ Use of agents infectious for personnel *[Provide IBC Approval]*
____ Use of a select agent or biological toxin *[See Appendix 2 of IBC permit form for list]*
___ Use of *non-commercial* genetically modified animals *[Provide IBC Approval]*
___ Captured wild animals or field studies *[Complete Attachment 4: Field Studies]*

Complete the Information Below:
Investigator/Instructor Name: David C. Zawieja Department: Medical Physiology
Mail Stop: 1114

Project/Class Title: Influences of lymph flow on the lymphatic pump

Is this AUP intended for continued work on a funded grant? (i.e. AUP was approved before grant?)
____No
__X__Yes (Previous AUP # 2001-252)

Is this AUP intended to replace another approved AUP?
_X__No
____Yes (Replaced AUP #_____)

FOR COMMITTEE ACTION ONLY

Animal usage (pertains to project design, not to species):

_____*Experiments involving food or fiber research or production (IAACUC)*
_____*Experiments of a biomedical nature (ULACC)*
_____*Client-Owned Animals (CVM CRRC)*
_____*Experiment Station (PHS or USDA Regulated Species, ULACC)*

Pain Stress Category Assigned:	I	II	III	IV
USDA Category Assigned:	N/A	C	D	E

_____ Returned for modification
_____ Approved by ULACC/IAACUC Date: _____ Signature:
_____

INVESTIGATOR'S/INSTRUCTOR'S ASSURANCE

Texas A&M University (TAMU) recognizes the importance of the use of animals in its research, teaching, and testing programs, and is committed to maintaining high standards for the care and use of animals in research, teaching, and testing. TAMU has adopted the "U.S. Government's Principles for the Utilization and Care of Vertebrate Animals Used in Testing, Research and Training" and complies with all applicable portions of the Animal Welfare Act, the Public Health Service Policy for the Humane Care and Use of Laboratory Animals, and all other federal, state, and local laws which impact the care and use of animals. TAMU investigators, teachers, staff, and students accept responsibility for determining that research, teaching, and testing involving the use of animals fulfills these principles, policies, and regulations. To assure compliance:

•**APPROVAL OF AUPS** Approval of an Animal Use Protocol (AUP), by the appropriate Institutional Animal Care and Use Committee (University Laboratory Animal Care Committee, ULACC, or Institutional Agricultural Animal Care and Use Committee, IAACUC), is required for all vertebrate animal use. All vertebrate animals must be covered by an active AUP, even after termination of a project.

•**DURATION OF APPROVAL** AUPs are approved for a three-year period and require two annual reviews. The first annual and second annual reviews are due on the anniversary of the date the ULACC/IAACUC approved the protocol. A new AUP approval is required for continuation beyond the three-year period.

•**AMENDMENTS TO AUPS** Any proposed change in personnel, species usage, animal procedures, anesthesia, post-operative care, or biohazard procedures to the animal portion of a study must be reported in writing to the ULACC/IAACUC for approval. Committee approval of the proposed amendment is required prior to proceeding with the revised animal procedures.

•**INFECTIOUS BIOHAZARDS, RECOMBINANT DNA** All animal research projects involving infectious biohazards and recombinant DNA, including procedures such as introduction of recombinant organisms into animals and generation of transgenic or knockout animals, must be registered and approved by the TAMU Institutional Biosafety Committee (IBC).

•**TRAINING OF PERSONNEL** All personnel working with animals, from the animal care staff to the persons doing the experiments/teaching must be qualified by training and/or experience to do so. Such training and/or experience should be documented in the AUP. All personnel working with animals must be informed of the TAMU Occupational Health and Safety Program for Animal Care and Use Facilities, and have the opportunity to participate fully in the program.

•**PROGRAM EVALUATIONS** All approved animal housing locations will be inspected twice annually. Unannounced inspections and observations of animal quarters and/or experimental or teaching procedures may be performed by the attending veterinary staff. Where procedures are causing severe distress to an animal and the pain cannot be relieved, veterinarians are authorized to humanely destroy that animal. Institutional Veterinarians will make a concerted effort to discuss these situations with investigators/instructors prior to initiating such action. The Committee is authorized to suspend research/teaching which does not conform to approved procedures outlined in the AUP.

Signature certifies that the Principal Investigator/Instructor:

1. Understands the requirements of the Public Health Service Policy for the Humane Care and Use of Laboratory Animals, applicable portions of the Animal Welfare Regulations (Animal Welfare Act), and the Institution's policies governing the use of vertebrate animals for research, testing, teaching, or demonstration purposes.
2. Will conduct the project/course in full compliance with the aforementioned requirements.
3. Will assure that personnel are appropriately trained and will conduct all procedures as described in this AUP.
4. Assures that this AUP accurately reflects the research/teaching described in any accompanying grant proposal.
5. Assures that the proposed work does not unnecessarily duplicate previous experiments.

6. Understands that work with animals is limited specifically to what is approved in this document.

David C. Zawieja Ph.D _____

Typed Name of Investigator/Instructor Signature of Principal Investigator/Instructor

Date

(NOTE: Graduate students need countersignature of Advisor)

David C. Zawieja Influences of lymph flow on the lymphatic pump
2001-252 _
Principal Investigator/Instructor Title of Project/Class
AUP#

Certification of ALL Participants in Research/Teaching Procedures
(Anyone whose name appears in the AUP)

Signature certifies that the participant:

1. Understands the requirements of the Public Health Service Policy for the Humane Care and Use of Laboratory Animals, applicable portions of the Animal Welfare Regulations (Animal Welfare Act), and the Institution's policies governing the use of vertebrate animals for research, testing, teaching and for demonstration purposes.
2. Will conduct the project/class in full compliance with the aforementioned requirements.
3. Understands his/her role in the AUP, agrees to perform it and assures that he/she has the appropriate skills to do so.
4. Further understands that work with animals is limited specifically to what is approved in this document.

Typed Name of Participant **Signature** **Date**

David C. Zawieja Ph.D.
_____

Anatoliy Gashev
M.D./Ph.D._____

Steven T. Greiner D.V.M.
_____

_____

_____

_____

Please add as many lines as necessary.

ANIMAL USE PROTOCOL (AUP)

(For Institutional Review Only)

Instructions to Investigators: All questions must be answered even if not applicable (N/A). **This form must be type written.** PLEASE USE AS MUCH SPACE AS NECESSARY TO COMPLETELY ANSWER EACH QUESTION.

SECTION I. PROJECT/CLASS IDENTIFICATION

A. Investigator/Instructor Name: David C. Zawieja
Dept:Medical Physiology, Mail Stop:1114

Work Phone: 979/845-7465 Emergency Phone: 979/846-3713

E-mail: dcz@tamu.edu

B. Title of Project/Class: Influences of lymph flow on the lymphatic pump

Funding Source: NIH
(e.g., NIH, USDA, AHA, Teaching, Internal)

Campus Routing Office: RF
(e.g., RF, TAES, TEES, none)

C. Project Animal-Care Contact Person *[Who is to be contacted in case of an animal emergency]*:

David C. Zawieja, Anatoliy Gashev, Steven Greiner
Work Phone: 845-7465, 862-8575 Emergency Phone: 846-3713, 731-1147, 731-8838

E-mail: dcz@tamu.edu, gashev@tamu.edu, stgreiner@msn.com

D. Abstract: Please provide a brief statement, in LAY TERMINOLOGY, understandable by someone with a high school education, with no acronyms or scientific jargon, outlining the purpose of the experimental/teaching procedures of this protocol. *[Why you are doing this experiment/class and what you propose to learn/teach.]*

The lymphatic system is a network of vessels and nodal tissues dispersed throughout the body that has important roles in body fluid and protein circulation, fat absorption and immune function. These experiments are designed to determine how fluid flow inside the lymphatic vessels affects the pumping activity of the lymphatic vessels. This pumping activity is necessary for the generation of lymph flow and for normal lymphatic function.

E. Animal Procedures: These protocols are available to, and may be read by, the lay public. Describe in narrative form, using LAY TERMINOLOGY, understandable by someone with a high school education, no acronyms or scientific jargon, the experimental procedures and manipulation or teaching protocol that will be performed on the animals (not scientific rationale). *[Be brief and specific in describing the animal procedures. However, it is not necessary to go into detail (in this section) regarding surgical procedures—that information should be addressed on the Surgical Procedures Attachment 1.]*

The experiments will involve the study of lymphatic vessels removed from the rat. This will require tissue harvest from the small intestinal mesentery of the rat after the animal has been first fasted overnight and then anesthetized. After the lymphatics are removed from the animal, the animal will be sacrificed.

F. Justify why you chose to use this (these) species in your research/class. *[Describe characteristics of the animal model that make it appropriate for use in your studies/teaching*. Body size, comparative data from prior studies or unique physiological features may be considered in justification of species. Cost alone is not an acceptable justification for selection of the animal model.]*

The rat is the animal model of choice because of a number of reasons. The first important consideration is size. The animal is small enough to allow us to study the lymphatics intact (in situ) on our intravital microscopes, while the vessels are large enough to allow us to microscopically observe them but still allow us to manipulate and isolate them. Another important factor is that this model has one of the largest literature base published on lymphatics and is one in which we have extensive (20years) of experience with both in situ and in vitro.

* If this is a teaching protocol please justify the use of live animals to achieve your teaching objectives.

G. Experimental Design/Teaching Protocol

1. Describe the number of animals per experiment/class, including a breakdown within experiments/lessons of animals per treatment condition *[Including number of replications and relevant controls.]* If the project involves breeding animals, indicate how many breeder stock will be required and how many offspring will be used for the studies. If the project utilizes a colony or herd which will be maintained for the purpose of supplying animals to other approved protocols, please contact the Chair of the ULACC/IAACUC for information on procedures for documenting colony numbers.

A CHART OR TABLE PROVIDING EXPERIMENTAL TREATMENT/TEACHING LABORATORY AND NUMBER OF ANIMALS PER TREATMENT/TEACHING LABORATORY WILL HELP EXPEDITE REVIEW.

See accompanying addendum for table and explanation

2. Explain WHY you chose a certain number of animals per treatment/teaching laboratory condition. *[Taking into account known variation of the dependent variable, subject losses, etc. Statements such as "this number is required for statistical significance", without an indication of how you know this, are not adequate answers. Numbers of animals required to obtain enough tissue to adequately quantify parameters may be important, but PI must supply indicators of expected tissue content and assay parameters.]* The following URL is used for Statistical Calculations: Number of Animals Needed:
http://www.stat.uiowa.edu/~Rlenth/Power/index.html.

Based upon our previous experience and power analyses with similar microlymphatic studies, approximately 10 successful experiments will be needed per group, given typical variability and measurement sensitivity for these experimental groups. Usually we have about about a 75% success rate with these types of experiments meaning we'll need ~15 animals per group. However because of the technical difficulty of Project 8, we have proposed a greater number of attempted experiments (~20 animals per group) because of anticipated, potential lower initial success rates. However we also anticipate

that our success rate will improve after the initial studies with new experimental paradigms.

SECTION II. ANIMAL PROCUREMENT/MAINTENANCE INFORMATION

A. List the total number of animals used, by species, for the duration of the project:

SPECIES	**TOTAL NUMBER FOR DURATION OF AUP**
Rat	**430**

If the project involves breeding animals, please also complete the table below. These numbers, for the duration of the project, should be included in the overall Total above.

SPECIES	**TOTAL NUMBER OF ADULT BREEDERS NEEDED**	**ESTIMATED TOTAL NUMBER OF OFFSPRING TO BE PRODUCED**

B.Where will you obtain the animals? [*If wild-caught by you, please describe applicable permits, method of capture and evaluation of health risks to personnel. Please provide a copy of permit approvals (Please contact the chairperson of ULACC if this presents a problem). Complete Field Studies Form, Attachment 4, for wild capture studies.*]

Commercial Vendors, normally Harlan

C.HOUSING ***(It is the investigators responsibility to assure availability of housing with the facility.)***

1. Where will you house animals? __ Reynolds Medical Building _ Bldg. #_____
2. Is it ULACC/IAACUC approved?

_X_Yes

_____ No ***(Please contact the ULACC office at 845-1828 to schedule a facility evaluation.)***

3. Describe any special housing, caging, diet, environment or other requirements necessary for this study/class (example: grid floors, special diets, food/water deprivation, identification of genetically modified animals).
None other than fasting the animals the night before their use.

D. Who will provide veterinary medical care for the animals? LARR staff Veterinarians

E.What will happen to the animals after you complete the experiment/class? [*If you plan to transfer the animals at the end of your study, please complete an Animal Transfer Form prior to such a transfer. This form is available on the ULACC website. If the animals are to be euthanized, please describe the agent and method employed. Decapitation or cervical dislocation without anesthesia requires written justification below.*]

Animal Transfer:

_____ Internal to another AUP (requires ULACC approval)

_____ External (outside agency, slaughter, adoption, etc.)

If adopting animals to private homes, please provide your laboratory procedures and guidelines.
Transfer to a private destination requires prior approval. Assure appropriate drug withdrawal times if applicable.

Euthanasia (This section must be completed on all AUP's. *Exceptions must be clearly explained (e.g. protected species).

Method: lethal overdose

Agent: sodium pentobarbital

Dose: 120 mg/kg Route: IP

Justification of decapitation / cervical dislocation without anesthesia, if employed:

Even when euthanasia is not an integral part of the AUP, please provide an adequate protocol for euthanasia in case there is an unexpected event.

F. Name(s) of individuals(s) administering euthanasia. [*Note: Other than CMP or Vet Med Park staff, only the persons listed below will be authorized to perform the euthanasia procedure.*]

David C. Zawieja, Anatoliy Gashev, Steven Greiner

G. Specify the education, training and experience which qualifies each person named in Section IIF to perform euthanasia.

David C. Zawieja, Ph.D., 22 years experience with rat models, TAMU LARR training "Rats: Basic Handling and Techniques" and "Asepsis and Aseptic Techniques".
Anatoliy Gashev, M.D. Ph.D., 19 years experience with rat models, TAMU LARR training "Rats: Basic Handling and Techniques".
Steven Greiner, D.V.M., 9 years experience with rat models, TAMU LARR training "Rats: Basic Handling and Techniques", TAMU LARR training "Mice, Basic Handling & Techniques"

SECTION III. ANIMAL PROCEDURES

A. Where will you conduct animal procedural/teaching work? *[List Bldg. and Room # for each procedure to be done]*: Reynolds Medical Bldg. Room 347

B. Briefly indicate below any non-surgical procedures to be used. Identify each species involved [*If more than one*]:

1. Method & duration of restraint:
The rats will be briefly manually restrained, no more than a minute or two, in order to give the anesthetic drugs

2. Method of obtaining blood or other tissues: [*Indicate the technique to be used, the volume to be collected, the frequency of collection, and the interval between collections. Terminal blood collections require use of a suitable anesthetic.*]
Lymphatic tissues will be collected after anesthesia, see details in Attachment 1 Surgical Procedures

3. Agents to be administered (other than anesthetics/adjuvants), including dose, volume, route, & frequency:
NA

4. Other procedures such as food or water deprivation, administration of noxious stimuli or substances and procedures which might induce clinical illness.
The animals will be fasted overnight the day before they are used. This is important for our studies in order to study basal lymphatic function under fasted conditions. We have extensive experience with this brief period of fasting and have not seen problems associated with it.

5. Names and qualifications of personnel to perform the specified procedures (Include training and experience in the techniques listed above):
David C. Zawieja, Ph.D., 22 years experience with rat models, TAMU LARR training "Rats: Basic Handling and Techniques" and "Asepsis and Aseptic Techniques".
Anatoliy Gashev, M.D. Ph.D., 19 years experience with rat models, TAMU LARR training "Rats: Basic Handling and Techniques".
Steven Greiner, D.V.M., 9 years experience with rat models, TAMU LARR training "Rats: Basic Handling and Techniques", TAMU LARR training "Mice, Basic Handling & Techniques"

C. Anesthesia/Analgesia

1. If anesthesia is necessary, please describe the agent to be used, dosage and route of administration for each species. *[Also indicate any other pre-anesthetic procedures, such as duration of fasting from food and water. Repeat for each species and/or surgical procedure if different.]*

Preanesthetic: none Dosage: NA Route: NA
The animals will be fasted overnight the day before they are used. This is important for our studies in order to study basal lymphatic function under fasted conditions. We have extensive experience with this brief period of fasting and have not seen problems associated with it.

Anesthetic: Fentanyl-Droperidol Dosage: 0.3 ml/kg Route: IM
Muscle relaxant: Diazepam Dosage: 2.5 mg/kg Route: IM

(the initial anesthetic dose is indicated in the LARR Animal Care and Use Handbook from TAMU and TAES and after extensive consultation and collaboration with LARR

veterinarian Dr. Kasari to find an anesthetic regimen that provides appropriate anesthesia/analgesia without inhibiting the lymphatic function we are scientifically trying to evaluate. It has been shown that of the typical drugs used for surgical anesthesia the barbituates, and gas anesthetics (other than ether) when "used in doses similar to plasma levels found during general anaesthesia, significantly depressed lymphatic contractility" (McHale NG and Thornbury KD. The effect of anesthetics on lymphatic contractility. Microvasc Res 37: 70-76, 1989). Thus we CANNOT use barbiturates, halothane of isoflurane anesthetics for these studies as they will render the results useless. We take care to test stimulatory reflexes of the rats to ensure that the animals are at an appropriate stage (III) and plane (2-3) of anesthesia and without normal responses to noxious stimuli (close hand clap, tail pinch and palpebral reflex). If the animal is not at an appropriate level of anesthesia/analgesia we will redose, although our experience for this regimen and experiment indicates this is usually not needed. In the past we have used a ketamine-xylazine mixture (100-300 mg/kg) for some experiments. However, we did not include this anesthetic regimen in this AUP because often the time needed to study/isolate the lymphatics for these experiments is longer (45-60 minutes) than what was indicated to us (as well as what we experimentally observed) was the optimum length of appropriate surgical plane (15-30 minutes) for ketamine-xylazine mixture regimen, thus requiring at least one redosing. This appeared to us to increase, not decrease the likelihood that our animals may experience pain during the procedure. Thus after careful consideration of all these factors we opted to use the Fentayl-Droperidol anesthetic regimen.)

Analgesics: Dosage: Route:

2. Identify each person who will administer/monitor anesthesia and their qualifications. ***[Indicate previous experience, education, and specific training for this specie and with this anesthetic agent. A listing of academic degrees is not an adequate response to this question. Anesthesia training is available; for information on training, visit the ULACC website, http://animal.tamu.edu/training.html. In teaching activities, students under the direct supervision of qualified personnel may be appropriate.]:***

David C. Zawieja, Ph.D., 22 years experience with rat models, 7 years experience with this anesthetic & species TAMU LARR training "Rats: Basic Handling and Techniques" and "Asepsis and Aseptic Techniques".
Anatoliy Gashev, M.D. Ph.D., 19 years experience with rat models, 5 years experience with this anesthetic & species, TAMU LARR training "Rats: Basic Handling and Techniques".
Steven Greiner, D.V.M., 9 years experience with rat models, 4 years experience with this anesthetic & species, TAMU LARR training "Rats: Basic Handling and Techniques", TAMU LARR training "Mice, Basic Handling & Techniques"

D. Assessment of Pain and Distress

1. Does the project/class exercise involve the use of painful procedures or paralytic drugs without the benefit of anesthetics or analgesics? Yes_____ No___X___
IF YES, justify why anesthetics/analgesics are inappropriate for your experiments:

2. Could the procedures or outcome of this project/class cause more than slight or momentary pain or distress to animal subjects? **Be advised that the USDA has ruled that**

any surgical procedure has the <u>potential</u> for pain and/or distress. (Please see the ULACC Website at http://animal.tamu.edu/p&d.html for examples of procedures which may cause pain or distress.)

NO _____

YES __X__ (Complete below)

A. __X__ As described in Section III.D.I. any potential pain or distress to these procedures will be relieved through use of anesthetics and analgesics and alternatives to these procedures are not available. ***COMPLETE THE SECTION ON ALTERNATIVES BELOW***

B. _____But as described in Section III.D.I., anesthetics and analgesics are inappropriate for these procedures. Alternatives to these procedures are not available. ***COMPLETE THE SECTION ON ALTERNATIVES BELOW***

Describe the methods and sources you used to determine that alternatives to these **procedures** are not available. These might include computerized database searches (BIOSYS, Current Contents, Medline, PubMed, AgriCola). Be advised that database searches are not the only source of alternatives.

Databases searched: Medline, PubMed

Dates searched (inclusive): 1966-2004

Keywords: lymphatic function, animal models, alternatives

A narrative of the results of alternatives search, addressing **Refinement** (new anesthetics, new analgesics, new surgical techniques, etc.) **Reduction** (please feel free to include reduction in numbers that have occurred during your career), **Replacement** (non-animal techniques) and a justification as to why these options were not used is required: **We have looked in the literature and consulted with Dr. Kasari from LARR for better refinements of anesthetics/analgesics and were not able to find significant refinement of these options given the scientific problems associated with most other anesthetics and lymphatic function. In terms of reduction of animal numbers over the course of my career here we have significantly reduced our numbers through refinement of expertise and technique to the point where the numbers needed reflect the true biological variability of the lymphatic biology and not our capabilities to accurately perform these studies. Replacement is simply not a viable alternative for these studies. While we use cell cultures for certain aspects of similar work, cultured cell DO NOT reflect what happens in situ in these tissues. Computer models are too simple and can truly only predict what we already know and that is not what our studies represent.**

3. Is there a possibility of any illness in the animals as a result of experimental/teaching procedures? Please include any clinically significant side effects that may occur in genetically modified animals.

No__X__ Yes_____ if yes answer a-d below:

a. describe those effects and explain at what point and by what objective criteria (such as clinical condition) the animals may be euthanized or permanently removed from the study/class:
B. describe the frequency per day that you or your staff will observe the animals after treatment administration:
C. describe the monitoring and recording procedures for determining physiological or behavioral abnormalities:
D. State what measures will be taken to minimize or alleviate problems associated with experimental/teaching procedures:

4. Is death (without euthanasia) an endpoint of the study? Yes____ No__X___
IF YES, justify why an earlier end point is not acceptable:

ATTACHMENT 1

SURGICAL PROCEDURE

Instruction to Investigator/Instructor: **Fill out one copy of this page for each different surgical procedure.** Please make an entry for each category. Carefully list the personnel names for those who will monitor anesthesia, conduct the surgery and monitor recovery. Only those persons listed below will be authorized to perform these functions. All survival surgical procedures require use of aseptic technique. This includes use of sterile surgical gloves, sterile instruments and aseptic preparation of the surgical field.

A. Surgical Procedure: Specify: __Laparotomy___

1. Where will the surgery be performed? [*List Bldg, Room #*]:
Reynolds, room 347
2. Indicate the nature of the surgical procedure [*check one*]:

__X__Non-survival
_____Survival
_____ Multiple Major Survival [*Provide justification*]:

3. Provide a brief description of the surgical procedure [*Include relevant details from initial incision to wound closure.*]:
A 2 cm long midline abdominal incision will be made through the skin, underlying fascia, and abdominal muscle layers. Bleeding will be controlled by electrocautery. A loop of small intestine, 4-5 cm long, will be gently exteriorized onto a specially designed preparation board so access to mesenteric collecting lymphatics is possible for observation and tissue collection. The exposed tissue will be continuously superfused with warm (37°C) physiological buffer. This preparation will be briefly observed with the aid of a stereomicrosope to pick a lymphatic suitable for isolation. The vessel will then be carefully dissected free from the surrounding tissue. After tissue collection, the animals are euthanized as described earlier.

4. Identify each person who is authorized to perform the surgical procedure. Indicate the qualifications of each person who will conduct the surgical procedure. ***[Indicate previous experience, education, and specific training for performing the procedure. A listing of academic degrees nor curriculum vitae (CV's) are an adequate response to this question. Surgical training is available; for information on training, visit the ULACC website, http://animal.tamu.edu/training.html. In teaching activities, students under the direct supervision of qualified personnel may be appropriate.]:***
David C. Zawieja, Ph.D., 22 years experience with rat models, TAMU LARR training "Rats: Basic Handling and Techniques" and "Asepsis and Aseptic Techniques", "Mice, Basic Handling & Techniques", "Asepsis and Aseptic Techniques".
Anatoliy Gashev, M.D. Ph.D., 19 years experience with rat models, TAMU LARR training "Rats: Basic Handling and Techniques", TAMU LARR training "Mice, Basic Handling & Techniques" Asepsis and Aseptic Techniques".
Steven Greiner, D.V.M., 9 years experience with rat models, TAMU LARR training "Rats: Basic Handling and Techniques", TAMU LARR training "Mice, Basic Handling & Techniques", "Asepsis and Aseptic Techniques".

B. Post Operative Care:
1. Where will the animals recover from surgery? [*List Bldg, Room #*]:
NA

2. Indicate what post-surgery complications might be anticipated and how they will be managed:
NA
3. List the names of the individuals who will monitor post-operative recovery and **frequency** of observation: NA
4. Describe the post-operative medication(s) to be given. [*List each agent, the dosage (e.g. mg/kg), route (e.g. IP) and the frequency of administration. If no analgesics are planned, please justify withholding analgesics following any surgical procedure.*]: NA

Analgesics:
Antibiotics:

Other:

ATTACHMENT 2
ANTIBODY PRODUCTION

Instructions to Investigator: Appropriate use of any adjuvant involves minimization of volume for injection and maintenance of sterility of material to be injected. Please contact one of the CMP veterinarians (845-7433) if you need more information. **NOTE:** USDA has determined that the use of Freund's complete adjuvant has the potential to cause more than momentary or slight pain or distress. If you plan to use Freund's complete, please answer "YES" to question III.D.2. on the AUP and document your search for alternatives. NA

A. Describe your immunization protocol. [*Please include adjuvant to be used including justification if complete Freund's is required. The committee discourages the use of Freund's Adjuvant due to the tendency of Freund's to contribute to tissue damage. Describe the route, volume, and number of sites for injections as well as time intervals between injections.*]:

B. Describe route and volume of blood collection and interval between collections. [*Note: Volume and frequency of collection must be limited to that which causes no anemia or hypovolemia. If there are questions concerning safe volumes, please contact one of the CMP veterinarians. Exsanguination must be performed under general anesthesia. Bleeding from the orbital sinus of rodents should be performed under anesthesia. Special authorization may be provided to individuals with experience and technical expertise for performance of orbital sinus bleeds without anesthesia.*]

C. Describe ascites fluid collection procedures. [*Note: After inoculation for ascites production, animals should be observed at least 3 times per week the first week and daily thereafter by the PI or the PI's staff to monitor the degree of abdominal distention and illness. Fluid should be removed when distention is comparable to a term pregnancy. Only one survival tap followed by one terminal tap under anesthesia is recommended. Euthanasia should be performed on any animals showing signs of poor condition.* **NIH expects that if the ascites method is to be used, justification is provided for why in vitro alternatives are not suitable.]**

D. Name(s) and qualifications of individual(s) performing techniques described including injections, abdominal taps, anesthesia, and blood collection. [*Include education, training and experience in these techniques.*]

ATTACHMENT 3

APPROVAL FOR USE OF HAZARDOUS MATERIALS IN ANIMALS

Instruction to Investigator/Instructor: If you will be using any hazardous substances (e.g., radioactive materials, toxic chemicals) in your animals (*in vivo*), you must complete this page. We will forward it on your behalf to the appropriate safety official. **Do not use this form for infectious agents. Obtain separate IBC approval. NA**

INVESTIGATOR/INSTRUCTOR: DEPT.: AUP #:
(to be assigned by ULACC)

PROTOCOL TITLE:

AGENT(S) TO BE USED:

SPECIES TO BE USED:

ANIMAL HOUSING SITE (include Bldg. & room. #):

LOCATION OF LABORATORY:

DESCRIPTION OF PROPOSED ACTIVITY:

How is the agent to be introduced into the animal?
____topical ____oral ____inhalation ____injection (give route, volume and concentration)

Major containment equipment to be used for personnel protection:

Personal protective gear to be worn:
____Face Shield ____Goggles ____Face Mask ____Full Face Respirator ____Shoe Covers
Lab Coats
____Rubber Boots/Coveralls ____Other (specify):

Describe type and quantity of hazardous waste to be generated and method of disposal:

Describe how contaminated materials are to be treated after usage (animals, bedding, glassware, benchtops, hoods, etc.):

Indicate which of the following resources are available in the area the procedure will be performed
____Fire Extinguisher ____Eyewash Station ____Spill Kit ____Emergency shower

Describe emergency procedures to be followed in case of accident (personnel exposure, spill, fire, etc.)

Last date of certification for any hood required:

Qualifications of Involved Personnel (give names, experience, certifications, etc.):

ATTACHMENT 4

FIELD STUDIES

Assurance of Health and Safety of Personnel Performing Field Studies Involving Animals

Instructions to Investigator/Instructor: The purpose of this Attachment is to assure that consideration is given to safety and well being of university personnel participating in field studies. It is a part of the institutional compliance with the Guide for the Care and Use of Laboratory Animals and the Guide for the Care and Use of Agricultural Animals in Agricultural Research and Teaching.

I hereby certify that there is a program in place to assure the safety of personnel participating in this proposed work. The program involves hazard identification and risk assessment, appropriate equipment for safe conditions for the work, personnel training and education, and preventive medical oversight. It includes an emergency plan which covers the following:

A mechanism to evacuate personnel if necessary in a timely fashion

A permanent and dependable system such as telephone, cellular phone, or radio for continuous emergency communication capability

A local contact for health and safety emergencies

Necessary medical coverage (insurance)

Appropriate individual medical preparedness

Vaccine and preventive medical precautions as deemed necessary by a physician

Adequate supplies of prescription drugs/devices

First Aid and Cardiopulmonary Resuscitation skills

Method to assure contact of University Human Resources Department in the event of accident/injury

Credentials and or training in safety procedures necessary for carrying out the work as determined by the Principal Investigator

_____

Signature of Investigator/Instructor **Date**
(*Signature does not imply transfer of liability*)

Experimental Design Addendum

The following table describes our projection of the number of animals needed for each of the experimental Project originally described in this proposal. However since this grant has been active for almost 2 years some of the projects have been completed and some have been removed from the grant due to funding limitations. The table below thus only reflects the animals needed for those projects still left to be finished.

Project #	# of groups	# of animals/group	Total # /Project
1	1	Completed in years 1-2	
2	1	Completed in years 1-2	
3	1	15	15
4	1	15	15
5	1	Project removed in renewal	
6	1	Project removed in renewal	
7^	20	15	300
8*	5	20	100
Total number of animals for the remainder of the proposal equals			430

* Project 8 will require 20 animals per group because of **anticipated potential difficulties** in the proposed research paradigm briefly described below:
Project 8: "Measure the changes in intracellular calcium in the endothelial and muscle cells of isolated mesenteric lymphatic that occur in response to imposed flow" has 5 experimental groups (endothelial calcium measurement, smooth muscle calcium measurement, endothelial denuded smooth muscle calcium measurement, SNP group with smooth muscle calcium measurement and DEA-NONOate group with smooth muscle calcium measurement) all of which require the measurement of intracellular calcium in intact tissues and thus are more difficult experiments based on our previous studies. Thus we anticipate needing larger number of animals in these groups.

^ Project 7 is an extensive project (20 experimental groups) that is the heart of this proposal that investigates the roles of nitric oxide (NO) pathway, the prostanoid pathways, and the EDHF pathways in the flow-mediated effects on lymphatic contractile function. There are 4 different groups studying the role of nitric oxide, 8 different groups studying the role of prostanoid, and 8 different groups studying the role of EDHF pathways. 20 experimental groups times 15 animals per group yields 300 animals for this project.

VITA

James Brandon Dixon was born on September 4, 1979 in Austin, TX to James & Marilyn Dixon. He grew up in Round Rock, TX as the oldest of five children and moved to College Station to attend Texas A&M University in September of 1998. Brandon received his B.S. in biomedical engineering from Texas A&M in December 2001. He immediately began graduate school in January working in the Optical Biosensing Laboratory under the direction of Dr. Gerard Coté. During his time in graduate school he worked on a variety of projects in addition to this one. Some of these projects include: Monte Carlo modeling for perfusion monitoring, non-invasive glucose detection using polarized light, and non-invasive skin cancer diagnostics using Mueller matrix imaging. He also served as an Assistant Lecturer, teaching five different undergraduate courses over the span of September 2002 to May 2006. He received his Ph.D. in biomedical engineering from Texas A&M in May 2006 and immediately left for Switzerland where he is a visiting research scientist at EPFL in Lausanne. His permanent address is 1908 Greenhill Dr., Round Rock, TX 78664.